A NEW APPROACH FOR PERFORMANCE EVALUATION OF BRIDGE INFRASTRUCTURE USING TERRESTRIAL LIDAR AND ADVANCED MATHEMATICAL MODELING

by

ALI SHAFIKHANI

Presented to the Faculty of the Graduate School of

The University of Texas at Arlington in Partial Fulfillment

of the Requirements

for the Degree of

DOCTOR OF PHILOSOPHY

THE UNIVERSITY OF TEXAS AT ARLINGTON

August 2018

Acknowledgements

First and foremost, I would like to take the opportunity to express my special appreciation and thanks to my advisor, Professor Anand J. Puppala to give me the opportunity to work in his great research group. It is not possible to accomplish this work without his generosity, inspiration and support. His expertise in geotechnical engineering and passion towards implementing new technologies to evaluate safety of the bridge infrastructure and communities are the driving factors to this research. Beyond research, the very friendly and professional atmosphere he managed in his research group was a driving factor that always encouraged me during my PhD program. Undoubtedly, it is not possible to express my appreciation and thanks to him in a few words. His attitude toward teamwork, leadership, passion and hard work will role as a great standard to follow during my future careers.

I would like to express my deep appreciation to Professor Laureano Hoyos for his remarkable discipline, patience and approach of explaining the very basic concepts in geotechnical engineering. I would like to extend my thanks to Dr. Xinbao Yu, who was a great representative of hard work and passion. I also thank Dr. Pranesh B. Aswath for his willingness to serve in my examination committee. My very special thanks to Dr. Tejo Bheemasetti for his unconditional supports and great advices. As a professional leader and friend, he made such a peaceful atmosphere to work during my PhD program.

I would like to express my greatest acknowledgments and thanks to my parents, siblings, and niece, Manouchehr, Shahla, Mona, Neda, Iman, Masood and Sophia for their unsparing encouragements and blessings. Without their supports, it was not possible to accomplish my PhD as another great goal in my life. I also want to acknowledge my very special friends Dr. Reza Saeedzadeh and Tram Ngo for their encouragements and supports.

I would like to extend my thanks to my friends and fellow students Dr. Aravind Pedarla, Dr. Ujwalkumar D. Patil, Tom Taylor, Dr. Raju Acharya, Dr. Alejandro Pino, Dr. Santiago Caballero, Leila Mosadegh, Anu George, Puneet Bhaskar, Sarat Chandra, Burak boluk, Leooldo Cardiel, Manikanta Saladhi, for your supports. Special thanks to Dr. Minh Hai, Shi He (Danny), Sayantan Chakraborty, Dr. Aritra Banerjee Dr. Jasaswee Das, Rice, Jun Lin for helping me to collect data from the US 67 bridge site. You never left me alone and I will never forget your supports. I also want to acknowledge Dr. Pinit Tuttanaporamakul (Tom) for his hard work and collecting such great dataset from the US 67 test site.

I am also grateful to entire faculty and staff in the Department of Civil and Environmental Engineering at The University of Texas at Arlington for your supports, advice and suggestions. A special acknowledgment is extended to Shelly Douglass for managing all of my paperwork during my PhD program.

Last but not the least, I thank to the great Mother Nature for leading me through such a beautiful pathway. Thank You for giving me everything I need. Thank you for your beautiful colors and I will keep on trusting you for the rest of my life.

July 17, 2018

Abstract

A NEW APPROACH FOR PERFORMANCE EVALUATION OF BRIDGE INFRASTRUCTURE USING TERRESTRIAL LIDAR AND ADVANCED MATHEMATICAL MODELING

Ali Shafikhani, PhD

The University of Texas at Arlington, 2018

Supervising Professor: Anand J. Puppala

High plastic expansive clays when subjected to different climatic conditions undergo large ground movements causing distress to infrastructures including bridges, pavements, buildings, retaining structures, and others. Performance assessment of these structures built on problematic soils such as expansive clays is important to reduce maintenance and extending the design life of infrastructure. Rapid developments in remote sensing technologies with precise evaluation have influenced the monitoring techniques for assessing the health condition of civil infrastructure projects. While these technologies have considerably aided in performance evaluation, cogent procedures for evaluating the ground movements are still required that integrates technologies, climatic factors, soil behavior models. This research study presents an integrated approach using the Three-Dimensional Terrestrial Laser Scanning (3D-TLS) technique and advanced mathematical modeling (system identification approach) for assessing the performance of the bridge infrastructure including highway embankment, bridge deck, bridge approach slab, bridge abutments, and columns. First, an optimized framework is developed to evaluate ground movements using 3D-TLS technique, which is an active-remote sensing Light Detection and Ranging (LiDAR) remote sensing technology that uses near-infrared light to monitor physical characteristics of earth's surface. The ground movements from the processed scans, and climatic factor parameters including temperature and precipitation variations were used to develop advanced mathematical models of dynamic systems using

collected time-series data. The validation of the developed integrated framework is illustrated on a test site built on high plastic expansive clay soils located in North Texas. Cost-Benefit Analysis (COA) is performed to compare 3D-TLS remote sensing and prevalent monitoring approaches. This research highlights the integration of latest technological developments with advanced mathematical models to predict the condition of a bridge infrastructure.

Table of Contents

List of Illustrations

List of Tables

Chapter 1: Introduction

General Overview

Geotechnical Structural Health Monitoring (GSHM) refers to the process of evaluating the condition of the infrastructure with respect to defined allowable tolerance criteria using different monitoring techniques. The condition of a bridge infrastructure is often addressed based on incurred ground movements, including vertical, lateral, and structural movements, corrosion of rebar system, and integrity of structure (Chen and Chai 2010; Das et al. 2018; Huston 2010; Karbhari and Ansari 2009). To evaluate these movements, engineers primarily relied on visual observations and technologies including in-situ sensors, such as inclinometers, extensometers, piezometers, pressure cells, deformation gauges, and elevation surveys (Dunnicliff 1993). Figure 1.1 presents a joint extensometer that can measure the relative displacements between concrete slabs.

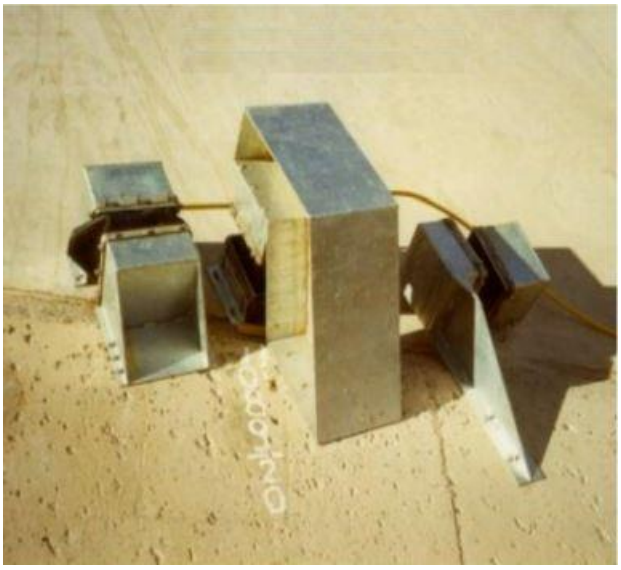

Figure 1.1 LVDT installed joint extensometer in a concrete dam site (Brylawski and Asce 2007)

Current monitoring techniques adopted by different agencies and researchers are labor-intensive, time consuming, point based measurements, and often difficult that can lead to unsafe practices (Eberhardt and Stead 2011; Jooste and Cawood 2006; Rezaeifar 2013; Su et al. 2006). Despite the accuracy of some of these techniques, the reliability of the point measurements data over the entire test site is not always valid, as the failure can be triggered at any location of the infrastructure (Indicator 2004; LIU et al. 2007; Mikkelsen and Wilson 1983). This uncertainty prompted engineers to constantly adopt new technologies to precisely evaluate ground movements. Remote sensing, which is an upcoming promising technology that is extensively being used in other disciplines, (Davenport 2001; Jensen 2005; Kerr and Ostrovsky 2003; Petite and Huff 2002; Siegal and Gillespie 1980) is considered in this study, for infrastructure monitoring purposes in this study.

Remote sensing is a multi-disciplinary science that includes optics, spectroscopy, photography, computer sciences, electronics and telecommunication disciplines (Aggarwal 2004; Choudhury 2008; Panigrahi and Goyal 2016). The main objective of remote sensing is to monitor atmosphere or the Earth's surface and capture objects' physical characteristics without direct contact (Aggarwal 2004; Campbell and Wynne 2011; Curran 1985). Depending on the monitoring target, different systems, including satellites, aircrafts, or stationary scanners, can be employed (Aggarwal 2004; Ehlers et al. 2003; Hausamann et al. 2005).

Satellite, aerial, and terrestrial remote sensing images provide valuable geological information about the monitoring site (Gupta 2017; Sabins 2007; Siegal and Gillespie 1980). Terrain mapping and analysis, identification of existing faults, areas of instability in mines, potential landslide assessment, and soil moisture and texture are some applications of these imageries (Dewitte et al. 2008; Jones 2006; Kayen et al. 2006; Mukoyama 2011;

Stewart et al. 2009). This research study focuses on evaluating ground movements using a terrestrial active remote sensing technique, Light Detection and Ranging (LiDAR).

LiDAR is an active remote sensing technology that uses ultraviolet, visible, or near-infrared light rays to scan objects (Lefsky et al. 1999; Lim et al. 2003). This technology was developed in the second-half of the 20th century to provide visual models of the earth's surface (Aggarwal 2004; Campbell and Wynne 2011). During the last decade, technological advancements in remote sensing and site instrumentation techniques have enabled engineers and researchers to collect highly accurate time-series data from civil infrastructures. One of the most important applications of collected time-series data is to develop prediction models for ground movements, which is considered a key step to geo-structural health monitoring and performance evaluation of infrastructure projects (Hashash and Whittle 1996; Kolay et al. 2008; O'reilly and New 1982; O'rourke 1993; Puppala et al. 2014, 2016). Current prediction models for ground movements of different soil types rely on analytical, empirical, and numerical methods (Adem and Vanapalli 2013; Alonso et al. 1999; Banerjee and Viladkar 2015; Briaud et al. 2003; Lowe et al. 2006; Nelson et al. 2007; Overton et al. 2006; Puppala et al. 2014; Vanapalli and Lu 2012; Vu and Fredlund 2004; Wray et al. 2005; Zhang 2005). However, these models do not account for climatic factors, which play a key role in governing the movements of high plastic clay soils. For example, expansive soils swell when they absorb water and shrink during dry periods, causing huge distress to civil infrastructure (Banerjee et al. 2018a; Chen 2012; Nelson and Miller 1997; Pedarla et al. 2015; Phanikumar and Singla 2016; Punthutaecha et al. 2006; Puppala et al. 2006). Hence, it is important to incorporate climatic factors, such as temperature and precipitation, to accurately predict the ground movements, which in turn will assist to evaluate the performance of bridge infrastructures. In this research study,

a new advanced mathematical modeling approach, using system identification theory, is conceived to overcome some of the current limitations with prediction models.

System identification, in essence, is the process of capturing physical characteristics of a system and matching it to a mathematical model structure (Fassois and Rivera 2007a; Keesman 2011). Applications of this technique transcend from engineering practices to other fields, including economics, biology, medicine, ecology, and geology (Fassois and Rivera 2007a; Natke 2014). Unlike the soil constitutive models that deal with limited parameters to describe the very complex behavior of soils, the system identification approach follows cause and effect concepts. For example, consider the relationship between the swell-shrink behaviors of expansive soils with respect to moisture content variations; the system identification approach is capable of considering the dynamic effect of ambient conditions, such as temperature and precipitation changes, directly.

Consequently, the objective of this research study is to develop a framework that integrates technology driven data measurements, time-series climatic data sets, and advanced mathematical modeling that assists in developing long term ground movement prediction models for bridge infrastructures. In this research study, the ground vertical movements are determined using LiDAR technology, and advanced mathematical modeling is performed using system identification approach. The following sections present the research objectives and thesis organization for the performance evaluation of geotechnical infrastructure using the integrated terrestrial LiDAR remote sensing technique and system identification approach.

1.1 Research Objectives

The main objective of this dissertation research is to develop a framework that could be used to evaluate the condition and performance of a bridge infrastructure and to develop advanced mathematical models that could predict ground movements using site

parameters, collected time-series measurements, and climatic factors. The framework is developed by integrating the in-situ testing techniques and system identification approach. The following are different research activities formulated to achieve the proposed objective:

a) Develop an optimized methodology for evaluating the ground movements using the 3D terrestrial LiDAR technique. In this task, different combinations of scanning plans, resolution, and quality settings are evaluated for the optimization of LiDAR scanning patterns to develop a 3D visualization model of a bridge infrastructure;
b) Validate the developed optimized methodology by performing a series of LiDAR surveys at a bridge infrastructure located in North Texas. This site was selected based on the history of the differential settlements that occurred at the bridge approach slab in reference to the bridge deck and extensive measurements including vertical displacements, vertical and lateral pressures obtained over a span of five years;
c) Develop advanced mathematical ground movement prediction models using system identification approach by considering measured ground movements using LiDAR, horizontal inclinometers, and site parameters, including temperature and precipitation;
d) Validate and evaluate the efficiency of the developed models with ground truth parameters and existing prediction models in the literature. Evaluating the cost-benefit analysis of the LiDAR technique in assessing the ground movements in comparison to conventional monitoring techniques;
e) Develop final recommendations and guidelines for implementing the 3D terrestrial LiDAR and system identification approach in evaluating the

performance and condition of bridge infrastructure that is beneficial to various transportation agencies, including city public works and department of transportation.

1.2 Thesis Organization

This thesis is comprised of seven chapters: Introduction (chapter 1); Literature Review (chapter 2); Development of Framework for Performance Assessment of Geo-Infrastructure; (chapter 3); Application of the Developed Framework for a Bridge Approach Embankment (chapter 4); Development of a Ground Movement Prediction Model for the Studied Approach Embankment by Using the System Identification Approach (chapter 5); Cost-Benefit Analysis (CBA) of Surveying Techniques (chapter 6); and Summary, Conclusions, and Future Research Recommendations (chapter 7).

Chapter 1 provides the introduction to performance assessment for bridge infrastructure projects, research objectives and thesis organization. The importance of using remote sensing techniques for performance monitoring of bridge infrastructure and developing soil movement prediction models are highlighted.

Chapter 2 provides a summary of the performance assessments of a bridge infrastructure based on laboratory testing, modeling approach, and field techniques. Application of Satellite and LiDAR remote sensing techniques for geotechnical and geological purposes and an introduction to the system identification theory are highlighted.

Chapters 3, 4, 5 and 6 provide the development of framework for 3D terrestrial laser scanning (3D-TLS) field operations, optimization of LiDAR scans, validation of the developed methodology, and development of a settlement prediction model for a bridge approach slab and CBA for monitoring a bridge approach slab site.

In chapter 3, the development of framework for performance evaluation of bridge infrastructure by using 3D terrestrial laser scanning (3D-TLS) remote sensing monitoring technique and system identification modeling approach is presented.

In chapter 4, the validation of the developed framework at the top of a bridge approach embankment is presented.

In chapter 5, the model identification process of vertical movements at the top of the bridge approach embankment is performed and a mathematical prediction model for ground vertical movements is proposed for the potential future natural hazards.

Chapter 6 presents Cost-Benefit Analysis (CBA) of surveying techniques for measuring ground vertical movements over the pavement surface of the bridge approach embankment.

Chapter 7 presents a summary of the research, conclusions and recommendations for future research.

Chapter 2: Literature Review

2.1 Introduction to Bridge Infrastructure

Bridges in civil infrastructure are referred to as structures that provide passage over a river and chasm, making vehicular movement possible between different geographical areas (Duan and Chen 1999; Lin and Yoda 2017; Troyano 2003). Bridge infrastructure is generally subjected to high cyclic loads and severe environmental conditions. Determining the required maintenance level to achieve optimized lifespan for bridge infrastructure has been challenging for transportation agencies and asset managers for several decades (Rashidi et al. 2013).

Based on the American Society of Civil Engineering (ASCE) infrastructure report card, there were 614,387 bridges in the United States (U.S.) in 2017. It was estimated that almost four in 10 of these bridges were operated for at least 50 years (ASCE 2017; Matthews 2017; Narayanan 2017). Approximately 9.1% of the entire bridges in the U.S. encountered structural issues. Recent studies demonstrated that an average of 188 million trips were made daily across these structurally deficient bridges in 2016 (ASCE 2017). While most of the bridge infrastructure projects in the U.S. were designed to operate for 50 years, the average age of the existing bridges is 43 years old. Hence, the number of the bridge infrastructure projects that soon require major rehabilitation increases substantially (ASCE 2017; Nguyen 2018; Rana 2017). Figure 2.1 classifies America's bridge infrastructures by age.

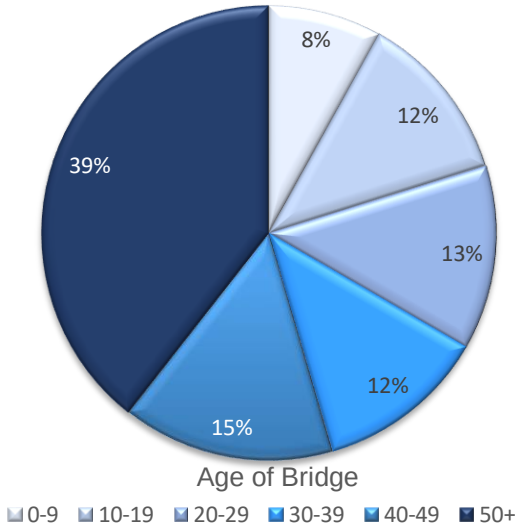

Figure 2.1 Classification of America's bridge infrastructure by age (ASCE 2017)

Annually, the U.S. government allocates billions of dollars to maintain aged bridge infrastructure systems. It was reported by the U.S federal government that $11.5 billion was spent to rehabilitate bridges in 2006. This amount increased dramatically to $17.5 billion in 2012. According to the most recent U.S. federal government estimates, $123 billion was reported to be required on the maintenance projects of the nation's aged bridge infrastructure systems in 2017 (ASCE 2017; Malheiro et al. 2018; writers 2018). Figure 2.2 depicts the top and bottom five U.S. states with structurally damaged bridges by number and percent.

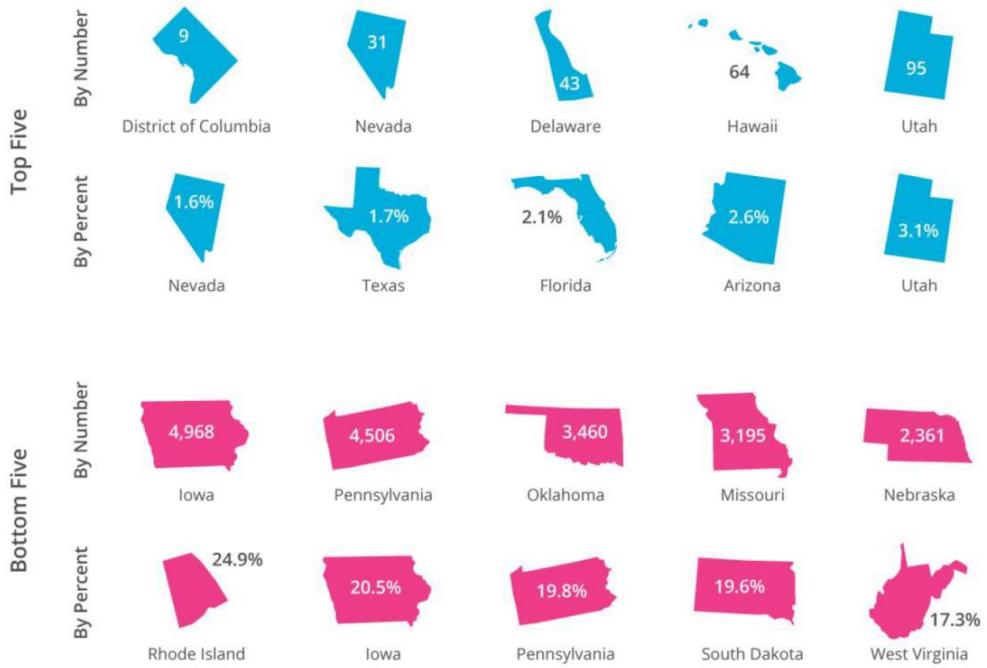

Figure 2.2 Top and bottom five U.S. states with deficient bridge infrastructure systems (ASCE 2017)

The aging bridge infrastructure together with limited financial resources for rehabilitation measures paved the way from radical departure of conventional monitoring techniques and evaluation methods for assessing the condition of the infrastructure (Onoufriou and Casciati 2015). This new challenging research area is conceptually motivated to lower the maintenance costs and extend the life of existing bridge infrastructure (Brownjohn 2007; Frangopol and Liu 2007; Karbhari 2009; Karbhari and Ansari 2009; Kirkham et al. 2004; Sanford et al. 2003).

In general, performance monitoring of bridge infrastructure consists of global health monitoring and local health monitoring methods (Chang et al. 2003; Farrar and Worden 2007; Murray et al. 2004). In the local health monitoring approach, the intensity of potential or occurred damage in infrastructure can be determined only in specific

monitoring areas. Installation of field instrumentations such as inclinometer casings, pressure cells, and joint extensometers are some examples of the local health monitoring approach. However, in the global condition assessment method, health and performance of the entire infrastructure can be assessed by detecting the potential or occurred damage locations (Chang et al. 2003). Based on functionality of different components, different monitoring systems are employed. The following sections present different components of a bridge infrastructure and their functions and performance evaluation methods.

2.2 Bridge Infrastructure Components

Bridge infrastructure is mainly composed of bridge decks, bearings, abutments, approach slabs, and embankments. Each of these components have a specific function in order to provide complete structural integrity to withstand the design loads safely and reliably throughout its designed service life. The following sections present each component and their functionality.

2.2.1 Bridge Deck

Bridge decks are structural parts of the bridge superstructure that provide direct passage for moving loads. Traffic loads are transferred from the moving vehicles to the major load-carrying members via bridge decks (Drains et al. 2011). The bridge deck can be constructed of different materials such as concrete, steel, open grating, or wood (Clouston et al. 2005; Horvath and Hendrickson 1998). Bridge decks are normally covered with asphalt or concrete pavement system. A typical view of a post-tensioned reinforced concrete bridge deck slab is shown in Figure 2.3.

Figure 2.3 Post-tensioned concrete bridge deck slab (Kromel and Maher 2010)

2.2.2 Bridge Bearings

Bridge bearings are designed to transfer traffic loads from bridge deck to the bridge abutments. In a bridge infrastructure, three different types of bridge bearings are used: elastomeric, plane sliding, and roller bearings. Elastomeric bearing provides rotational and translational movement degree of freedom for the bridge deck. This type of bearing supports the bridge deck against longitudinal, transverse and vertical loads. Plane sliding bearings are made from low friction polymer, polytetrafluoroethylene (PTFE), and sliding against a metal plate to resist against vertical movements and loads perpendicular to the keyway. Multiple rolling bearings are designed to accommodate large movements in the longitudinal direction and to resist against vertical loads (Eggert and Kauschke 2002; Mazroi et al. 1983). A schematic view of these three types of bridge bearings is demonstrated in Figure 2.4.

(a) (b) (c)

Figure 2.4 (a) Elastomeric bearing, (b) plane sliding bearing, and (c) Multiple rolling bearing (Childs 1998)

2.2.3 Abutments

Abutments are bridge elements connected to the deck at either end of a bridge to provide support for the bridge structure. Abutments are composed of bridge seats, wing walls, back walls, piles, and footings. There are several types of bridge abutments (Chen et al. 2000). A typical type of abutment system, which is commonly used by many state Department of Transportations (DOT's), is shown in Figure 2.5.

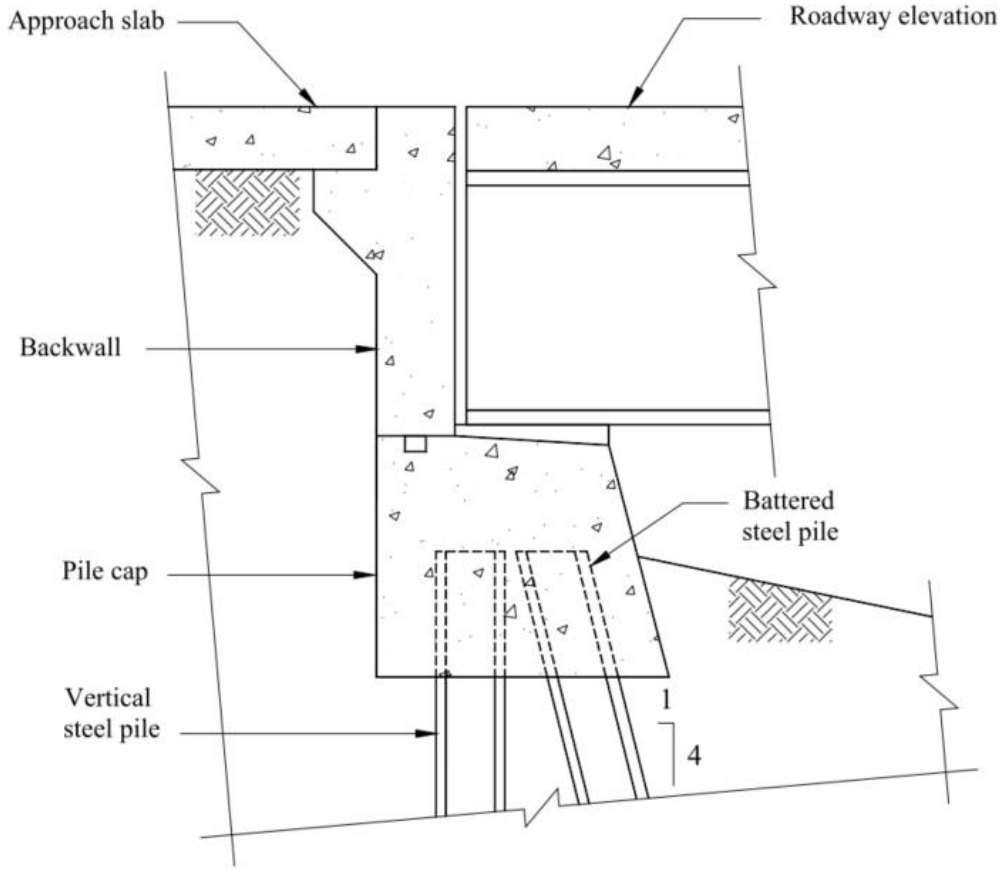

Figure 2.5 Typical bridge abutment system (Klaiber et al. 2004)

2.2.4 Bridge Approach Slab

Bridge approach slabs are built over the approach embankments to provide smooth transition of moving wheel loads from the approach embankment to the bridge

deck. Indeed, approach slabs are considered an intermediate bridge between the bridge approach embankment and bridge structure (Authority 2002; Hoppe 1999; Kramer and Sajer 1991). Figure 2.6 demonstrates a schematic view of a bridge approach slab.

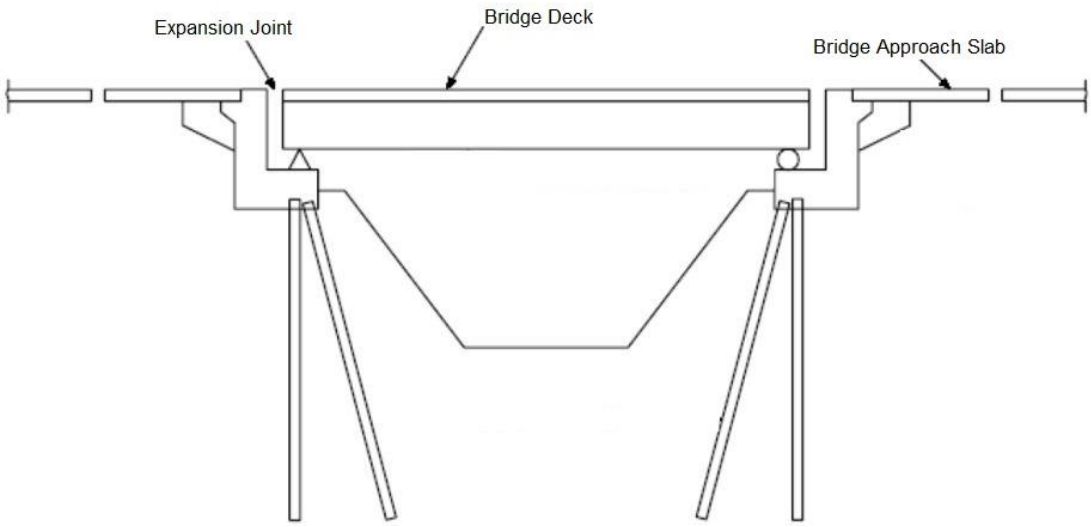

Figure 2.6 Schematic view of bridge approach slab (Paraschos et al. 2016)

However, a differential settlement at the end of a bridge near the interface between the abutment and the embankment is considered a serious problem for highway agencies, commonly called “bump phenomenon” (Briaud et al. 1997; Hassona et al. 2017; Nicks 2009). Several rehabilitation techniques including grout injection, soil nailing, hot mix overlays, micro-piling, and fill replacement methods include using light-weight materials such as the Expanded Polystyrene (EPS) geofoam, rubber tires are some solutions attempted to mitigate bump phenomenon.

2.3 Performance Evaluation Measures for Bridge Infrastructure

This section presents different performance evaluation measures of a bridge infrastructure that are currently being adopted by different state agencies practitioners, and researchers. The key steps used for performance evaluation are instrumentation, monitoring, and development of prediction models. Instrumentation and monitoring are

essential measures for successful performance evaluation of bridge infrastructure projects. Collected data from the monitoring phase should be employed to predict future probable concerns in order to reduce maintenance costs and increase the bridge infrastructure design life. The following sections present detailed background of different performance evaluation approaches focusing on field instrumentation and remote sensing techniques. A detailed review of the numerical, empirical, and analytical modeling approaches is elaborated subsequently.

2.3.1 Performance Evaluation Using Sensor Instrumentation

According to the Federal Highway Administration (FHWA) bridge inspector's reference manual, all public bridges in the U.S. should undergo visual inspection once every two years (Ryan et al. 2012). Although human sensing abilities such as visual inspection are noticeable, several health factors of a system cannot be measured. This includes ground and structural elements displacements, strain, pressure, temperature, cracks, fatigue, etc. are some examples (Huston 2010). Hence, more accurate sensing techniques are required to produce detailed information about the physical characteristics of a bridge system.

Installing sensors within the bridge components can provide a detailed response of each component with respect to different loading and environmental conditions (Catbas et al. 2008; Park et al. 2000). It should be noted that infrastructure, sensors, information, and their interactions with the decision-making process are all internally connected. The interrelationship between these steps is depicted in Figure 2.7 (Ettouney and Alampalli 2011). There are several types of sensors used to evaluate performance measures of different components of a bridge infrastructure. The following are some of the most commonly used sensing instrumentations for geotechnical engineering applications.

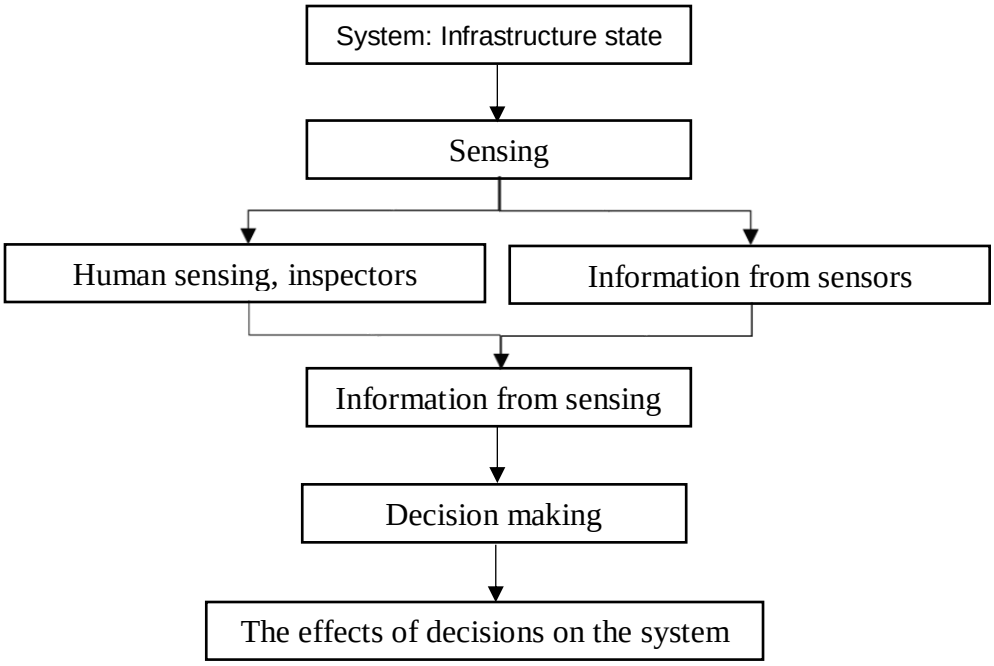

Figure 2.7 Interrelationship between infrastructure, sensors, and collected information

Settlement cells are used to monitor settlement and heave in embankments, embankment foundations- during dewatering or preloading- and for subsidence monitoring due to tunneling and mining. In a settlement cell, the transducer measures the pressure, induced by the column of liquid in the attached tube. As the installed transducer settles with the surrounding ground, the height of the liquid increases in the tube and the transducer shows a higher pressure. Settlement is calculated at different periodic intervals by converting the change in pressure to the liquid head. Figure 2.8 depicts a typical type of settlement cell and its components, including a reservoir and tubing (Indicator 2004).

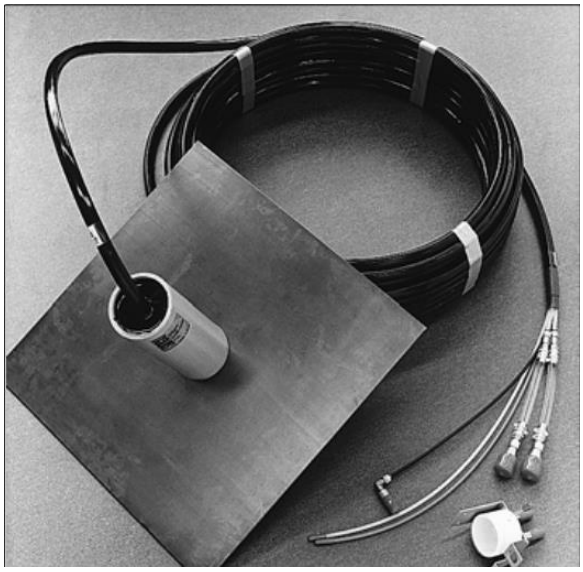

Figure 2.8 A typical type of settlement cell (Indicator 2004)

Magnet extensometers and Sondex settlement systems are the other two most commonly used settlement cells for measuring heave and settlement in embankments. The magnet extensometer system consists of a probe, a graduated cable, a reel with built-in light and buzzer, and a number of magnets positioned along the length of an access pipe. The magnets move with settlement or heave of the surrounding ground and the readings are obtained by drawing the probe through the access pipe to find the depth of the magnets (Indicator 2004). In Sondex settlement systems, a probe, a signal cable, a cable reel with a built-in voltmeter, and a number of stainless steel sensing rings are used. Collecting data from these systems can be performed by drawing a readout probe throughout the installed magnets alo0ong the entire length of a casing. A schematic view of the magnetic extensometer system is shown in Figure 2.9 (Spathonis 2011).

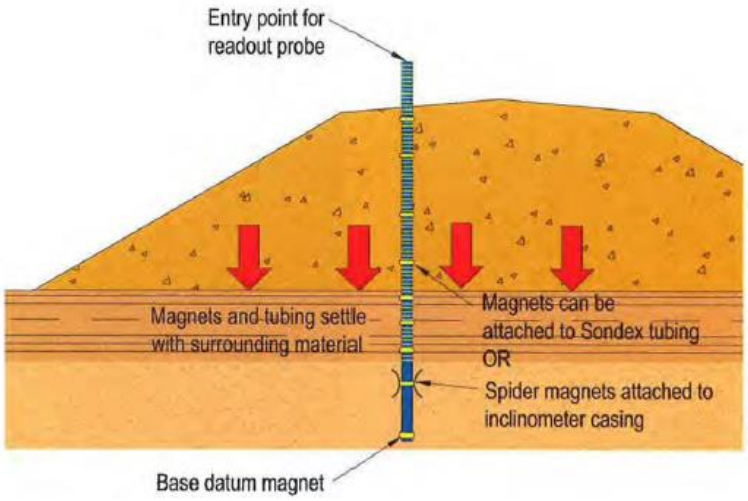

Figure 2.9 Schematic view of Magnetic extensometers and Sondex settlement systems (Spathonis 2011)

Horizontal Profile Gauges (HPG) or Inclinometers are widely used to monitor settlement in bridge approach embankments. There are two types of inclinometer systems including the portable-traversing system and in-place system (Geo-Enterprises 2006). In the traversing system, the wheeled portable inclinometer probe is steered into a graved casing to measure ground vertical, lateral, or differential movements. However, in an in-place probe system, the inclinometer is positioned into a span when continuous reading is required. It should be noted that both systems require inclinometer casings to operate. Figure 2.10 presents different types of inclinometers (Geo-Enterprises 2006; Hanna 1985).

(A) (B)

Figure 2.10 Inclinometer probe systems (A) portable traversing probe, (B) in-place probe system (Geo-Enterprises 2006)

Reliable measurement of lateral and vertical pressures in a soil media makes an important contribution to assess the performance of a bridge infrastructure. Interaction between a bridge structure and approach embankment, evaluation of traffic loading effects on underneath soil movements, and structural movements and fluctuations of vertical pressures due to shrink-swell behavior of a foundation expansive soil media are some examples.

Monitoring lateral and vertical pressures was a challenge to practitioners and researchers for several years since most sensing techniques include compliance in the measurement concept (Talesnick 2013). The Earth Pressure Cell (EPC) transducers have been used widely for several years to measure average vertical and lateral pressures in soil. Depending on the type of soil, expected earth pressure magnitudes, ambient conditions, and required accuracy, different types of EPC can be used to monitor earth pressures (Theroux et al. 2000; TN and SM n.d.). A sensitivity parameter is provided along with measured soil pressure as an accuracy indication for different types of pressure cells (Hvorslev 1976; Selig 1980; Wachman and Labuz 2011; Weiler and Kulhawy 1982). Figure

2.11 depicts a common type of EPC that is commonly used to measure vertical and lateral earth pressures (Talesnick 2013). In order to consider the effects of ambient conditions on bridge infrastructure performance, some earth pressure cell models are equipped with thermometers to measure the temperature variations and pressure changes simultaneously (Shafikhani et al. 2017).

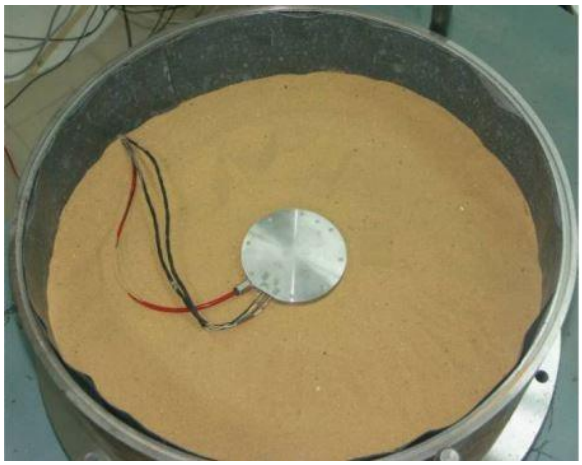

Figure 2.11 A typical type of earth pressure cell gage (Talesnick 2013)

2.3.2 Performance Evaluation Using Impact-Echo Method

Impact-Echo is a non-destructive test that is based on propagation of sound waves through a material. Small cracks, delamination, voids in concrete and pavement, and pavement thickness can be detected from acoustical responses (Grosse et al. 2005; Hoła and Schabowicz 2010). A typical design of the impact-echo instrument is a four wheeled device in which a built-in striker part produces the acoustic wave to pass through the target; whereas, the reflected response of strikes is measured from an installed microphone. Figure 2.12 depicts a typical handheld design of impact-echo equipment.

Figure 2.12 Handheld impact-echo non-destructive testing equipment (Hoensheid et al. 2012)

This method is most widely used to evaluate the integrity of different components in a bridge infrastructure with a high accuracy (Scott et al. 2003; Yehia et al. 2007). The major concern with this test is traffic interruption and the low rate of data collection and in the active traffic areas (Hoensheid et al. 2012).

2.3.3 Performance Evaluation Using Ground Penetrating Radar (GPR)

Ground Penetrating Radar (GPR) is a non-destructive geo-physical method that uses radar pulses to image the subsurface. GPR is a wide bandwidth-low frequency electromagnetic wave data acquisition technique with center frequency of less than 500 MHz. The wide bandwidth wave transmission mechanism enables the GPR to detect features with maximum embedment depth. GPR waves can transmit through different types of material such as soil, concrete, and water. According to the conductivity of various materials, the reflected energy will be measured by a processor to produce images. A

skilled operator is required to interpret the acquired data from the GPR. One of the primary applications of this technique is to detect subsurface material density beneath the bridge approach slab and close to the bridge structure, where the bump phenomenon usually occurs (Acharya et al. 2014; Berns et al. 2011; Islam 2010; Seo 2005). A typical GPR system structure is illustrated in Figure 2.13 (Anderson et al. 2016).

Figure 2.13 Ground Penetration Radar (GPR) system structure (Anderson et al. 2016)

2.3.4 Performance Evaluation Using Ultrasonic Surface Wave (USW)

The USW is a method of the Spectral Analysis of Surface Waves (SASW) used to estimate the properties of the near surface materials. In this method, by using high-frequency range waves, the penetration depth of dispersed waves is limited to the thickness of the target object. The USW is based on impacting the surface of a medium to estimate its layer thickness and elastic modulus by considering the velocity of propagation as a function of frequency and wave length. In this test, at least two transducers should be employed to record the response energy from impacts. The USW is commonly used as an in-situ bridge infrastructure inspection test to evaluate bridge deck condition. Figure 2.14 demonstrates a schematic view of the USW method (Baker et al. 1995; Chakraborty et al. 2018; Nazarian et al. 1997).

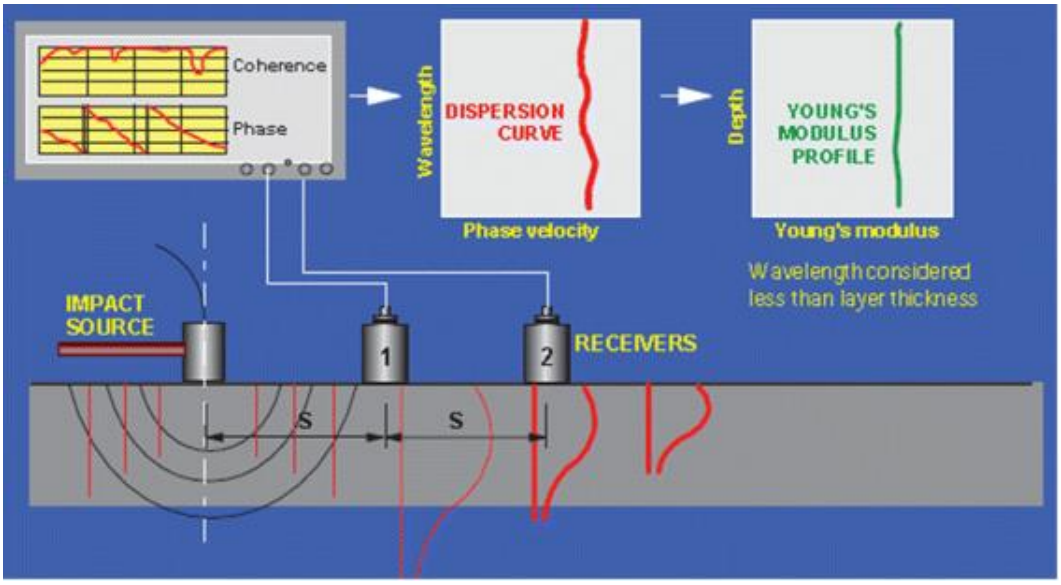

Figure 2.14 Schematic view of evaluation of a layer modulus by the USW method (La et al. 2015)

There are several advantages of using the USW test to inspect bridge infrastructure conditions. The penetration depth in the USW test for flaw detection is more than other Non-Destructive Techniques (NDT). Both subsurface and surface discontinuities can be detected with this highly portable device and the results can be deciphered instantaneously. Although these advantages, there are some limitations of performing the USW test. A highly skilled operator is required to perform signal and spectral analysis of the USW outputs. Since the USW is a local testing approach, it is not possible to monitor the condition of the entire bridge infrastructure. Also, traffic control strategies may be required while performing the USW test (Kogias 2007).

2.3.5 Performance Evaluation Using Total Station Surveys

Total station is the most commonly used traditional surveying tools used by various state agencies to obtain three-dimensional coordinates of target points. A total station is a combination of an electronic theodolite, an Electronic Distance Measuring (EDM) device,

and a data collector with a memory unit. A graphical explanation of the total station surveying mechanism is depicted in Figure 2.15.

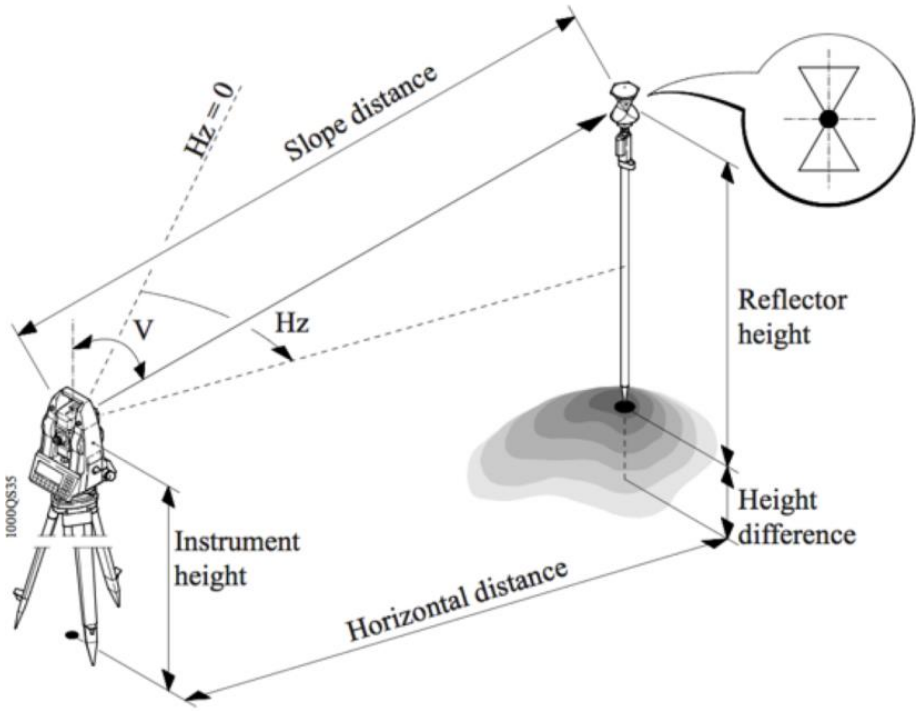

Figure 2.15 Elements of measurement in total station (Wang 2017)

Total station is technically set up on a tribrach attached to the top of a tripod. A prism pole is used to locate three-dimensional coordinates of a target point with respect to a specific reference point. Ground movements can be measured with a total station by comparing the coordinates of target points from consecutive surveys. According to Figure 2.16, ground vertical movement of a target point can be calculated from the following equation:

$$H_T = H_s + H_I \pm L \sin\left(\frac{\pi}{2} - V\right) - H_R \qquad 2.1$$

Where, H_T represents the elevation of the target prism, H_S is the elevation of the station point, H_I is the total station instrument height, L is the slope distance between the total station and the prism pole, and H_R is the reflector height (Wang 2017).

Total station is a quick setup, multitasking, accurate surveying tool in which a graphical view of the land and plots can be exhibited in advanced equipment versions. Different errors associated with total station surveys are operator mistakes, measurement error, and stationing error. The errors in each step can accumulate and decrease the reliability of the measurements; however, due to the relative ease of employing this technique at the test site and use of skilled labor can provide high accurate point-based measurements. Also, depending on the location and traffic conditions, it is not always feasible to accomplish total station surveys. For instance, total station survey cannot be performed without stopping the traffic in an active traffic area (Cuypers et al. 2009; Fröhlich and Mettenleiter 2004).

2.3.6 Remote Sensing Techniques

Remote sensing refers to the science of obtaining reliable information from the physical objects and environment through the process of recording, measuring, interpreting, and digital representations of energy patterns derived from noncontact sensors (Campbell and Wynne 2011; Curran 1985). The history of remote sensing dates back to the inventory of photography in 1826, when a number of scientists conducted experiments with photosensitive chemicals (Campbell and Wynne 2011). The theory of electromagnetic energy was developed in 1873 and the application of photography as an aerial reconnaissance technique was initiated for military purposes during World War I in the 1910's. Operation of photography was expanded and photogrammetry was developed in the 1920's and during 1930's radar technology was developed in Germany, UK, and USA (Jensen 2005). For the first time, the term "remote sensing" was used between the

1930's and 1960's by using the infrared and microwave energy spectrums for military projects (Campbell and Wynne 2011). The improvement of analog imagery to digital format during the 1970's and rapid advances in digital image processing made it possible to analyze imagery by using computers. Finally, remote monitoring and analysis was began to be widely utilized for engineering applications in the 1990's. A brief history of remote sensing is presented in Table 2.1 (Jensen 2005).

Table 2.1 History of remote sensing technology (Jensen 2005)

Date	Remote Sensing History
1826	The invention of photography
1850's	Photography from balloons
1873	Theory of electromagnetic energy by J. C. Maxwell
1909	Photography from airplanes
1910's	World War I: aerial reconnaissance
1920's	Development and applications of aerial photography and establishment of photogrammetry
1930's	Development of radar in Germany, USA, and UK
1940's	World War II: application of infrared and microwave regions
1950's	Military research and development
1960's	The satellite era: Space race between USA and USSR
1960's	First use of term "remote sensing"
1970's	Rapid advances in digital image processing
1990's	Remote sensing was started to use widely for engineering purposes

Remote sensing equipment records information of an object or phenomenon without direct contact by utilizing different types of sensors that are located on orbital or

sub-orbital platform (Aggarwal 2004; Gao 2008). Figure 2.16 depicts different remote sensing techniques for orbital and sub-orbital platforms.

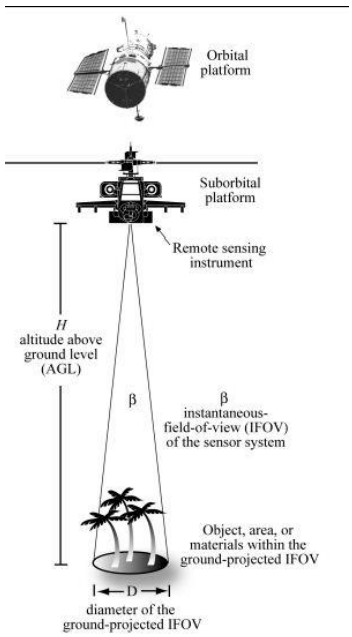

Figure 2.16 Orbital and sub-orbital platform (Gao 2008)

Two types of sensors are used for the data collection and interpretation: 1. Optical sensors, which consist of visible reflectance, near infrared reflectance, and thermal infrared radiation sensors; 2. Microwave sensors are divided into two categories of passive (scattering) and active (backscattering) types of sensors. Figure 2.17 depicts a schematic of both active and passive remote sensing techniques (Tsang et al. 1985; Ulaby et al. 1986; Woodhouse 2017).

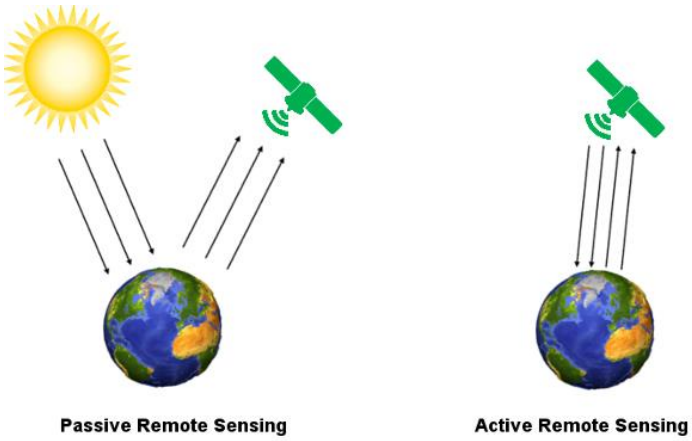

Figure 2.17 Passive and active remote sensing mechanisms (Ulaby et al. 1986)

In active remote sensing, the energy is produced from the remote sensing platform. Whereas, in the passive remote sensing measurements depend upon a natural or external energy resource, it is referred as passive remote sensing. The sections below present a brief overview of the passive and active remote sensing techniques.

2.3.6.1 Passive Remote Sensing

Passive remote sensing refers to a technique in which a passive sensor measures the amount of reflected visible or invisible solar energy from a target object to capture physical characteristics of the object such as distance, color, and size. The most common types of passive sensors include satellite-based sensors operated from an orbital platform (Lyzenga 1978; Päivinen and Anttila 2000). Advanced Space-borne Thermal Emission and Reflection (ASTER), Land satellite (Landsat), Advanced Very High Resolution Radiometer (AVHRR), Moderate Resolution Imaging Spectro-radiometer (MODIS), and Satellite SPOT (French: Pour l'Observation de la Terre) are some examples for passive remote sensing satellites (Aggarwal 2004; Al-Rawabdeh et al. 2016; Nageh and Saturday 2014; Sabins 2007).

There are two main limitations to the passive remote sensing technique. First, reflected visible and near-infrared radiation from a target object can be assessed only during daylight hours. Second, even during the daylight, clouds interfere with both incoming and outgoing radiation at near-infrared wavelengths (Scaioni et al. 2014).

2.3.6.2 *Active Remote Sensing*

The active remote sensing process is performed by sensors that rely on their own energy source for illumination. In active remote sensing, the sensor emits radiation toward a target object (Campbell and Wynne 2011; Nageh and Saturday 2014). Physical characteristics of the object can be measured by assessing the amount of reflected radiation from the target with the sensor. The most popular techniques for active remote sensing include: Radio detection and ranging (RADAR), Synthetic Aperture Radar (SAR), Light Detection and Ranging (LIDAR), and space and air-borne RADARs and LiDARs.

Passive and active remote sensing can be performed from orbital and sub-orbital platforms. Satellite Based Imagery (SBI) is the most common approach for sensing from orbital platforms, whereas LiDAR is considered as one of the most recent technologies for sensing from sub-orbital platforms. SBI and LiDAR remote sensing techniques are discussed in more detail in the following sections.

2.3.6.2.1 *Satellite Based Imagery (SBI)*

Even though photography has proven to be an important visualization technique to produce analog maps, the associated need to telemeter imagery in digital format has given rise to the development of SBI as an important remote sensing technique. SBI remote sensing is a combination of data collection techniques from the Earth's surface or the atmosphere along with mathematical interpretation of collected data from space using satellites (Aggarwal 2004; Lazecky et al. 2015; Nageh and Saturday 2014). Installed sensors on the satellite receive radiated electromagnetic energy with different spectrums

from objects on the Earth. The radiance (amount of radiation from an object) measured by sensors represents properties of targets by producing an image of sensed region.

Since the human eyes can only recognize the reflected solar light by objects within the range of 400 to 700 nm, several types of equipment are utilized to make electromagnetic reflection beyond this range (near infrared, middle infrared, thermal infrared, and microwaves) visible. Scientifically, the electromagnetic wavelengths are very broad, and not all of them are applicable for remote sensing. Also, only limited wavelengths interact with the Earth's surfaces, as the shorter wavelengths are absorbed significantly from the atmosphere. Figure 2.18 depicts the electromagnetic wave production from the solar spectrum wavelengths radiations of the sunlight (Gao 2008).

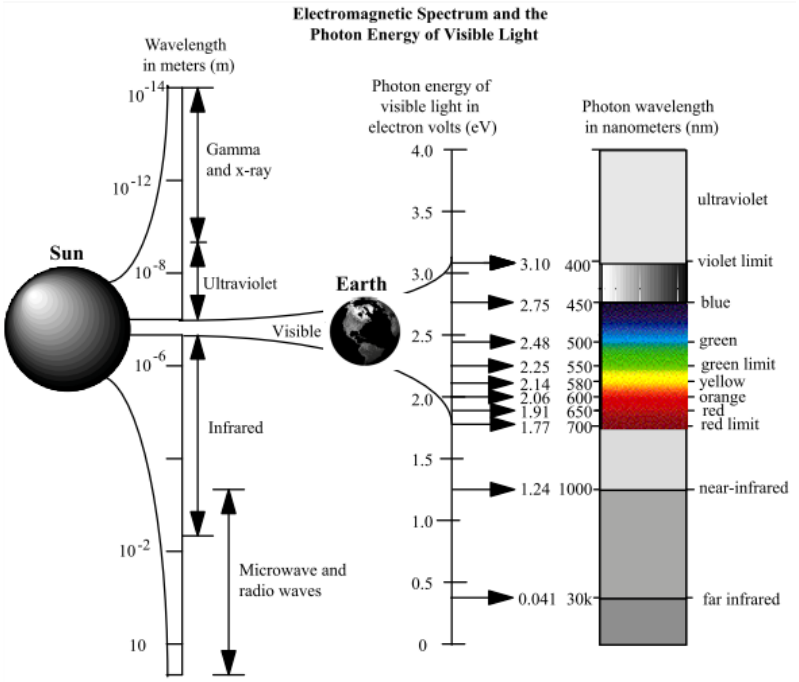

Figure 2.18 Electromagnetic wavelengths (Gao 2008).

The scanning mechanism in SBI is based on collecting data within the instantaneous field of view (IFOV) of objects. The process of scanning is fulfilled by

sweeping a small field of view in a west to east direction at the same time the satellite is moving in a north to south direction (Lazecky et al. 2015; Thyagarajan and Minden 2002). Thus, with regard to the type of sensors mounted on satellite, different types of data can be collected from diverse objects.

There are several satellite systems operating to collect imagery for specific characteristics for particular applications. The most common satellite systems and their applications are described below (Al-Rawabdeh et al. 2016; Thyagarajan and Minden 2002):

a) The ASTER passive sensor is used in glaciology, urban change, evapotranspiration and surface fluxes, hydrology, volcanology, and geology.

b) Landsat sensors are used widely for crop acreage inventories, timber class identification and mapping, regional land use classification, geological mapping and interpretation, generation of photo maps, mining monitoring, and erosion evaluation. Landsat sensors collect Thematic Mapper (TM) data with different spatial resolutions and spectral ranges from target objects. Several other analyses can be performed on TM data, such as detection of beach erosion, areal snow assessments, pollution monitoring, mineral and petroleum exploration, and sea ice movement monitoring.

c) The AVHRR sensor provides full resolution data mostly for meteorological applications, such as drought early warming, regional and global vegetation monitoring, snow and ice mapping, dynamic oceanography, detection of forest fires, soil moisture analysis, geology, continental scale mapping, toxic algal bloom detection, and sand storm monitoring.

d) The mission of the MODIS sensor is to provide a wide series of visualization data from the entire surface of the Earth, oceans, and atmosphere. It has been designed to monitor the entire surface of the Earth every two days with the primary application of making decisions for environmental purposes.

e) The SPOT sensor was designed to detect visible near-infrared radiance data by focusing on geological exploration and the evaluation of major geologic faults and structures.

f) The Constellation of Small Satellites for Mediterranean Basin Observation (COSMO-SkyMed) system is composed of four radar satellites for Earth observation launched by the Italian Space Agency.

COSMO-SkyMed is at the forefront of technology and equipped with high-resolution radar sensors to observe the Earth day and night, regardless of weather conditions. The constellation has been fully operational since 2008 (Covello et al. 2010; Pulvirenti et al. 2011). The main purpose of the COSMO-SkyMed constellation is to monitor the Earth and provide global scale data for emergency situation prevention and management of environmental risks, land management, exploration of natural resources, as well as military, scientific, and commercial purposes (Bovenga et al. 2012; Covello et al. 2009). Additionally, there are other SBI sensors, such as the European Remote Sensing Satellite (ERS) and the Japanese Earth Resource Satellite (JERS), which are used widely for providing topographic and coastal maps (Kellndorfer et al. 1996; Simard et al. 2002).

Collected data from SBI systems can be used for geotechnical engineering purposes, such as land slide explorations, monitoring of post-earthquake ground movements, and assessment of liquefaction hazards in global scale investigations (Bouali et al. 2017; Johnson 1988; Lazecky et al. 2015; Sabins 2007; Yang and Yu 2016). Figure

2.19 demonstrates data interpretation using mathematical models to recognize landslide scrap. In this figure, higher eigenvalues represent landslide scrap aspects, because these areas are less clustered than other smooth terrain surface (Al-Rawabdeh et al. 2016).

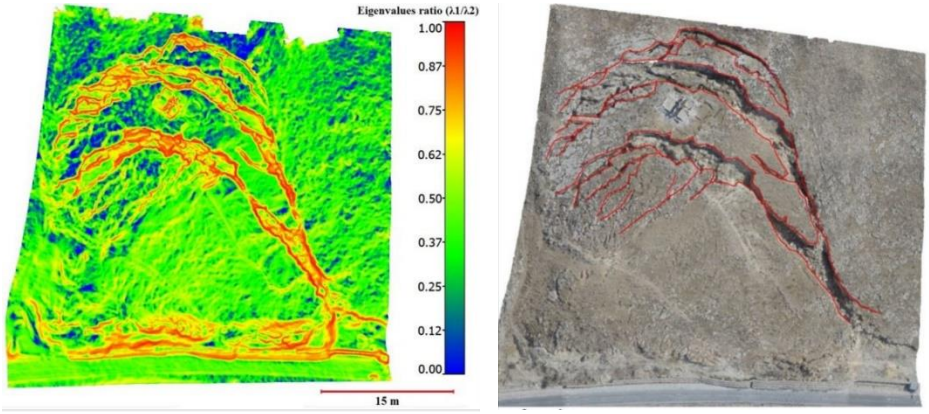

(a) (b)

Figure 2.19 Recognition of landslide scrap features (a) Mathematical approach (b) Manual approach (Al-Rawabdeh et al. 2016)

Figure 2.20 also depicts the collected data interpretation from COSMO-Sky Med of landslide occurrences before and after the landslide over Montescaglioso (Italy – square zone) by the University of Florence (Manconi et al. 2014). The analysis has been performed using an advanced InSAR algorithm for surface deformation monitoring to identify precursor movements.

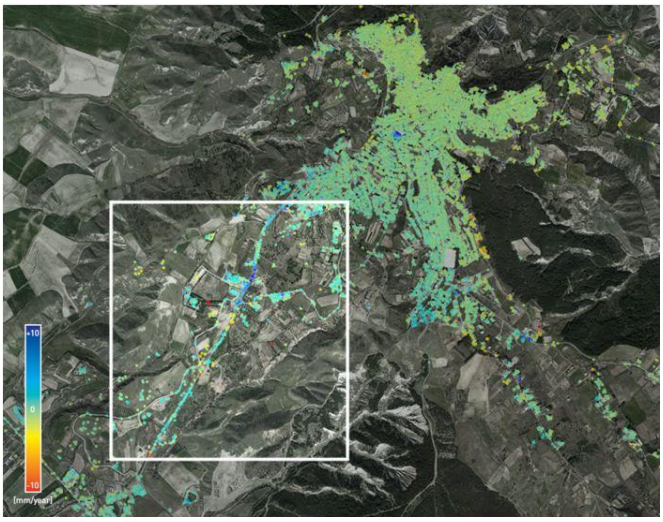

Figure 2.20 Ground movement analysis before landslide occurrence (Montescaglioso-Italy) (Manconi et al. 2014)

It is not always necessary to perform specific mathematical analysis to monitor movements corresponding to landslides, slope instability, and ground movements by using SBI technique. In order to have a reasonable visual analysis and interpretation, it is highly recommended to use small spatial resolution images. Figure 2.21 depicts the first NASA satellite images of the affected area by the M-6.9 earthquake in northern India (Gahalaut 2011; Rai et al. 2012).

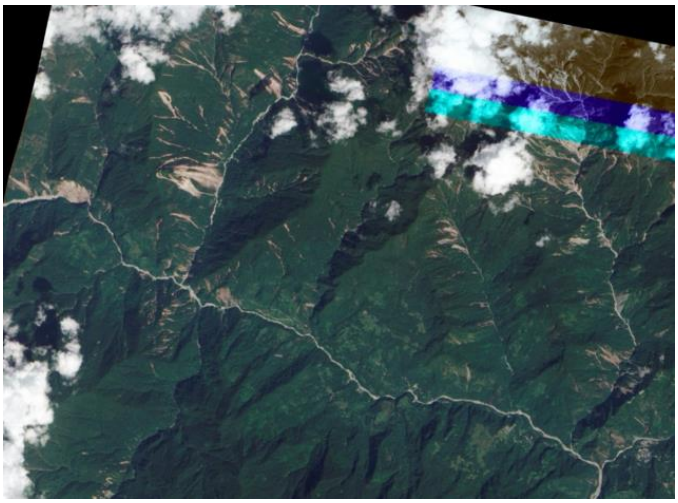

Figure 2.21 Landslide occurrence monitoring after earthquake in Northern India (Rai et al. 2012)

Analysis and interpretation of a 10 m spatial resolution image shows a rather high incidence of slides in the valleys at the north end part of the image. It is evident in the figure that many slides happened towards the east and the south. However, the epicenter was about 45 km to the northwest of this location. Thus, most slopes failed away from the epicenter rather than towards it. Also, most of the slides appear to be shallow rockslides that have connected to gully systems; many of them initiated high on the hillside. There are also some large slides nearer to the main channels (Rai et al. 2012).

Beyond physical aspects of objects, SBI made it possible to estimate some quality controls of objects. The European Space Agency's Soil Moisture and Ocean Salinity (SMOS) mission is to monitor the surficial water amount of soil and to estimate the concentration of salt in seawater's top layer for agricultural purposes (Jackson 1993; Njoku and Entekhabi 1996; Silvestrin et al. 2001; Zwissler et al. 2017). Figure 2.22 demonstrates surficial soil moisture content estimation using the SBI technique for agricultural purposes.

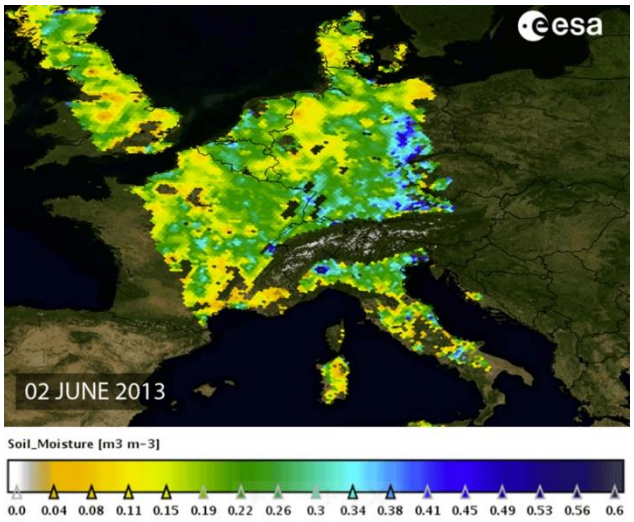

Figure 2.22 The amount of water held in ground surficial layers (Silvestrin et al. 2001)

Estimation of soil moisture content is feasible using data from thermal bands of optical sensors. NASA's Soil Moisture Active Passive (SMAP-launched at 2014) satellite mission is to estimate moisture content and freeze/thaw state of soil to understand changes on Earth. In another studied case, Landsat shows a devastating landslide happened after the M-7.8 Gorkha earthquake in Nepal, which led to form a new lake in the Manaslu trekking area of Nepal. Figure 2.23 demonstrates a landslide dam lake formation imagery of the region (Galetzka et al. 2015).

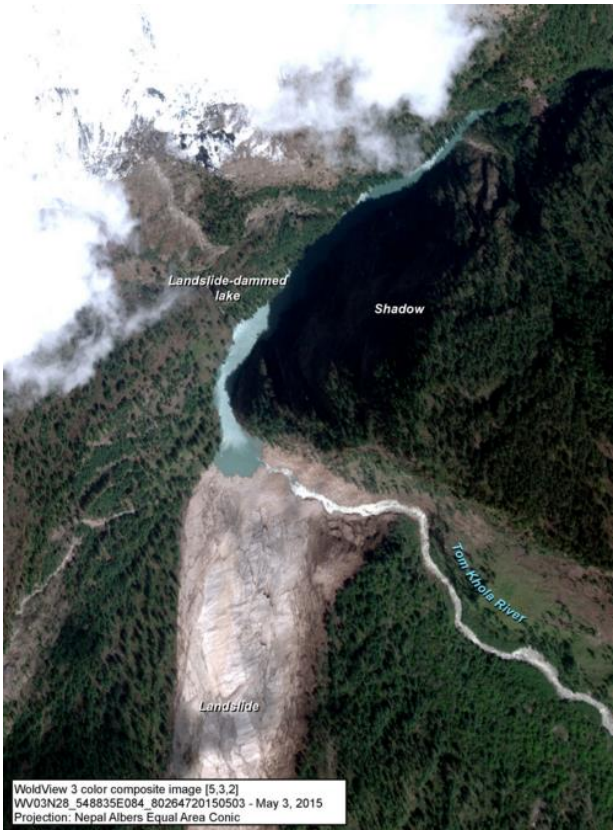

Figure 2.23 Dam-lake formation imagery from Landsat 8 (Galetzka et al. 2015)

The lake is formed at the upstream of the village Ghapsya (5 kilometers) after a landslide dammed the Tom Khola River. Thus, these satellite-based imageries can be used to perform analysis and interpretation, such as evaluation of risk for probable future earthquakes or aftershocks, which has not been done yet.

2.3.6.2.2 *Light Detection and Ranging (LiDAR)*

LiDAR is an active remote sensing technology in which laser beam pulses are discharged from a rotating mirror to provide geographic point cloud data from a target object (Carter et al. 2012). A point cloud is a set of millions of points in space from the external surface of a target object. Data output from LiDAR often look like 360 degree

digital images, which are made by recording clouds of points using one of the below techniques (Hu et al. 2010; Lato 2010; Lim et al. 2003):

a. An infrared laser resource discharges a stream of focused pulses at a rotating mirror and scatters them towards the surface of and object on the ground. When the receiver unit recaptures the reflected energy, the elapsed time between the emitted signal and received echo is calculated by the laser scanner. Terrestrial Laser Scanner (TLS) systems are used in this approach as a ground-based active imaging method to produce dense point clouds from an object.
b. A constant record of pitch, heading, and roll of an aircraft can be performed automatically during a flight by using an Internal Reference System (IRS)
c. A continuous documentation of the spatial position of an aircraft can be recorded by using a kinematic Airborne Global Positioning (ABGPS) throughout the flight.
d. An analog camera, digital camera or color video camera can be operated as an imagery collection system to record the terrain along the track of the LIDAR scan. The quality control of final processed data and planimetric feature collection can be performed by the recorded Imagery (Morgan and Falkner 2001). Figure 2.24 illustrates the aforementioned data collection techniques by using LiDAR schematically (Campbell and Wynne 2011).

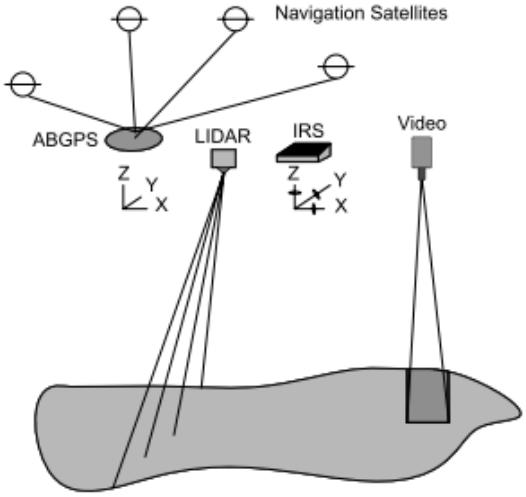

Figure 2.24 Schematic illustration of different LIDAR data collection techniques (Campbell and Wynne 2011)

LiDAR function in remote sensing started with preparation of mapping the heights of trees, producing contour maps and detailed maps of floodplains. More recently, new innovative engineering tasks are added to the LiDAR applications. Most new engineering applications of the LiDAR laser scanner are related to the detection of small deformations of structures, slopes, landslide occurrence risk analysis and interpretation, and settlement analysis of improved soil deposits (Fekete et al. 2009; Grejner-Brzezinska et al. 2015; Lato 2010; Stewart et al. 2009). Technically, there are four steps to collect, analyze, and interpret data using the LIDAR remote sensing technique, including Collecting data (scanning) by performing one of the four mentioned techniques in different time periods; Creation of point clouds and place all scans together; Reduce the data set to target zone and select some points (if required) for small displacement analysis; Compare the collected data from different time periods to the first set of scans and relocating specified set of points from the first set of scans in different time periods by using appropriate computational

applications. The following section presents the application of LiDAR technology in engineering.

2.3.6.2.3 *LiDAR Applications*

LiDAR technology has been increasingly applied to geomatics, archaeology, geography, geology, geomorphology, seismology, forestry, atmospheric physics, and structural and geotechnical engineering areas (Jones 2006; Kayen et al. 2006; Lefsky et al. 1999; Lim et al. 2003; Mukoyama 2011). LiDAR data can be used for several geo-engineering applications, such as identifying geological formations, performing small deformation analysis of human made infrastructures, and risk assessment of natural hazards due to landslides, rockfall, and ground movements with accuracy of mm level (Combs and Kemeny 2011; Hu et al. 2010; Jaboyedoff et al. 2012). Unlike the point monitoring approaches, the entire area of interest can be covered in LiDAR surveys. Figure 2.25 demonstrates a rockfall event on June 2010 at a Colorado site, situated along Highway 285 before (September 2009) and after (June 2010) the event (Silvestrin et al. 2001).

Figure 2.25 Rockfall monitoring by using LiDAR technique (Silvestrin et al. 2001)

High resolution point cloud data collected from laser scanner surveys can be analyzed for geological structure identifications by returning very sensitive intensity values in addition to point cloud location information. Figure 2.26 depicts a continuous geological formation of a site identified in raw laser point cloud data (Fekete et al. 2009).

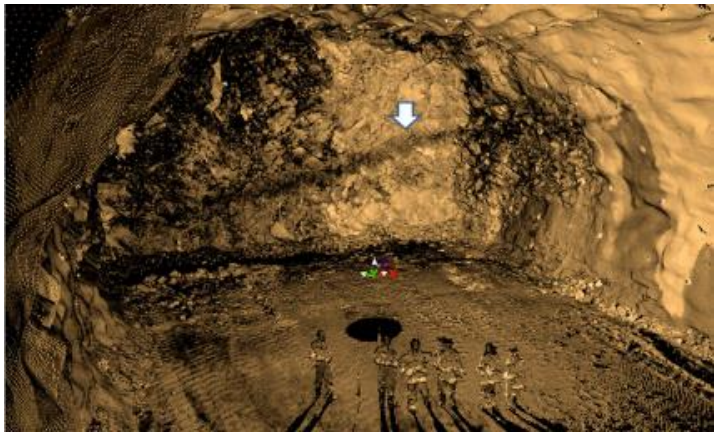

Figure 2.26 Continuous geological structure formation (Fekete et al. 2009)

Another application of produced point cloud data by terrestrial laser scanner is to identify specifications of structural elements. For example, thickness and other characteristics of a shotcrete layer can be evaluated based on different returned intensity values collected from before and after shotcrete placement scans. Figure 2.27 (a and b) illustrates the thickness of shotcrete layer, contrast of intensity for rock, and wet and dry shotcrete in a tunnel (Fekete et al. 2009).

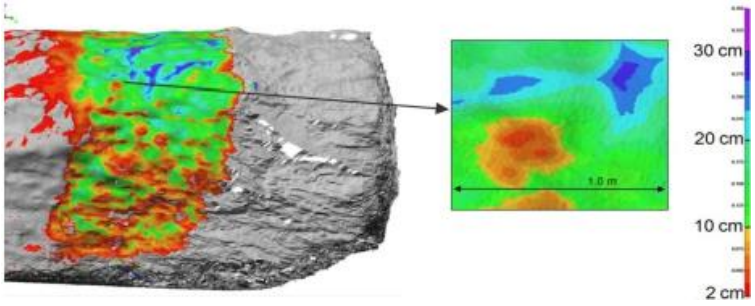

(a)

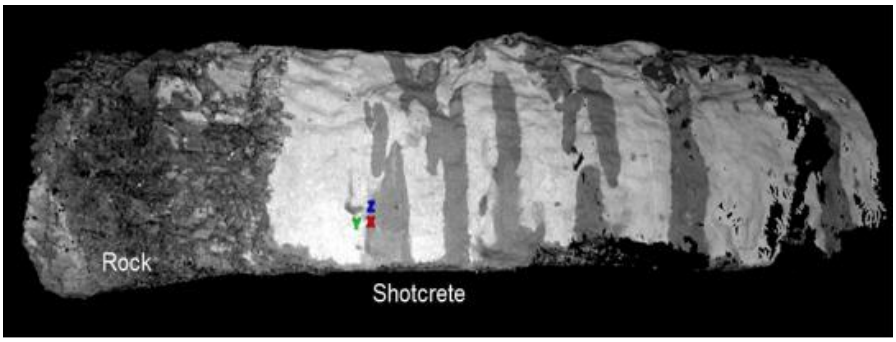

(b)

Figure 2.27 (a) calculation of shotcrete thickness and (b) contrast of intensity for rock, and wet and dry shotcrete in a tunnel (Fekete et al. 2009)

Evaluation of small deformations is considered one of the most recent and innovative applications of LiDAR remote sensing technology. Measuring small deformations plays an important role in long-term performance of infrastructures, such as dams and levees, tunnels, embankments, and roadways. For example, differential settlement of more than 38 mm (1.5 in.) on the top of a bridge approach embankment is considered as a bump phenomenon and rehabilitation is required (Ruttanaporamakul 2015). Small deformations of an infrastructure can be assessed by performing different sets of scans with reasonable resolution and quality settings.

Figure 2.28 (a and b) represents a typical cross section, front view and small deformation analysis of the Studena concrete dam situated in the west part of Bulgaria. The dam was built over a seven year span (1950-1953) (Antova 2007).

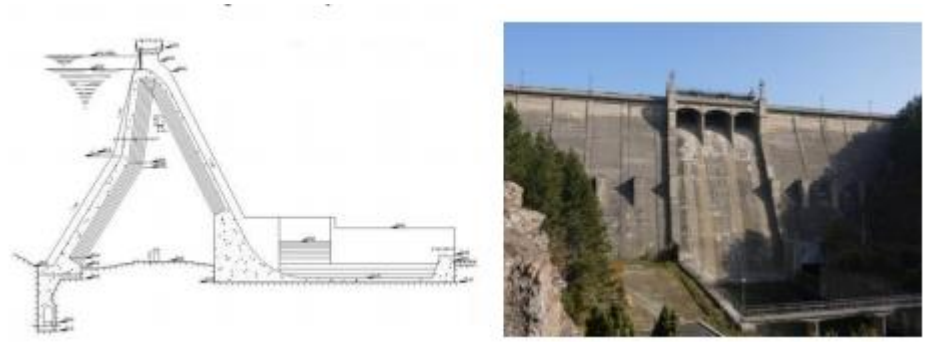

(a)

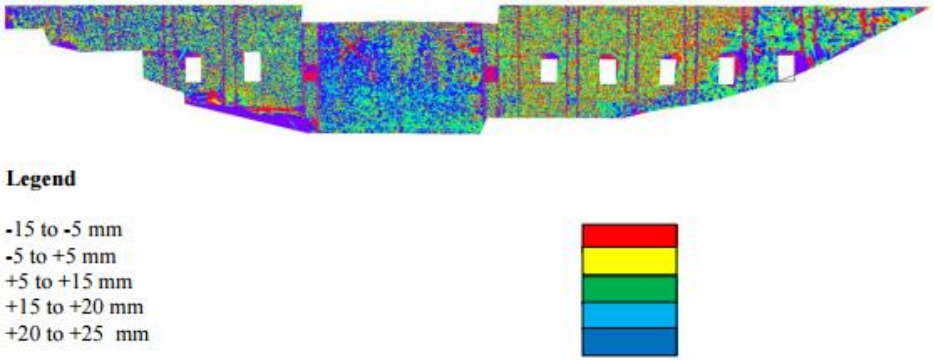

(b)

Figure 2.28 (a) cross section and front view of Studena concrete dam and (b) deformation monitoring over one year (December 2011- June 2012) (Antova 2007)

It is evident from the figure that laser scanner data analysis for surficial deformation demonstrates a range of -15mm to 25 mm movements during one year monitoring period from December 2011 to June 2012 (Antova 2007).

2.4 Modeling Approaches for Performance Evaluation of Bridge Infrastructures

Collected data from various monitoring approaches should be employed to evaluate the performance of infrastructures by implementing different modeling techniques. The main objective of this section is to provide a brief background on the modeling techniques used to evaluate the condition of bridge infrastructure components

including embankment slopes, pavement surface, columns, and drilled shafts. In recent decades computational modeling has been widely used to assess the performance of bridge infrastructures by analyzing several parameters, such as stresses, deformations, structural forces, ground movements, slope stability, bearing capacity, liquefaction, and ground water flow (Baecher and Christian 2005; Banerjee 2017; Banerjee et al. 2018b; Brinkgreve 2013; Chakraborty et al. 2017, 2018; Chakraborty and Nair 2018; Eberhardt 2003; Fenton and Griffiths 2008; George et al. n.d.; Shafikhani et al. 2017; Wanyan et al. 2014; Whitman 2000; Zhang et al. 2013). The following sections present numerical, empirical, and analytical modeling approaches along with their advantages and limitations.

2.4.1 Numerical Modeling

Numerical modeling in geotechnical engineering applications includes solving complex geotechnical problems analogous to several geo-mechanical parameters and their coupling effects. Coupling effects emerge from complex dual-phase interaction between more than two variables in a problem (Hicks et al. 2014). Compared to other engineering materials, soils are heterogeneous in nature and often exhibit complex non-linear, anisotropic behavior. Indeed, soils exhibit stress dependent stiffness and behave differently when subjected to loading, unloading, and reloading conditions (Dong 2017; Lipiński and Wdowska 2011; Papadopoulos et al. 2016; Ti et al. 2009b). In many geotechnical engineering problems, the analysis is performed with limited available information about the test site. In such cases, numerical modeling can be used to forecast the performance of the infrastructure with a fast and reliable approach.

Numerical modeling offers a fast and systematic solution to a problem by providing more realistic models of geomaterials. These benefits of numerical modeling can result in cost reduction and optimization in geo-engineering investigations (Hicks et al. 2014; Koliji 2013). In geotechnical engineering, numerical modeling analysis can be divided into three

fundamental components: initial boundary conditions, type of analysis, and soil constitutive model.

In mathematics, a boundary value problem includes a set of differential equations together with a set of additional constraints, called the boundary conditions (Brenan et al. 1996; Keller 1992; Marano 1994). In numerical modeling, these differential equations can be generated either manually or from computational tools. Accordingly, appropriate constraints and initial boundary condition values should be defined to the geometric boundaries of the problem (Carter 2001). Boundary conditions take on a pivotal role to define a successful, unsuccessful, fast, or slow computation. Any geo-engineering problem should be set into an initial boundary value problem. This can help to give a better insight and global picture of the problem. Appropriate initial boundary value problems can be considered based on the project concepts. For example, for a static analysis of a double arch concrete dam, double arch effects, seasonal water and temperature variation, and water and sediment load effects should be considered for the project concepts. Accordingly, the problem can be converted into a 3D numerical analysis by considering varying temperature and imposed loads as the initial boundary value concept.

Two types of uncoupled and coupled analysis can be performed for any initial boundary value problem. There is only one primary variable involved in uncoupled analysis such as displacement or pore water pressure. Whereas, more than two variables and their coupling effects are considered in coupled analysis. Coupling effects of displacement and pore water pressure in a hydro-mechanical problem is an example of a coupled analysis.

Geomaterials exhibit non-linear behavior due to their complex, heterogeneous and time dependent stress-strain nature; therefore, a realistic prediction/simulation of their behavior can be accomplished by using pertinent constitutive models to address such non-

linearity. Depending on the several applications and requirements of the problem, different constitutive models can be selected to produce more realistic models.

According to the selected constitutive model for soil, material parameters should be determined from correlation and routine laboratory tests (Nakase et al. 1988; Ti et al. 2009a; Xiao et al. 2016). Table 2.2 lists basic laboratory tests and respective standards to determine soil parameters (Ruttanaporamakul 2015).

Table 2.2 Basic laboratory tests for the performance assessment of an embankment

Materials	Experiment	Standard
Embankment fill soil and foundation subgrade	Determination of natural moisture content	ASTM D-2216-98
	Determination of in-place unit weight	ASTM D-2937-00
	Specific gravity of soil solids test	ASTM D-854
	Soil classification test	ASTM D-422
	Atterberg Limit tests	ASTM D-4318
	Falling head permeability test	ASTM D-5084
	Standard Proctor compaction	ASTM D-698
	One-dimensional consolidation test	ASTM D-2435-96
	Direct shear test	ASTM D-3080-98
	UU and CU triaxial compression test	ASTM D-2850-95

Once the geo-engineering is converted into an initial boundary problem and a pertinent constitutive model is selected to represent a more realistic behavior of the geomaterial, an appropriate numerical method should be selected to produce the model. Numerical methods can be divided into two main groups of continuum and discontinuum methods. Different numerical methods in general are presented in the Table 2.3. However, the detailed description of these methods is beyond the scopes of this research study.

Table 2.3 Numerical modeling methods (Koliji 2013)

Continuum Methods	Discontinuum Methods
Finite Element Method (FEM)	Discrete Element Methods (DEM)
Finite Difference Method (FDM)	
Boundary Element Method (BEM)	Discontinuous Deformation Analysis (DDA)

Technically, there are eight (8) steps that should be followed to produce a numerical model. These steps are illustrated in the Figure 2.29.

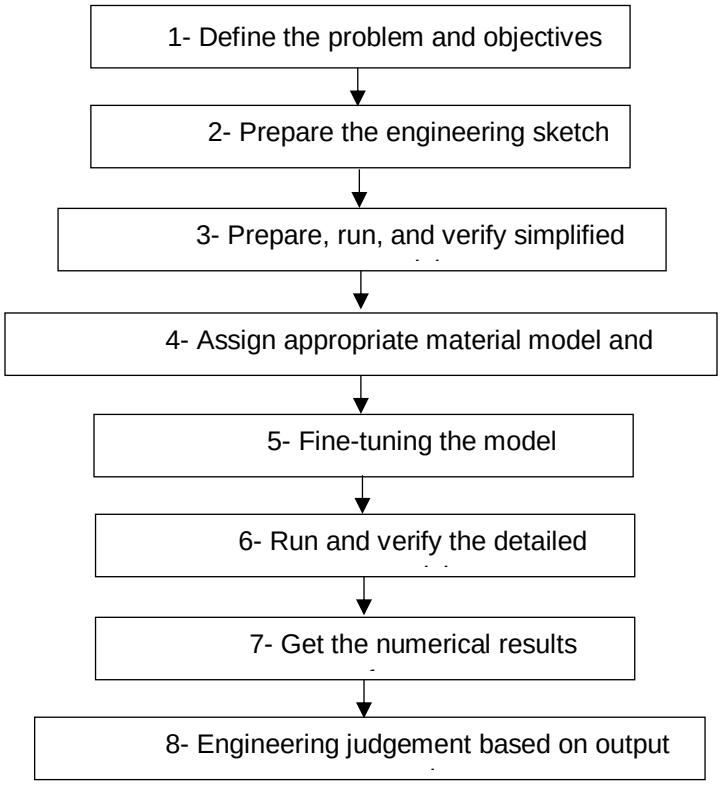

Figure 2.29 General Procedure for numerical modeling in geomechanics (Koliji 2013)

The final step in modeling is interpretation of the results in combination with engineering judgment. The issue of primary importance should be identified and sought in the results. The general trend of the results should be always should be compared with

knowledge-based engineering expectations. If anomalies are observed, the engineer should find out the numerical or physical reason behind it. If necessary, some or all the above-mentioned steps should be then repeated to achieve an enhanced model with realistic results. Figure 2.30 demonstrates long-term performance monitoring of a bridge approach embankment by using the FLAC3C-FDM approach. It should be noted that vertical displacements are presented in feet.

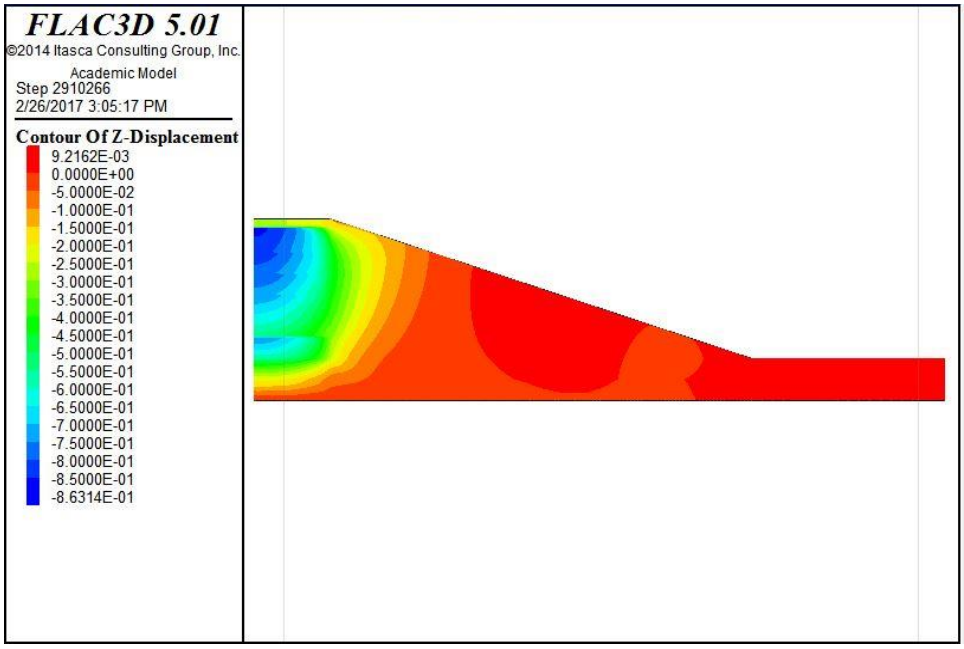

Figure 2.30 Long-term performance evaluation of a bridge approach embankment

In the Figure 2.30, long-term (17 years) performance of a bridge approach embankment is assessed based on predicted and measured ground vertical displacements. Maximum vertical displacement of more than 0.86 ft is predicted at the centerline of the roadway. However, field measurements revealed more than 1.33 ft of vertical displacement for 17 years lifespan of the approach embankment. The difference between the measured and predicted values from the site and the numerical modeling approach, respectively, can be mainly due to the limitation of the numerical modeling

approach to consider the effect of precipitation and temperature changes on the long-term performance of the bridge approach embankment.

2.4.2 Empirical and Semi-Empirical Statistical Modeling

Empirical Modeling (EM) is one of the most commonly used techniques in science, industry, engineering, and management (Mark 2016). There is a diverse range of problems modeled using this approach. EM refers to a specific variety of principles and algorithms in standard domains to construct models based on observations and experiments (Weibelzahl and Weber 2002). Like numerical methods, the application of empirical modeling in geotechnical engineering inherently embodies some advantages and limitations.

The Empirical modeling approach enables the user to get a deeper insight of the existing relationships among the different variables that belong to a particular system (Habib 2016). Recent developments in empirical modeling approaches, such as machine learning, genetic algorithm, and artificial neural network, are applied in different areas combined with fast and inexpensive computational tools (Adeli and Hung 1994; Goldberg and Holland 1988; Samanta et al. 2003). In recent years, it has been attempted to find ways of developing empirical models that are insightful, recursive, and practical, complementing the otherwise inherent versatility of the approach.

Empirical modeling has been used in geotechnical engineering applications for decades. Several empirical-semi empirical models have been developed for prediction and correlation purposes. Swell-shrink characteristics of expansive soils, ground movements, residual strength of liquefied soils, prediction of liquefaction induced lateral spreading, and earthquake induced sliding are some examples (Bartlett and Youd 1995; Kramer and Wang 2015; Oh et al. 2009; Puppala et al. 2014, 2016; Saygili and Rathje 2008).

A major criticism of the empirical modeling approach is that it provides less explanation of its output. In other words, empirical model principles and algorithms are not a formal proof of a fact (Papadimitriou 2003). Empirical studies always include uncertainties that can be expressed in statistical inference (Yun and Reddi 2011). An empirical method is best to use when there is no analytical modeling framework available.

2.4.3 Analytical Modeling

The term analytical modelling is defined as a mathematical approach to capture the behavior of a system with a closed form solution (Bender 2012). The analytical modeling approach has been used extensively in natural sciences, engineering disciplines, and social sciences. Unlike empirical approaches, which are based on observations and experiments, analytical models are developed based on mathematical concepts. Analytical models are formulated based on certain assumptions to explain a system, study the effects of different factors, and to make reasonable predictions over a wide range of component levels. Depending on how much historical information of a system is available to develop a model, analytical modelling can be categorized as either black or white box models. In white box models, all necessary information is available, While, black box models, are developed based on no priori information of a system.

During the last decades, analytical approaches, such as implementation of basic mathematical concepts, regression, and statistical analysis have been applied extensively (Baecher and Christian 2005; Hicher and Shao 2013; Schofield and Wroth 1968; Ti et al. 2009a; Yamamuro and Kaliakin 2005). However, the application of interdisciplinary analytical methodologies, such as artificial neural network, system identification, and machine learning approaches has been limited and yet to be developed (Oskay and Zeghal 2011; Shahin et al. 2001). Developing basic and advanced soil constitutive models to analyze the very complex behavior of different types of soil, interaction of soil-structure

systems, prediction of ground movements, and to model practical geotechnical applications, such as retaining structures, foundations, and dams are some examples (Zhang et al. 2013).

Besides the advantages, there are some limitations for applications of analytical modeling approaches in geotechnical engineering. Analytical models are very expensive in both time and data. Unlike empirical models, analytical models follow logical mathematical concepts. Hence, theoretical models may fail to represent the dynamic behavior of an infrastructure.

2.5 Summary of Past Research Works

Health monitoring and condition assessment of a bridge infrastructure has always been a concern for geotechnical engineers due to complex, non-linear, and anisotropic behavior of soils. Several monitoring techniques and modeling approaches were attempted to evaluate the performance of bridge infrastructure during its design life. However, each monitoring technique inherently possessed some major limitations in assessing the condition of an entire bridge infrastructure. Numerous empirical and analytical prediction models were developed to predict future probable concerns, mainly to reduce maintenance costs and increase the bridge infrastructure design life. However, their failure to consider the dynamic effects of ambient conditions such as temperature and precipitation variations on bridge infrastructure, resulted in undesirable predictions.

In this research study, a comprehensive framework is developed with the integration of the latest technological developments within advanced mathematical modeling approaches to better predict the condition of a bridge infrastructure. This research study also examines the cost effectiveness of the 3D-TLS remote sensing technology, LiDAR, as an effective alternative ground movement monitoring technique using Cost-Benefit Analysis (CBA).

Chapter 3: Development of Framework for Performance Assessment of a Bridge Infrastructure

3.1 Introduction

This chapter presents a framework developed for performance assessment of bridge infrastructures using 3D Terrestrial Laser Scanning (3D-TLS) LiDAR technology and system identification theory. The framework presents a step-by-step approach starting from designing an initial scanning plan at a test site to final ground movement analysis to evaluate the performance of a bridge infrastructure. Several factors such as project requirements, site conditions, atmospheric conditions, geometry of the scanning area, and climatic factors are considered in the developed framework. An optimization procedure of scanning plans to enhance the 3D visualization model of an infrastructure is developed considering different combinations of scanning plans, resolution, and quality settings. The following sections present the step-by-step details of development of the framework for 3D-TLS field operations and inclusion of system identification mathematical modeling approach.

3.2 Step-by-Step Procedure

This section presents a step-by-step procedure of the developed framework for health monitoring and performance assessment of a bridge infrastructure. The framework consists of four major steps as presented in Figure 3.1:

1) Define project requirements, including project history, including age of the bridge infrastructure and history of performance and maintenance measures, site conditions contain soil and environmental conditions including precipitation, dry periods and temperature variations, and different components of the bridge infrastructure as per the type of the bridge

2) Develop a monitoring approach using 3D-TLS LiDAR technology, including initial scanning plan, registration process, rotating scans to a single coordinate system, and develop an optimized methodology for evaluating the ground movements.
3) Develop database of time-series environmental data, including temperature, precipitation, and snowfall at the project site using nearby weather stations and deformation measurements using 3D-TLS technology. Determine the dependence and interdependence of different variables and develop an approach to incorporate all the parameters to develop long term ground movement prediction models.
4) Perform validation studies for determining the accuracy of the developed models. This is performed using the validation database that is not used to develop the models and also performing comparison studies with existing established models in the literature to determine their efficacy in performance assessment.

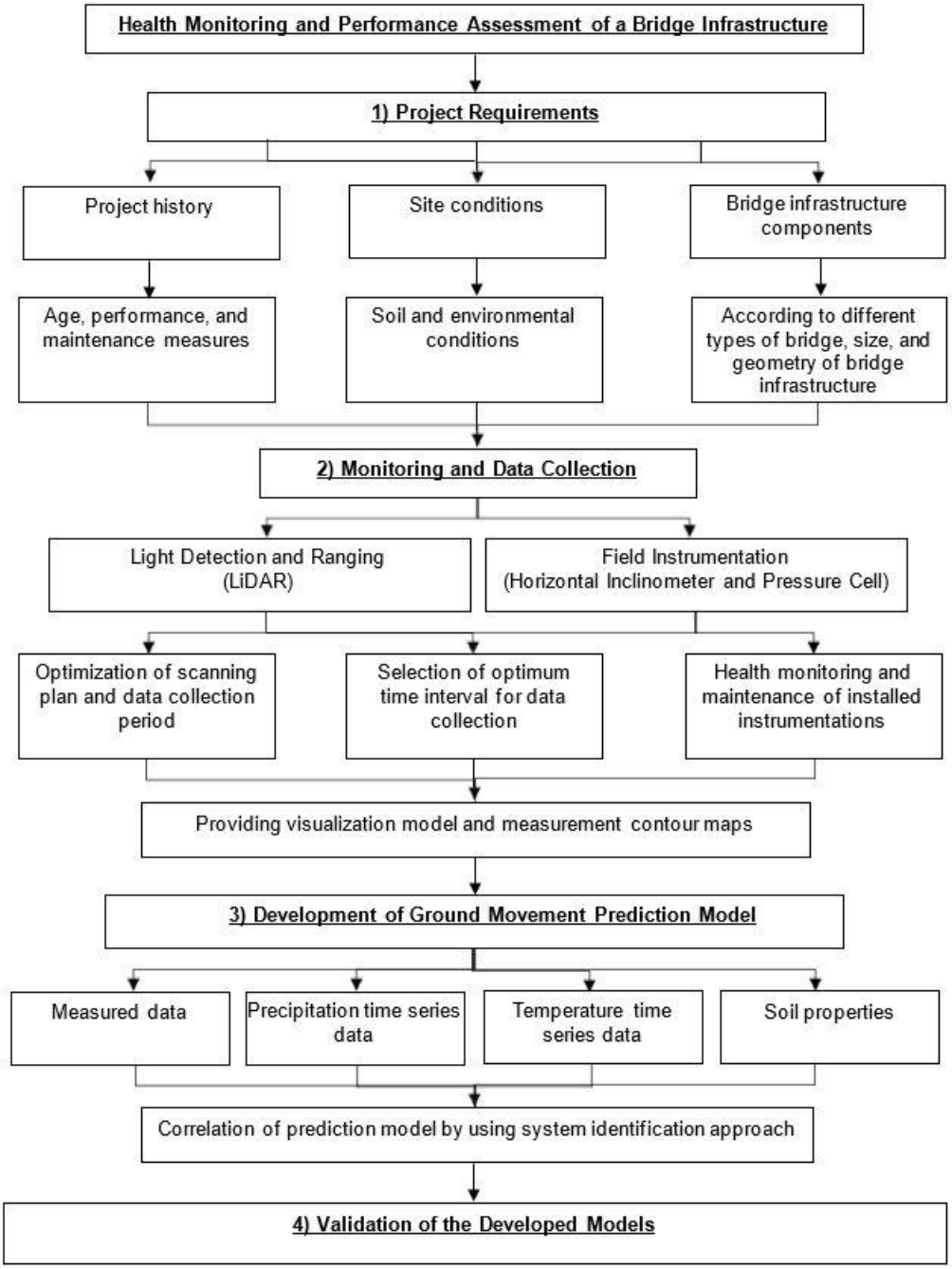

Figure 3.1 Procedural framework for performance assessment of a bridge infrastructure

The framework presented in Figure 3.1 comprises of four major steps. The first step is to collect a solid database from the project history, site conditions, and bridge infrastructure components. A detailed understanding of project requirements such as size, geometry, and soil and seasonal ambient conditions is indispensable to perform reliable monitoring and to develop ground movement prediction models for the project under consideration.

The second step is to collect relevant time-series data from bridge infrastructure test site using 3D-TLS technology. The validity of the data should be assessed by comparing the collected data from field instrumentations and terrestrial LiDAR surveys. Effective seasonal ambient factors such as precipitation and temperature variations should be considered during the data collection process.

After producing visualization models and comparison graphs based on the monitored parameters and 3D terrestrial laser scanner surveys, an accurate ground movement prediction model should be developed using system identification methodology. Several model structures should be attempted to estimate the best fit mathematical model structure to predict ground vertical or lateral movements. Considering effective ambient conditions, these sequential steps provide optimal unbiased estimates for cyclic ground movements, especially in expansive clays.

As the final step, predicted ground movements from the developed model should be evaluated and validated by using measured data from the test site and commonly used prediction model. The following sections present step-by-step procedure of health monitoring for bridge approach embankment by using 3D-TLS LiDAR technology. Each of the aforementioned steps are elaborated with more detail in the following sections.

3.2.1 Project Requirements

Health monitoring and performance assessment of a bridge infrastructure cannot be accomplished without collecting a comprehensive information database from the history of the infrastructure, soil conditions, and bridge infrastructure components (Yari 2018). Performance history of a bridge infrastructure project including age and performed maintenance measures can provide a valuable database for future risk assessments and prediction analysis (Hooks and Frangopol 2013). The maintenance history of a bridge infrastructure can provide useful information about a bridge that can be used for future repair and budget preparation. This can include details such as date, description of project, contractor, cost, project number, type of maintenance, and related data. Knowledge of bridge deterioration rates is crucial for cost-effective bridge management and long-term performance prediction analysis (Biggs and Mahony 2004; Manos et al. 2008).

Another important project requirement for health monitoring and performance evaluation of a bridge infrastructure is site conditions, including subsurface soil and environmental conditions. The effect of soil-structure interaction on the performance of bridge infrastructure cannot be investigated without having a deep insight of soil conditions. Soil conditions along with seasonal ambient precipitation and temperature variations reveal important information about potential hazardous problems below the surface. Liquefaction of sand deposits, differential settlements at the interface of a bridge structure and approach embankment, and swelling-shrinkage of expansive clayey soils are some examples. Additionally, developing accurate ground movement prediction models is not possible without collecting a solid database of site conditions.

According to different types of bridge in the United States, infrastructure components, size, and geometry of bridge infrastructure play a pivotal role in bridge asset management and performance assessment of the infrastructure. Girder Bridge is the most

common basic highway bridge type constructed in the United States (Yari 2018). The most common basic type of superstructure used in the construction of girder type bridges are I beam girders and box girders. The material normally includes structural steel, prestressed concrete, and/or composite of steel and reinforced concrete. However, bridge structure are normally supported by drilled shaft deep foundations and connected to the roadway from approach embankments (Yari 2018).

In the case of monitoring of ground movements using 3D-TLS LiDAR technology, project requirements on the object under consideration such as geometry and size of bridge infrastructure and seasonal ambient conditions make important contributions for designing both initial and optimized 3D-TLS scanning plans (Ahn and Wohn 2016; Zámečníková et al. 2014). Ideally, to scan the surface of a bridge component, the laser scanner should be placed in such a way that the laser beam is near perpendicular to the surface (Soudarissanane et al. 2008; Soudarissanane and Lindenbergh 2011). However, it is not feasible to place the scanner perpendicular to the target object's surface due to the survey limitations. This limitation can be reduced by designing an optimized scanning plan and using enhanced scan settings during LiDAR surveys. The next section presents scanning parameters, include resolution and settings, as another effective factor on LiDAR scanning plans.

3.2.1.1 LiDAR Scanning Plan

An initial scanning plan is vital and should be designed according to the geometry and size of the surveying area, type of monitoring object, and the distance between the scanner and the target object. Parameters such as resolution and quality also contribute to the scanning plan and survey efficiency. It should be considered that the length of time required for scanning is increased dramatically by enhancing the resolution and quality

settings. The significance of effective factors on LiDAR scanning plans is elaborated in the next sections.

3.2.1.2 Resolution and Quality Settings

The resolution and quality settings are the two most important scanning parameters that govern the quality of the bridge visualization model. An optimized scanning plan contains a minimum number of scans with specific resolution and quality settings that covers the entire monitoring area. Respective settings can be either obtained from relevant inspection manuals or can be estimated by updating the scanning plan following a trial-and-error approach. The resolution setting defines the distance between the sampled points. A higher resolution setting time is required if the measurements are required at very close distances. Whereas, the quality setting determines how long the scanner takes to measure a point and the duration of time a point is sampled. Higher quality scans provide less noise during the scanning survey. It should be noted that noise generally represents the turbulence from sensors and monitoring techniques. It should also be noted that with an increase in the quality and resolution settings, the scanning process time duration would be increased drastically. Figure 3.2 depicts the impacts of resolution and quality settings on the scanning survey (FARO Technologies 2011). The white dots in Figure 3.2 represent sampled points during the scanning survey.

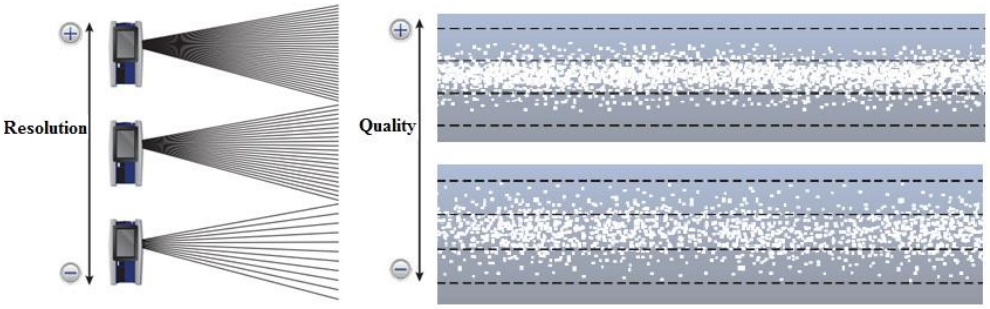

Figure 3.2 Resolution and quality setting effects on scanning surveys

3.2.1.3 Atmospheric Conditions

The atmospheric conditions can have significant impact on time-series measurements made by terrestrial laser scanning technology (Hejbudzka et al. 2010). Atmospheric conditions such as fog, rain, dust, and snow conditions can affect the scanner and the captured data (FARO Technologies 2011). Experimental surveys revealed that sampled points by the scanner were decreased drastically during the foggy atmospheric conditions (Hejbudzka et al. 2010). To ensure efficient scanning survey, the ambient temperatures should be within the range of 44°F and 104°F before performing surveys (FARO Technologies 2011).

3.2.1.4 Geometry of the Scanning Area

The geometry of the scanning area plays an important role in the accuracy of the resulting point cloud data (Schaer et al. 2007; Soudarissanane et al. 2011; Soudarissanane and Lindenbergh 2011). Geometry constraints at a monitoring site can deteriorate the quality and reduce the accuracy of scans. For instance, increasing the distance between the scanner view point and target zone can lead to an increase in incidence angles to the object surface, which would decrease the accuracy of the 3D-TLS survey. It should be noted that the incidence angle “α” is defined as the angle between the emitted laser beams with the normal (n) to the object surface (Figure 3.3).

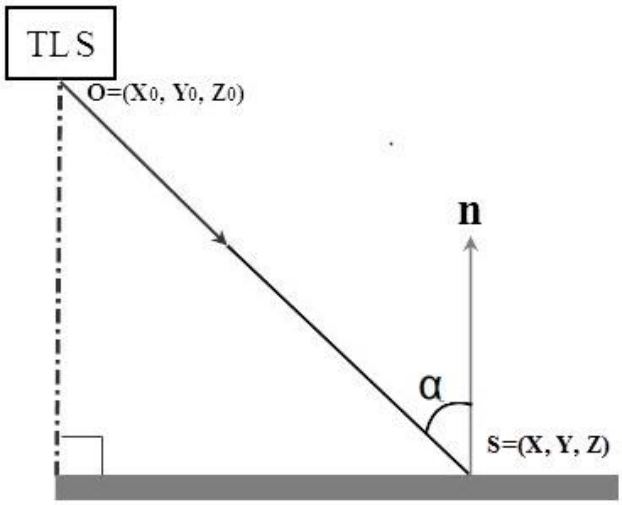

Figure 3.3 Performing field surveys and optimized number of scans

An optimized scanning plan to cover the monitoring area contains a minimum number of scans with specific resolution and quality settings. Respective settings can be obtained from relevant inspection manuals or can be estimated by updating the scanning plan, following a trial-and-error approach. An initial scanning plan with high resolution and quality settings is recommended to use as the reference point cloud database to cover the monitoring area. The numbers of scans can be decreased gradually by employing different combinations of settings. Finally, depending on the variation-time rate of the monitoring factor, an optimized scanning plan will be developed for performing the consecutive surveys. Each set of acquired scans should be registered to a single point cloud. Different registration techniques are described in the following section.

3.3 Registration

The registration process refers to moving all the individual scans to a single project point cloud and aligning them with a single coordinate system. This is an inherent procedure to be followed for test sites that require more than three scans. This process can be accomplished using target-based, target-less, or manual registration techniques.

The following sections present the details of the individual registration techniques that can be followed based on the test site conditions and project requirements.

3.3.1 Target-Based Registration

In order to register each set of collected scans to a single point cloud, at least three common reference points are required to be captured in two consecutive scans. In the target-based registration process, standard spheres, checkerboards, or natural targets are generally used as reference points (FARO Technologies 2011). A target-based registration is recommended to facilitate and expedite the registration process of scanning plans that have more than three scans to cover the entire test site. Target objects are categorized into two types: artificial and natural. Figure 3.4 demonstrates two commonly used types of artificial and natural targets including standard spheres and fixed structural elements of a bridge infrastructure.

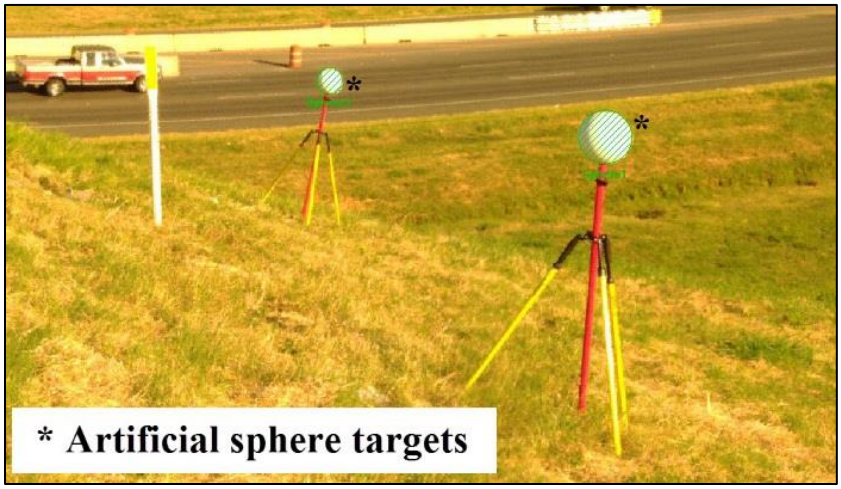

(a)

(b)

Figure 3.4 (a) Artificial target; (b) Natural target

The size and shape of the artificial and natural targets should be defined and set up manually in the processing tool as shown in Figure 3.5 ((a) and (b)). This is required for the processing software or the registration error may increase during the registration phase.

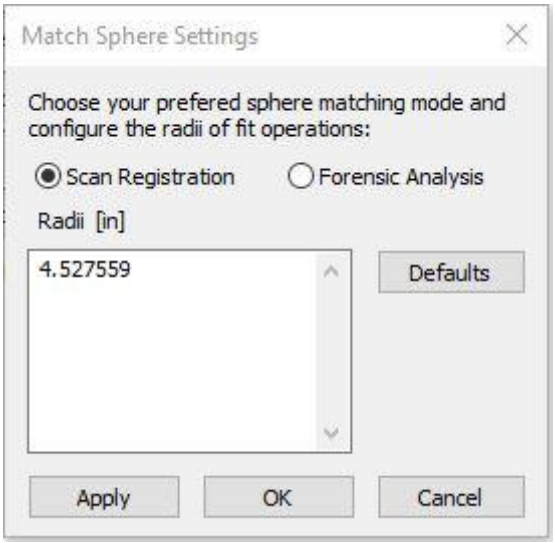

(a)

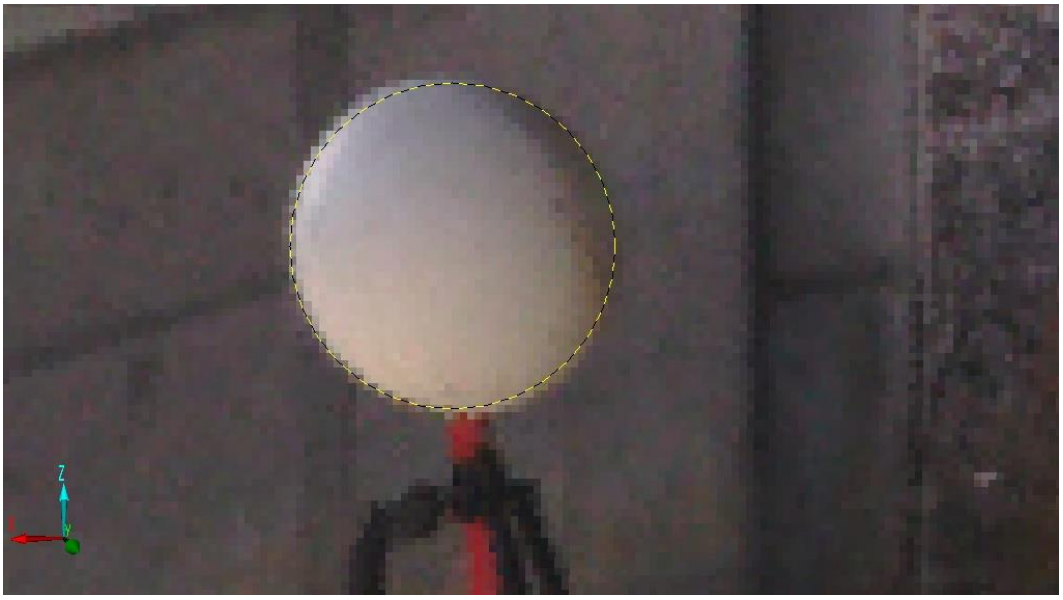

(b)

Figure 3.5 (a) sphere target dimension set up; (b) measuring of sphere diameter

3.3.2 Target-Less Registration

In many construction applications, physical targets cannot be installed for the registration process. However, setting up artificial targets such as spheres or flags are not always feasible due to space constraints and site limitations. In such cases, automatic target-less registration processes can be employed to produce an accurate visualization model of the surveyed area. Automatic target-less registration is a computational form of registration composed of cloud to cloud and top-view based registration approaches. Cloud to cloud registration is a form of target-less registration by overlapping the area that is identical between two scans. Hence, more identical points in two consecutive scans can lead to a more accurate target-less registration. However, there are some advantages and limitations corresponding to the automatic cloud to cloud registration approach.

For the case of closed surveying areas, automatic cloud to cloud registration is very exact, because in this case the calculation involves millions of identical points. In large

outdoor surveying areas, automatic cloud to cloud registration is often not possible since there are only points on the ground and scans cannot provide enough points at higher altitudes to perform the cloud to cloud registration process (Sanchez et al. 2017). However, for outdoor surveying purposes, automatic top-view based target-less registration can be performed. Automatic top-view based registration is a form of target-less registration approach by automatic identification of edges, corner points, and fast plane detection (FARO Technologies 2016).

Scanning plan makes an important contribution to perform the automatic target-less registration process. A complicated scanning plan can confuse the computational tool to place all scans accurately. Hence, simplifying the scanning plan to cover the target area may facilitate the target-less registration process. Additionally, appropriate overlapping between the scanned areas plays a key role in facilitating the target-less registration process. Over-scanning and considering a proper scanning distance in the scanning plan as per the scanning settings can assist to provide a reasonable overlapping between the collected scans using target-less registration techniques.

3.3.3 Manual Target-Less Registration

Target-less registration can be accomplished initially by the manual registration approach. In the manual registration approach, individual scans should carefully be aligned and adjusted together in correspondence view. Correspondence view refers to a close view of an unregistered set of scans in which each scan is presented in a specific local coordinate system. In correspondence view, each scan can be rotated and moved to a proper position according to the adjacent scans. Subsequently, a cloud-to-cloud registration should be performed in such a way that the distance between overlapped areas do not exceed a user-defined maximum search distance magnitude (Figure 3.6).

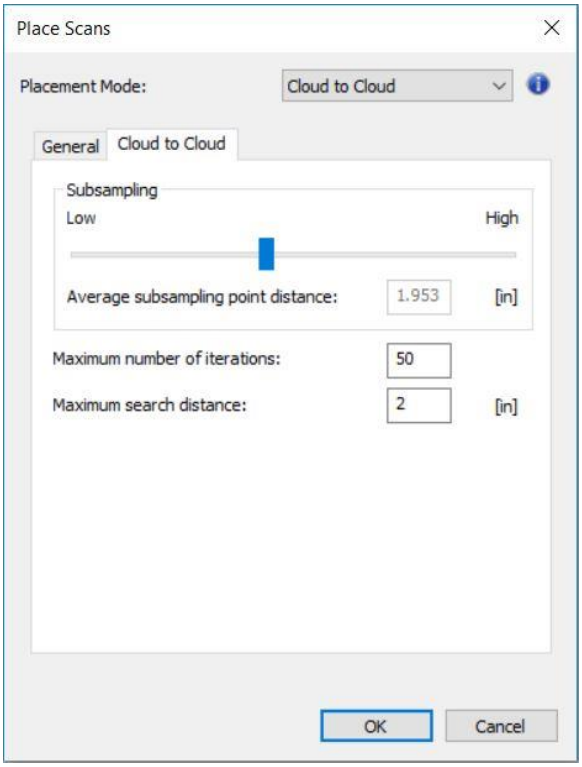

Figure 3.6 Maximum search distance in cloud-to-cloud registration

The maximum search distance is the farthest distance in which, a scan will search adjacent scans for common captured points to find a reasonable overlap. An appropriate value for the maximum search distance parameter can be found by performing several trial and error cloud-to-cloud registration process. Figure 3.7 illustrates a simple example for manually setting up scans in correspondence view.

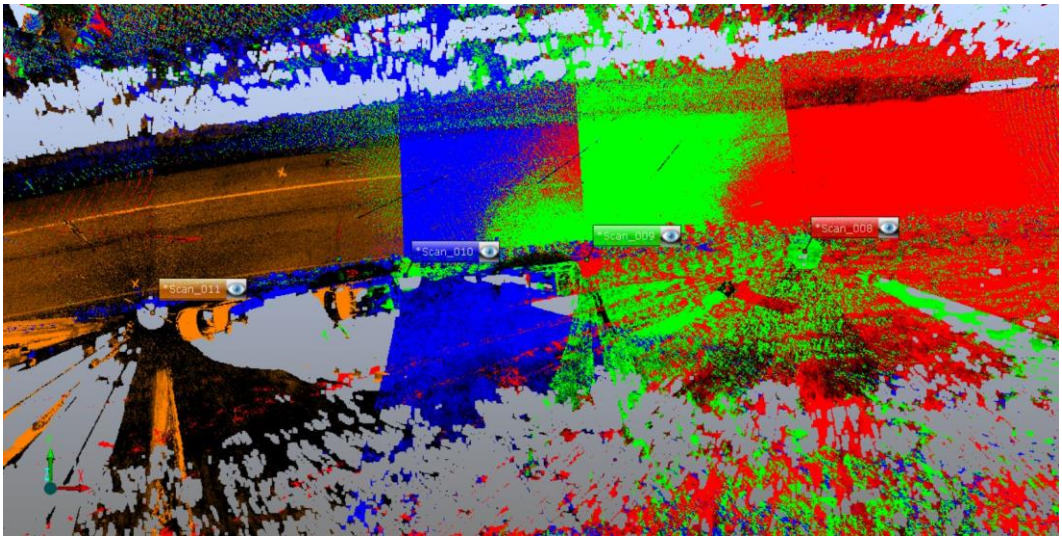

Figure 3.7 Appropriate linear scanning plan for top view-based registration

The manual registration method may require several time-consuming attempts to get the registration process completed with the highest accuracy. After the initial registration process is accomplished, several cloud-to-cloud registration updates should be attempted to achieve the highest accuracy for the registered visualization model. The following section explains how to perform cloud-to-cloud registration updates briefly.

3.3.4 Cloud-to-Cloud Registration Update

Both target-based and target-less registration approaches are considered as a primary registration process, which cannot provide a highly accurate database to perform small deformation analysis. According to the used 3D terrestrial laser scanner, several cloud-to-cloud registration updates should eventually be implemented to achieve a mean scan point tension of less than 0.15 inches (FARO Technologies 2011). Mean scan point tension represents the discrepancy in the global coordinate system between the position and the orientation of the two corresponding reference objects in Scans 1 and 2. For corresponding reference points, the distance between their positions serves as input for the calculation of the tension. For planar areas and pipelines, the position and the direction

serve as input for the calculation of the mean scan point tension value. Values close to zero indicate a good registration result (FARO Technologies 2011). Cloud-to-cloud registration updates increase the accuracy of the registered point cloud by matching the surfaces' sampled points from different scans (Akca 2007, 2008). By gradually decreasing the maximum search distance and increasing the average subsampling point distance, the accurate registration of scans can be accomplished (Figure 3.6). Subsampling, reduces and homogenizes the point density to a specified point distance. Whereas, maximum search distance determines the distance from each point within which a computational tool searches to find corresponding scan points (FARO Technologies 2011).

It should be noted that a combination of a higher value of the subsampling parameter and a minimum set up value for the maximum search distance may not be necessarily result in a better cloud-to-cloud registration update. Instead, an optimized combination of both settings should be attempted to accomplish the highest accuracy.

3.3.5 Ground Movement Analysis

The main objective of using 3D-TLS technology in this research study is to detect ground movements. After all sets of scans are registered to a single point cloud, there are three main steps to measure ground movements. Assessment of ground movements is attainable merely by rotating all the registered point clouds to a same coordinate system. Thereafter, monitoring points should be selected from the reference point cloud, and ground vertical displacements can be determined from the other sets of scans. These steps are elaborated briefly in the next sections.

3.3.5.1 Rotating Scans to the Same Coordinate System

Practically, each LiDAR survey is performed in a different local coordinate system. Hence, it is required to rotate all registered point clouds to the same exact coordinate system prior to performing ground movement analysis. Since this type of alignment

involves six degrees of freedom (three translations and three rotations), at least three common fixed reference points are required in all registered point clouds. Artificial reference points such as standard spheres or naturally fixed objects from the test site such as bridge piers supported by deep foundations. These piers can be used to rotate all point clouds to the same coordinate system.

3.3.5.2 Selection of Monitoring Points

The selection of monitoring points is crucial in evaluating the performance of the bridge infrastructure. The monitoring points should be selected from the reference point cloud database generated from the first set of scans. Depending on the type of infrastructure project, monitoring points can be selected from critical monitoring zones. For example, in a bridge approach embankment, ground vertical movements should be measured and evaluated for bump phenomenon on the top of the pavement surface, and the stability of embankment slope can be evaluated by monitoring of ground movements on the top of the pavement shoulders and embankment slopes.

3.3.5.3 Evaluating Ground Movements for Periodic Intervals

An appropriate automated computational tool is required to evaluate ground movements. For example, in an imaging processing software, SCENE, a new add-in was developed to evaluate ground vertical displacements. Mathematically, the deformation analysis will be conducted by evaluating the new location of the selected points by searching for the same coordinates in other scanned point clouds.

3.4 Summary of the Framework for 3D-TLS Field Operations

During the past few decades, terrestrial laser scanning technology has evolved and has been adopted for a variety of applications, including Industrial, architectural, structural, geotechnical, archaeological, and mechanical dimensional inspection (Ebrahim and Mostafa 2011; Lemmens 2011). Despite the versatility in the applications, very limited

studies were performed in developing a framework suitable to their respective application. The first step to develop a framework to evaluate the performance of a bridge infrastructure is to develop an optimized methodology for evaluating the ground movements using 3D-TLS LiDAR technology. Figure 3.8 depicts a summary of the developed multipurpose flexible framework for the implementation of 3D-TLS for performing field operations. The following sections present how time-series measurements can be utilized for development of ground movement prediction models.

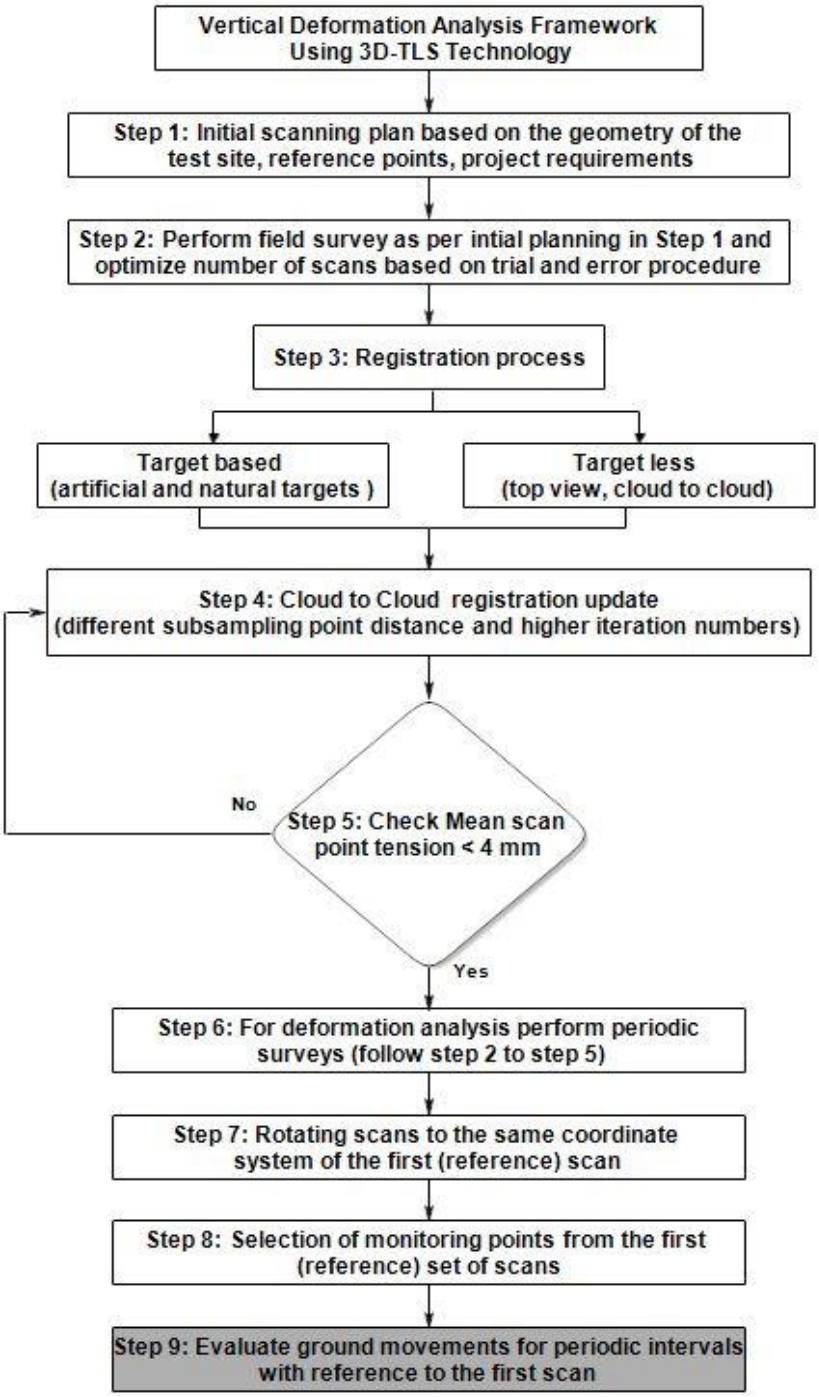

Figure 3.8 Terrestrial laser scanning step-by-step procedure (Shafikhani et al. 2018a)

3.5 System Identification

System identification is the process of capturing the physical characteristics of a system and matching it to a mathematical model structure (Fassois and Rivera 2007b; Keesman 2011). A system is a regularly interacting or interdependent group of factors, that form a unified whole. The applications of system identification techniques transcend from engineering practices and reach into fields such as economics, biology, medicine, ecology, and geology (Fu and Li 2013). The theory of system identification technique is briefly reviewed here, a detailed explanation can be found elsewhere (Ljung 1998; Natke 2014; Söderström and Stoica 1989).

Figure 3.9 demonstrates a system identification step-by-step procedure (Andersson et al. 1998). The identification process of a system is typically comprised of four main steps: (1) collection of suitable data from the system, (2) selection of the model structure, and (3) implementation of the identification algorithm, and (4) validation of the prediction model according to a criteria (Rabbani et al. 2013). An identification procedure usually involves numerous iterations between these steps. Based upon the number of factors involved in the model formulation, the system identification process can be categorized into single-input single-output and multi-input multi-output models (Aarts 2012). According to the availability of a priori data of a system, models can be generated as white-box, grey-box, or black-box (Chinarro 2014).

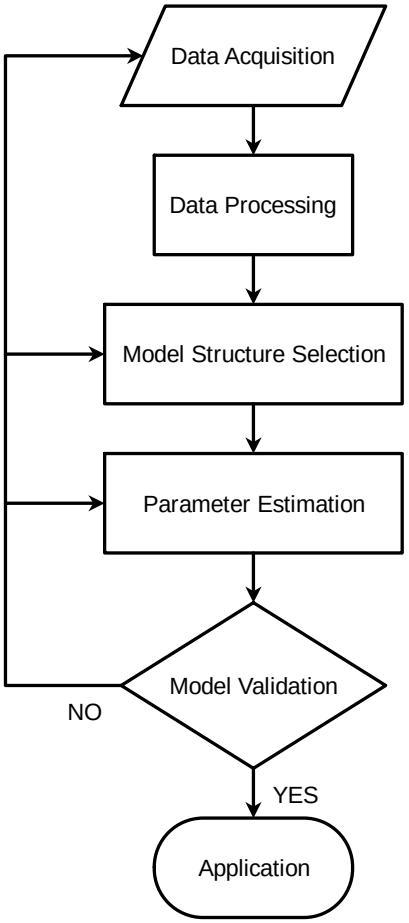

Figure 3.9 System identification procedure (Andersson et al. 1998)

White-box, also called glass-box or clear-box, is a system with all necessary available information. Accordingly, a white-box model is a pure mathematical model in which, if the available dataset employs appropriately, the derived model will behave correctly. In contrast, black-box refers to a system which can be viewed in terms of inputs and outputs with an unknown internal structure. Black-box models may be developed to estimate a nonlinear system (Chen et al. 1990; Leontaritis and Billings 1985). However, physical significance or structural properties of the system cannot be captured (Gawthrop et al. 1993; Lorito 1998; Tan and Li 2002). Non-linear auto-regressive moving average or artificial neural network models are two examples of black-box modeling techniques.

Sometimes, a combination of a partial theoretical model and some a priori information may complete a model. However, some of the minor nonlinearities cannot be modelled accurately due to the system complexity and constraints on physical ability to measure. Thus, this is seen as a partially known system and can be modelled as a grey-box model (Forssell and Lindskog 1996; Gawthrop et al. 1993; Sjöberg and De Raedt 1997; Tan and Li 2002). In practice, all systems are between white-box and black-box models. Hence, almost all systems can be considered as grey-box models. In other words, by transmitting from white-box to Black-box modeling approaches, the level of experimental modeling of a system is increased (Figure 3.10).

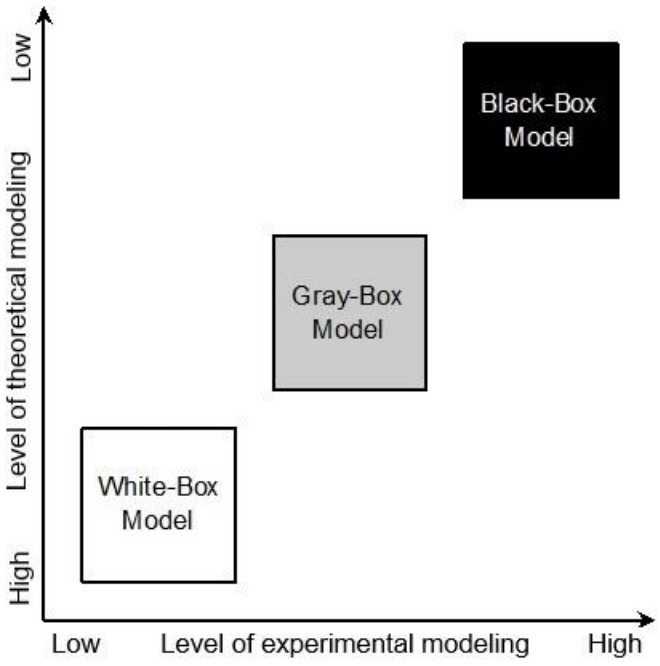

Figure 3.10 Different methods of mathematical modeling (X-engineer.org 2018)

Depending on the application, the identification algorithms can be divided into recursive (suitable for on-line setup) or non-recursive (off-line) methods. In many cases, it is beneficial to have a model algorithm available on online to be updated based on new observations. In such algorithms, model parameters can be computed repeatedly over time

when a new observation is recorded at next iterations (Chen 2009; Ljung and Söderström 1983; Pelckmans 2015). This type of algorithm in which current output(s) depend on previous output(s) is called recursive (on-line) models. However, in non-recursive (off-line) systems, current outputs do not depend on previous output(s) (Ghanem and Shinozuka 1995; Isermann 1981).

A variety of linear and non-linear model structures are available in the model identification approach to assist modeling an unknown system (Aarts 2012). Selection of an appropriate model structure to capture dynamics of a system depends significantly on several factors. Comprehensive understanding of the system identification modeling approach and possessing inclusive insight of the system undergoing identification are two major required factors (Andersson et al. 1998; Natke 2014). It has been revealed that employing complex nonlinear model structures does not necessarily result in an accurate model to capture dynamics of a system. However, models developed from linear model structures may result in more user-friendly and accurate models for practical purposes (Akshaykumar and Subbulekshmi 2016).

There are several linear model structures that are available to employ in the model identification process. One important class of model structures used in system identification modeling is the discrete-time linear models (Åström and Eykhoff 1971; Kailath 1980). Autoregressive models are mathematical-statistical algorithms that can represent a type of random process in which the output variable depends on stochastic and noisy terms (imperfectly predictable terms) and their previous values. Data used for building such models can be intrinsically discrete or might be samples of a continuous signal(s).

Generally, a system can be described by using the following linear polynomial equation (Akshaykumar and Subbulekshmi 2016; Ljung 1992, 1998):

$$y\,(n) = q^{-n}G(q^{-1},\theta)u(n) + H(q^{-1},\theta)e(n) \qquad 3.1$$

Where, $u(n)$ and $y\,(n)$ are input and output of the system, respectively. In this equation, $e(n)$ represents the noise in the system, and $G(q^{-1},\theta)$ and $H(q^{-1},\theta)$ are the transfer functions of the deterministic and stochastic part of the system, and q^{-1} is the "backward shift operator" such that $q^{-n}u(t) = u(t-n), n \in \mathbb{Z}$. The general-linear model structure is depicted in Figure 3.11. It is worthwhile to restate that noise generally represents the turbulence from sensors and monitoring techniques. While some unwanted variation of a system such as a step change in ambient conditions can create disturbance in a system, both noise and disturbance effects are considered in modeling process using system identification approach (Shinners 1998).

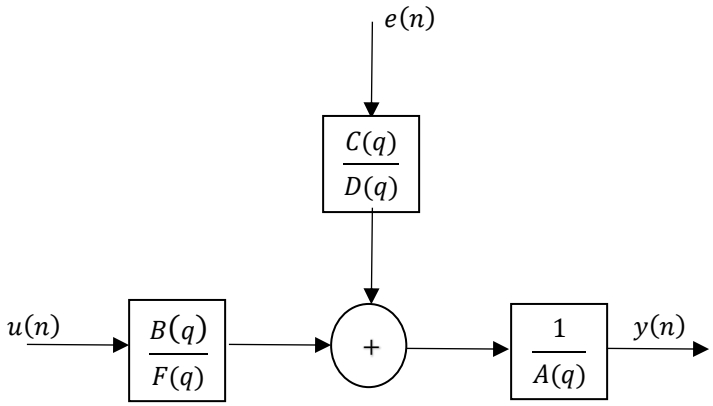

Figure 3.11 General-linear model structure (Andersson et al. 1998)

Equation 3.1 implies a comprehensive format of a linear model structure. However, simpler forms of general-linear model structures can be deduced by setting one or more of $A(q)$, $B(q)$, $C(q)$, $D(q)$, $F(q)$ polynomials as 1. These simpler models such as Auto Regressive (AR), Auto-Regressive with exogenous input (ARX), Auto-Regressive Moving Average with eXogenous input (ARMAX), Output Error (OE), and Box Jenkins (BJ) can be deduced for different real-world applications (Akshaykumar and Subbulekshmi 2016; Ljung 1992). It should be noted that the term exogenous refers to variables in which their values

are determined from outside the model. A summary of each model is discussed briefly in the next sections.

3.5.1 AR Model Structure

AR model structure is the simplest form of linear model structures in the model identification approach. In this model, outputs are only dependent on previous outputs and no system inputs or disturbances can be modeled using this model. Very simple time-series analysis and linear prediction coding are applications of this model. Figure 3.12 demonstrates the AR model structure (Akaike 1974).

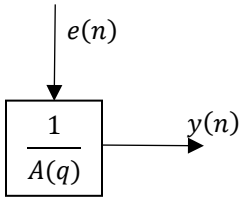

Figure 3.12 AR model structure (Akshaykumar and Subbulekshmi 2016)

3.5.2 ARX Model Structure

ARX model structure is one of the most efficient polynomial estimation methods in the linear system identification approach (Ljung 1998; Rachad et al. 2015). ARX model provides a unique solution by using linear regression equations in analytic form. ARX model is recommended when the required model order is high (Andersson et al. 1998; Ljung 1992).

In the ARX model, disturbance is considered as a part of the system dynamics, which is a limitation of this model. In other words, the deterministic and stochastic parts of the system have the same poles, which can lead to unrealistic results. This disadvantage of the ARX model can be optimized by setting high order models to minimize the equation

errors and increase the stability of the model. Figure 3.13 demonstrates a schematic view of the ARX model.

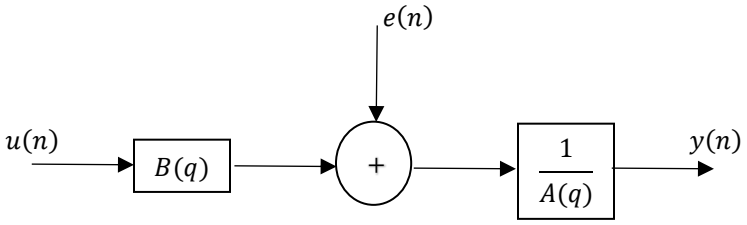

Figure 3.13 ARX model structure (Rachad et al. 2015)

3.5.3 ARMAX Model Structure

Unlike the ARX model structure, ARMAX model structure possesses more flexibility for modeling dominating disturbances that enter early in the system. For instance, a wind gust affecting an aircraft is considered as an early disturbance in the system. Figure 3.14 demonstrates the ARMAX model structure (Åström and Eykhoff 1971).

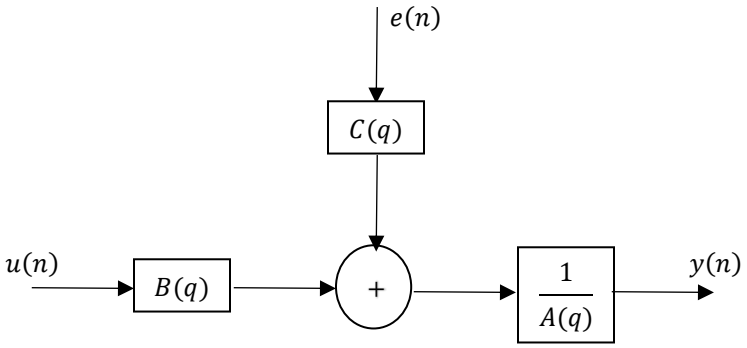

Figure 3.14 ARMAX model structure (Johansen and Foss 1993)

3.5.4 OE Model Structure

In the OE model, dynamic and stochastic effects of a system can be modelled separately. However, this model cannot capture the disturbance effects of a system. Figure 3.15 shows a schematic view of the OE model (Andersson et al. 1998; Ljung 1992).

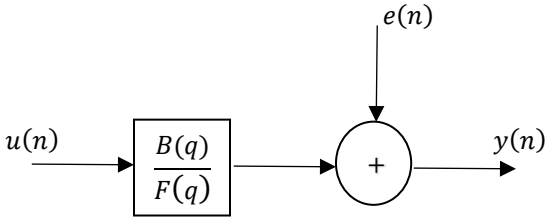

Figure 3.15 OE model structure (Akshaykumar and Subbulekshmi 2016)

3.5.5 BJ Model Structure

Between the linear polynomial model structures, the Box Jenkins provides a complete model in which disturbance can be modeled separately from system dynamics. Unlike the ARMAX model, the BJ model is useful when disturbances enter late into the system. For example, precipitation effect on expansive soil swell-shrink induced displacements can be considered as a late disturbance effect in a system. Figure 3.16 displays the BJ model structure.

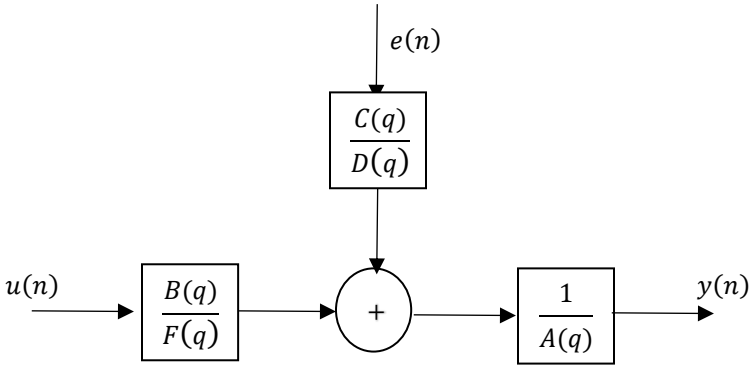

Figure 3.16 BJ model structure (Reilly 1980)

Table 3.1 summarizes the general-linear polynomial model structures of the AR, ARX, ARMAX, OE and BJ models (Croarkin et al. 2002; Xue and Chen 2013). In the given formulas, A , B, C, D, E, and F are polynomials of the shift operator, n_u denotes the total number of inputs, and n_k designates the i[th] input delay that characterizes the transport delay (Croarkin et al. 2002). It is worth emphasizing that the existence of shift operator q^{-1} in the models exhibits the fact that we are dealing with a discrete-time model rather than a continuous-time model. Table 3.1 presents different linear polynomial model structures that can be used for assessing the performance of a civil infrastructure based on the site conditions.

Table 3.1 Linear polynomial model structures (Croarkin et al. 2002; Xue and Chen 2013)

Model Structure	Equation
Auto-Regressive Exogenous (ARX)	$A(q)y(t) = \sum_{i=1}^{n_u} u_i(t - nk_i) + e(t)$
Auto-Regressive Exogenous (ARX)	$A(q)y(t) = \sum_{i=1}^{n_u} B_i(q)u_i(t - nk_i) + e(t)$
Auto-Regressive Moving Average Exogenous (ARMAX)	$A(q)y(t) = \sum_{i=1}^{n_u} B_i(q)u_i(t - nk_i) + C(q)\,e(t)$
Output Error (OE)	$y(t) = \sum_{i=1}^{n_u} \frac{B_i(q)}{F_i(q)}u_i(t - nk_i) + e(t)$
Box Jenkins (BJ)	$y(t) = \sum_{i=1}^{n_u} \frac{B_i(q)}{F_i(q)}u_i(t - nk_i) + \frac{C(q)}{D(q)}e(t)$

3.6 Summary

A framework is developed for health monitoring and performance assessment of a bridge infrastructure. The developed framework mainly consists of four major steps including project requirements, developing a monitoring approach using 3D-TLS LiDAR

technology, developing long term ground movement prediction models using system identification approach, and performing validation studies for determining the accuracy of the developed models. The impact of project requirements including project history, site conditions, and bridge infrastructure components on performance assessment of a bridge infrastructure, and the initial and optimized scanning plan is presented respectively. An introduction to the system identification approach is presented along with a step-by-step procedure for developing and validating ground movement prediction models.

The illustration of the developed framework is performed on a rehabilitated soil-geofoam bridge approach embankment located in Cleburne, Texas. The illustration is performed in two parts: performing field operations using 3D-TLS technology and developing prediction models by using the system identification approach, which are presented in chapter 4 and chapter 5, respectively.

Chapter 4: Application of the Developed Framework at the Top of a Bridge Approach Embankment

4.1 Introduction

This chapter presents the illustration of the developed framework using 3D-TLS technology and the system identification approach to assess the performance of a bridge infrastructure. In this study, a rehabilitated soil-geofoam embankment bridge infrastructure located in North Texas was considered. The following sections present the details on test site, project background, site geometry, in-situ instrumentation, evaluating the feasibility of 3D-TLS technique for ground movement data collection, scanning parameters, registration process, and analyses performed to obtain ground vertical movements over the pavement surface of the studied infrastructure.

4.2 Project Site Background

The bridge approach embankment considered in this study was constructed in 1995 and is located in Johnson County, North Texas. The abutments of this infrastructure are supported on drilled shafts, and the approach slab of the bridge was constructed over a 40 ft. high embankment composed of plastic clay. The sides of the embankment and abutment walls are supported by reinforced retaining walls (see Figure 4.1).

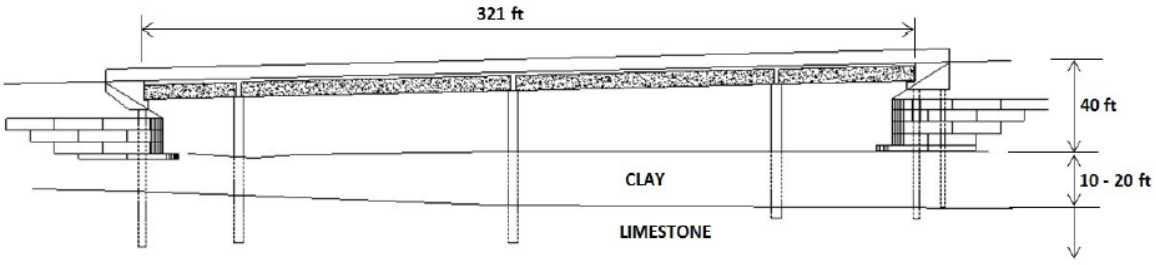

Figure 4.1 Schematic view of the US 67 bridge (Ruttanaporamakul et al. 2016)

The approach slab settled more than 16 inches over a period of 16 years, translating to an average settlement rate of 1 inch per year. The settlement at this site is

primarily due to the consolidation of the embankment and foundation soils (Ruttanaporamakul et al. 2016). Figure 4.2 demonstrates the measured ground vertical displacements at the top of the bridge approach embankment in January 2012 (Ruttanaporamakul 2015).

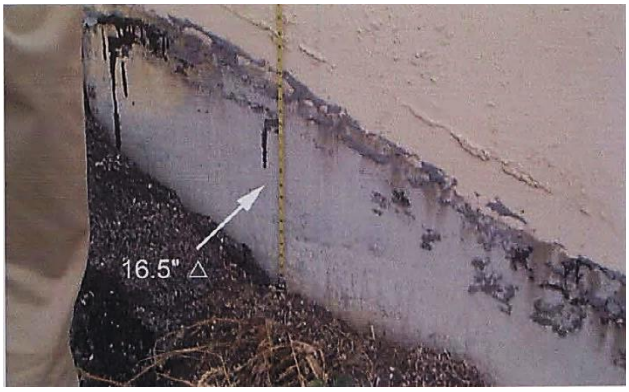

Figure 4.2 Measured ground vertical movements (January 2012) (Ruttanaporamakul 2015)

Several rehabilitation measures, including soil nailing, grout injections, and hot mix overlays, were attempted, but none of the applied techniques were found to be effective in mitigating the differential settlements. This was because all the techniques were not alleviating the overburden pressure, which caused the consolidation settlements of the foundation and embankment soils. In 2012, the top 6 ft of the approach embankment was replaced with lightweight expanded polystyrene (EPS) geofoam blocks, primarily to reduce the overburden pressure (Figure 4.3). The details of the design and construction of this rehabilitated embankment can be found elsewhere (Puppala et al. 2017a; Ruttanaporamakul 2015).

Figure 4.3 Installation of geofoam blocks in January 2012 (Ruttanaporamakul 2015)

4.3 Geometry of the Scanning Area

In this research study, approximately 26,640ft^2 of a bridge infrastructure site was covered using LiDAR surveys. The main intent of performing LiDAR surveys was to monitor vertical displacements over the large pavement area of 4,400ft^2 located at the top of approach embankment. A top view of the test site and monitoring area is depicted in Figure 4.4. The dashed line represents the scanning area under consideration.

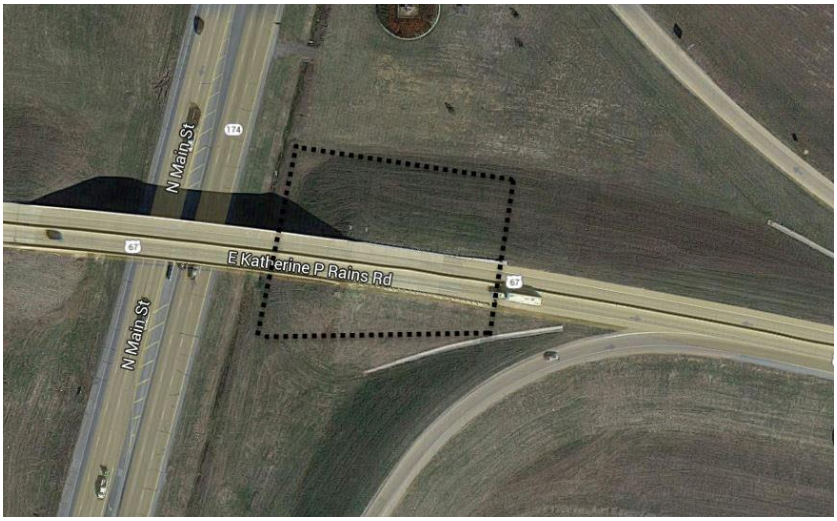

Figure 4.4 Top view of the test site and surveying area

4.4 Site instrumentation

In order to evaluate the performance of the soil-geofoam bridge approach, the test site was monitored using horizontal inclinometers and pressure cells. Four horizontal inclinometer casings were installed on the top of the geofoam layer, which was approximately 2 ft. below the pavement surface. Inclinometer readings were taken monthly from each casing using a data logger. It is worth noting that horizontal inclinometer applications were limited to vertical displacement monitoring along the installed casing sections. So, collected data from the horizontal inclinometer is not adequate for quantifying ground displacements over the monitored pavement area. Figure 4.5 ((a) and (b)) demonstrates a schematic illustration of four inclinometer casing locations and the measuring process of ground vertical movements.

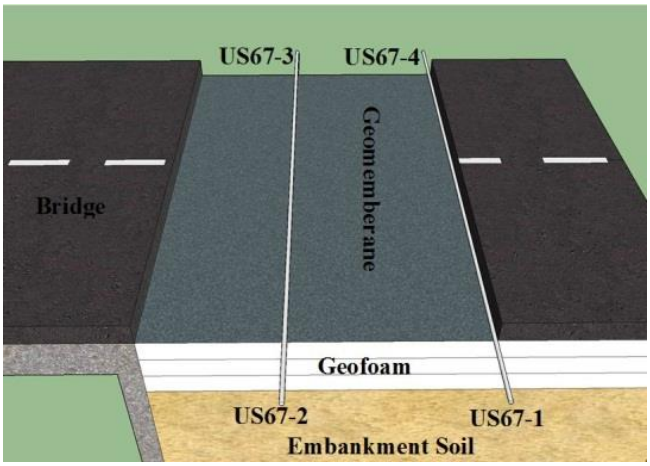

(a)

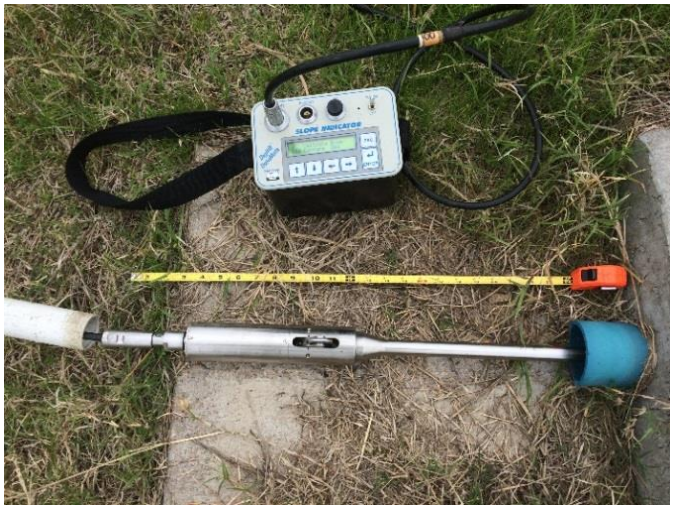

(b)

Figure 4.5 (a) Horizontal inclinometer casing locations; (b) Measuring process of ground vertical movements

Additionally, to monitor vertical and lateral pressures at the top and bottom of the Geofoam layer, four pressure cells equipped with thermometers were installed in the rehabilitated area. Figures 4.6 (a) and (b) represent the pressure cells installed at the top and bottom of the Geofoam blocks to measure the vertical pressures. Figures 4.6 (c) and (d) represent the pressure cells installed on both the abutment and the north wing wall in contact with the Geofoam blocks to measure lateral pressures at their interface.

(a)

(b)

(c) (d)

Figure 4.6 Four pressure cells installed at the bridge approach slab

The pressure cells were connected to a Quattro logger, where the algorithm was set to automatically record the readings for each 15-minute time interval. It shall be noted that the VW Quattro Logger's electronics are impervious to humidity and condensation, which is rated to collect reliable data from -4º to +150º F (Ruttanaporamakul 2015). It is observed that the soil-geofoam bridge embankment has undergone less than 1.5 inches of settlement over the five-year period from January 2012 to December 2016, which is considered as the threshold for the Bump phenomenon. The laterally installed pressure cell on the inside wall of the bridge abutment (Figure 4.6 c) showed occasional negative values. Also, the pressure cell installed at the bottom of the inside of the north wing wall (Figure 4.6 d) stopped working properly, which could be due to loss of contact with the Geofoam layer (Figure 4.7).

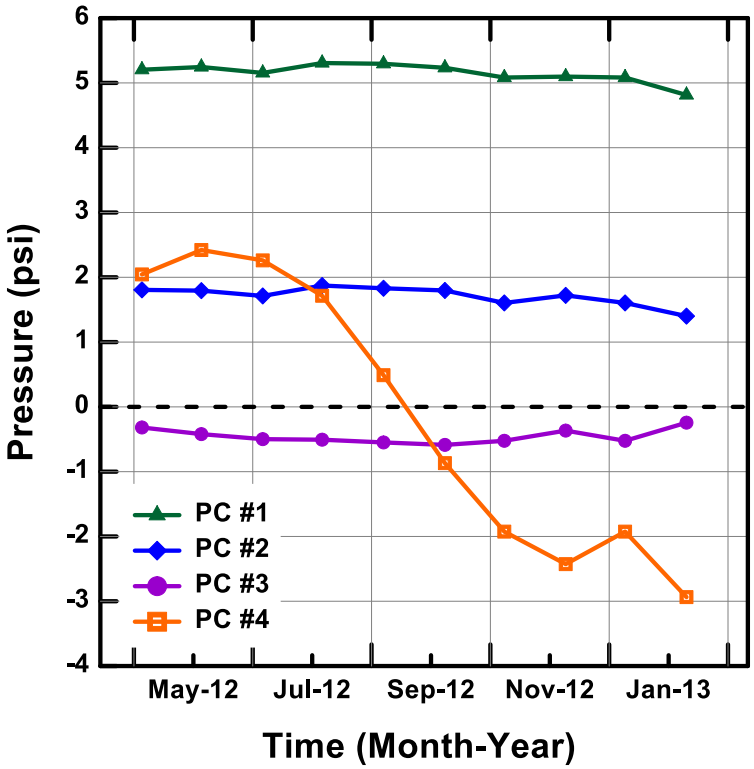

Figure 4.7 Lateral and vertical pressure cell data, 2012

These observations led researchers to analyze the physical interaction between the abutment and wing wall and the Geofoam layer due to temperature variation effects. Since the main objective of this research is to evaluate the performance of the bridge approach slab over a geofoam modified soil embankment with respect to seasonal temperature variations, the temperature variations were recorded in the pressure cells at 15-minute time intervals. Even though the horizontal inclinometer provided the deformation readings, the measurements depict only a specific section along the bridge approach slab. In order to evaluate the deformations on the bridge deck and approach slab, the LiDAR technology was adopted as presented in the following sections.

4.5 Evaluation of the Potential of LiDAR for Ground Movement Data Collection

Since ground movement monitoring over the large pavement area was not feasible using in situ instrumentation techniques, remote sensing surveys were performed using 3D-TLS technology. In this study, long-range scanner technology was used, which was capable of scanning objects up to a distance about 1080 feet from the scanner. Figure 4.8 depicts a scanning survey using the FARO Focus^{3D} X 330 3D terrestrial LiDAR, which is used in this study.

Figure 4.8 Long range 3D TLS LiDAR survey

4.6 Initial Scanning Plan

This section presents the initial scanning plan developed for covering the entire bridge site using 3D-TLS technology. Several site inspections, 3D map analysis, and trial

and error scanning plans were carried out to design an approximately optimized scanning plan for the current test site. The effective factors for the optimized scanning plan consist of required scan parameters for the pavement monitoring purposes, reference points for registration process, and monitoring points for performance evaluation.

For pavement forensic analysis, the minimum required scan point density of 0.1 ft. or less is required at a distance of 125 ft. from the scanner (Caltrans 2011). Accordingly, the LiDAR surveys were scheduled with ¼ resolution and 4x quality. The selected resolution and quality setting provide a point density of 0.07 ft. at the distance of 125 ft. from the scanner (FARO Technologies 2011). Figure 4.9 illustrates the basic working mechanism of a laser scanner and conditions for pavement forensic surveys.

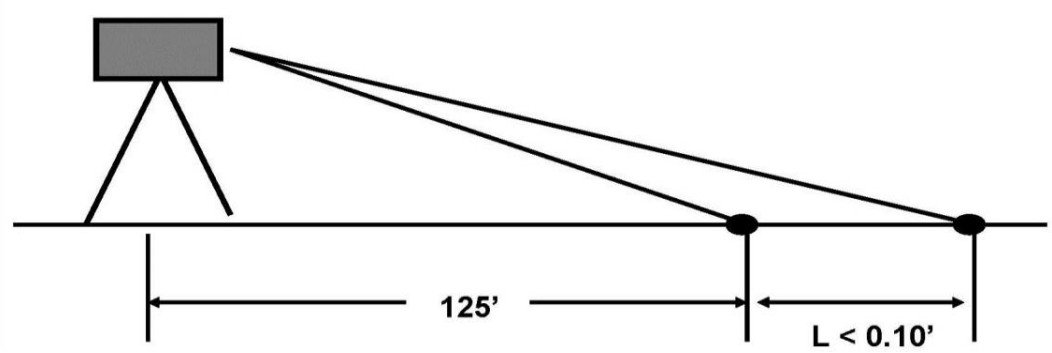

Figure 4.9 Minimum required point density for pavement analysis scans (Caltrans 2011)

In order to perform deformation analysis on the collected point clouds from different time intervals, at least three fixed reference points are required to rotate all the scans to the same coordinate system. In the current project, since the bridge abutments are supported by drilled shaft foundations, a part of the bridge structure close to the abutments was considered as the fixed zone. Thus, small steel anchor bolts were anchored onto the bridge deck to hold eight standard spheres as the fixed reference points (see Figure 4.10).

(a) (b) (c)

Figure 4.10 (a) Anchor bolts, (b) & (c) locations of fixed reference points

According to the different scanning plans, different sets of spheres were used to rotate the collected scans to the same coordinate system after the registration process. However, all eight reference points were covered in all scanning plans to evaluate the accuracy of respective produced digital models after rotating them to the same coordinate system.

Based on the selected scan parameters, reference point locations, visual inspections, and performed trial and error scanning plans, an initial set of 10 scans was scheduled to cover an area of approximately 26,640 ft^2 of the bridge infrastructure test site. It was anticipated that this plan would provide high quality visualization of the test site, which would be beneficial for any future holistic assessments of the bridge infrastructure test site.

Among ten scans, four scans were planned to monitor 100 ft. in length of the pavement surface. Additionally, four scans were considered to cover the side slope embankments and concrete shoulders and two scans were scheduled to record the bridge structure movements. Figure 4.11 (a to c) shows the initial scanning plan and a top view of the test site from the collected scans. In Figure 4.11 (a), the numbers represent the counterclockwise sequence of the scanning plan that was performed at the test site. Scans 1 to 3 and 8 to 10 covered the approach slab pavement and the embankment slopes

(Figure 4.11 a). Whereas, scans 4 to 7 were planned to cover the bridge structure movements.

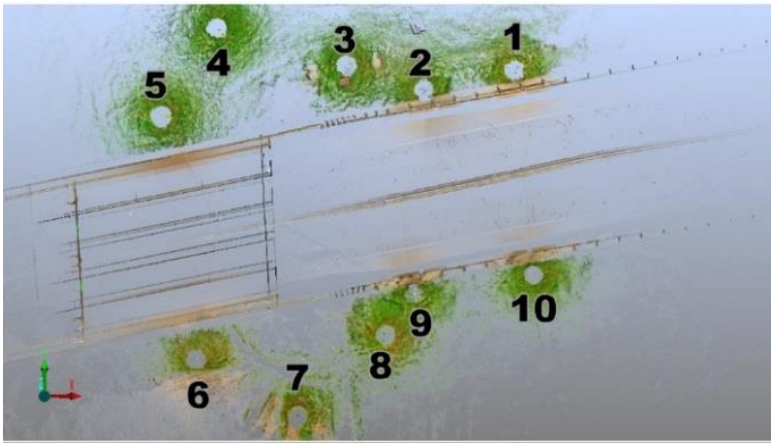

(a)

(a) (c)

Figure 4.11 (a) initial scanning plan (top view), (b) Top view from the processed scans, and (c) satellite top view

Figure 4.11 (b) depicts a top view of the test site from the processed scans. Unlike the satellite top view (Figure 4.11 c), the temperature-induced expansion joint between the bridge structure and the approach embankment and even bridge decks are evident from the top view of the test site from the processed scans (Figure 4.11 b). Performing a scanning survey includes scanner set up for each scan and conducting a set of 10 scans. This process required more than 200 minutes of surveying, which was time consuming and laborious.

4.7 Optimization of LiDAR Scans

In order to increase the accuracy of the collected point cloud and reduce the scanning time period, an attempt was made to reduce the number of scans and to find an optimized scanning plan. Hence, the scan number 3 and 8 were eliminated initially in the third consecutive survey. The scans numbered 3 and 8 were primarily designed to cover the embankment slope surface and to provide a better visualization model of the monitoring area. However, the main purpose of conducting LiDAR surveys was to monitor vertical displacements over the pavement surface.

Figure 4.12 (a) depicts a top view of the monitoring area from the enhanced scanning plan. It is worthwhile to state that the spheres numbered 1, 5, and 7 were used to rotate the digital models produced from the latter two surveys to the same coordinate system of the collected point cloud from the initial survey (Figure 4.12 b & c). The spheres numbered 1, 5, and 7 were utilized as the fixed reference points mainly because they were installed very close to the bridge structure that supported by drilled shaft foundations.

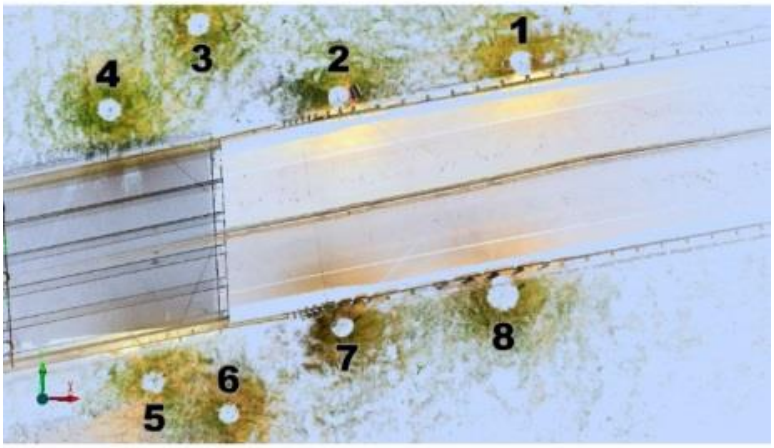

(a)

(b) (c)

Figure 4.12 (a) enhanced scanning plan (top view), (b) & (c) reference points

According to the scanning plan, scans 3 through 6 (Figure 4.12 (a)) were considered to cover the bridge structure and the fix zone, including reference points 1, 2, 5, and 6 (Figure 4.12 (b & c)). An attempt was made to optimize the scanning plan by eliminating scans 3, 5, and 6 (Figure 4.12 (a)) since five scans were likely to be sufficient to cover the entire pavement surface area, bridge deck, and embankment slopes (Figure 4.13).

In order to evaluate the influence of using different reference points during the initial registration process on the accuracy of the produced models from different scanning plans, the scan numbered 1 was retained in the optimized scanning plan to cover the reference points below the bridge structure. It is worthwhile to restate that placing all individual scans to a single project point cloud and aligning them onto a single coordinate system is called registration. Subsequently, two sets of fixed reference points including point numbers 3, 4, 8 and 1, 5, 7 (Figure 4.12 (b & c)) were used to rotate the registered point cloud from the optimized scanning plan to the previously produced model's coordinate system.

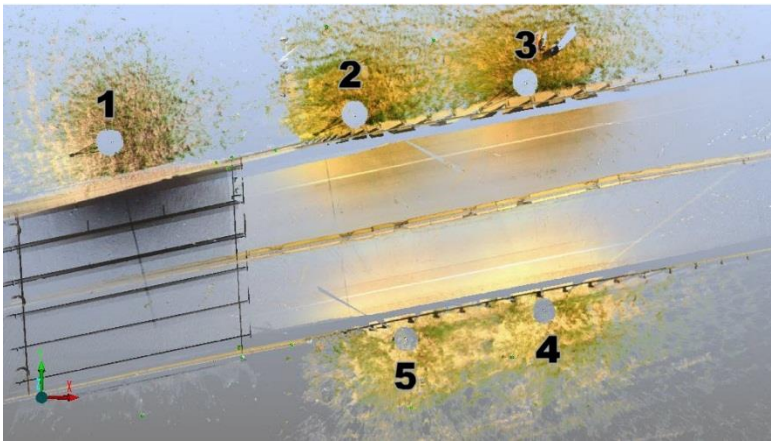

Figure 4.13 Optimized scanning plan (top view)

It is evident that the first two scanning plans, including sets of 10 and 8 scans were registered in a counterclockwise sequence (Figures 4.11 (a) and 4.12 (a)). However, a clockwise registration sequence was performed for the optimized scanning plan comprises of 5 scans (Figure 4.13).

4.8 Registration Process and Cloud-to-Cloud Registration Updates

A target-based registration approach was performed initially to facilitate and expedite the registration process for each set of scans. Several cloud-to-cloud registration updates were performed to achieve the maximum possible accuracy of the point cloud. Several combinations of cloud-to-cloud registration settings were attempted to achieve the highest possible accuracy (Figure 4. 14 (a to c)).

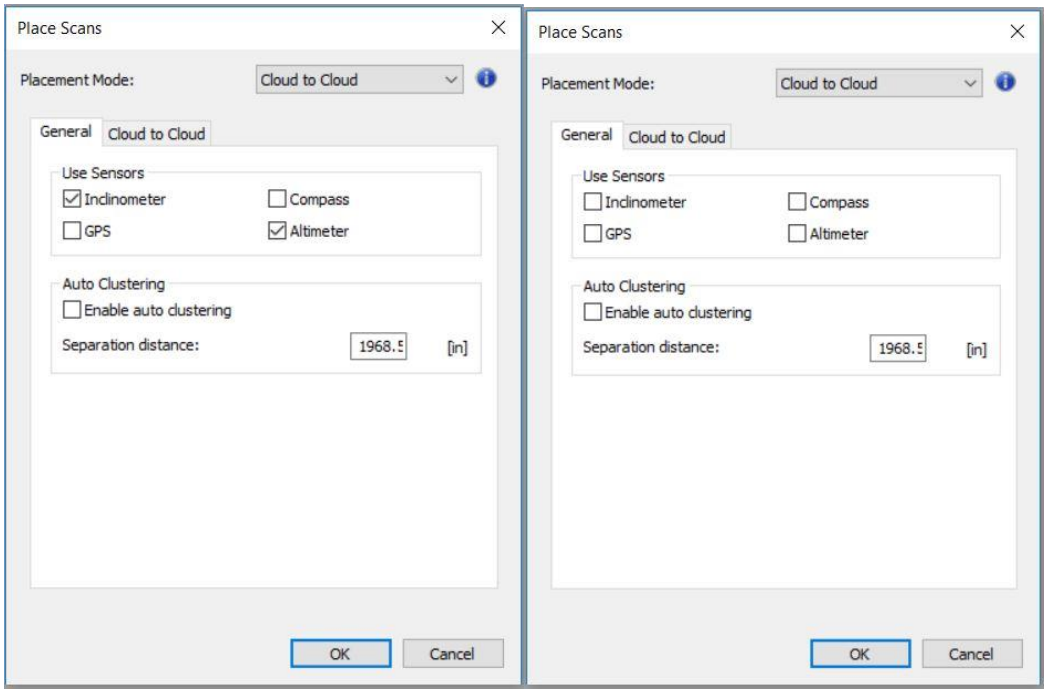

(a) (b)

Figure 4.14 Cloud to cloud scanning update settings

It was recommended that more accurate point cloud registration can be accomplished by using digital inclinometer and altimeter data resources rather than the collected data from the digital GPS and compass within the scanner (FARO Technologies 2011). Subsequently, overall mean scan point tension values of less than 0.15 in. were achieved after the cloud-to-cloud registration update process was performed for all sets of scans. Figure 4.15 depicts overall statistics of an updated point cloud with 0.1133 in. of mean scan point tension value.

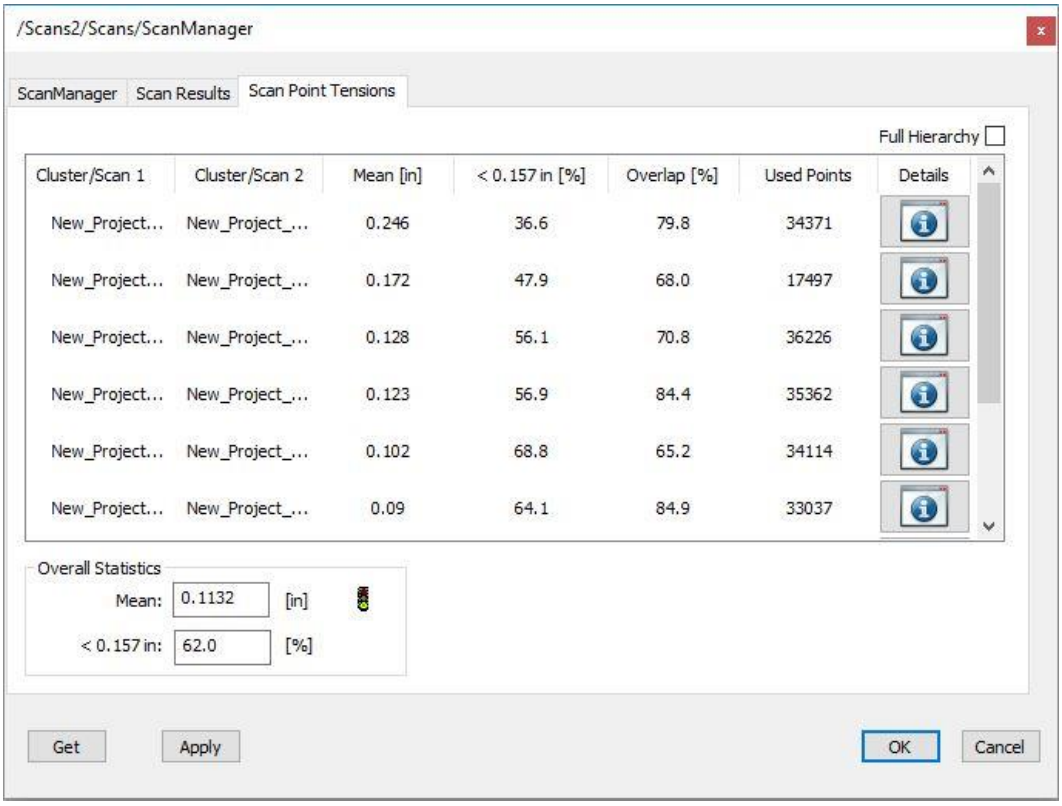

Figure 4.15 Over all mean scan point tension of less than

After conducting several periodic LiDAR surveys, all the registered point clouds were rotated to a single coordinate system. Detailed information about this step is provided in the next section.

4.9 Rotating Scans to the Same Coordinate System

After the registration process, at least three fixed reference points were required in all the registered point clouds to rotate them to the same coordinate system. Since the bridge abutments are supported by drilled shafts, a part of the bridge structure close to the abutments was considered as the fixed zone. Thus, small steel anchor bolts were planted and affixed to the bridge deck to hold eight standard spheres of radius 4.5 in. as the fixed

reference points (see Figure 4.12). The spheres were used for both the registration process and for rotating scans to the same coordinate system.

A negligible error of less than 0.002% was calculated after the rotation of scans into the same coordinate system. The accuracy of the rotated sets of scans was controlled by the selection of ten similar random points from all sets of scans. The distance of each point was calculated from the origin of each survey coordinate system, then the error was estimated for each rotated point cloud by comparing the distances of selected points from the origin. The first scan survey performed in April 2016 was considered as the reference data set for performing movement analysis of the embankment during subsequent time periods.

4.10 Selection of Monitoring Points

More than 850 monitoring points were selected and analyzed for assessing the vertical movements at the top of the approach slab pavement, concrete shoulders, and bridge deck, as shown in Figures 4.16 (a & b).

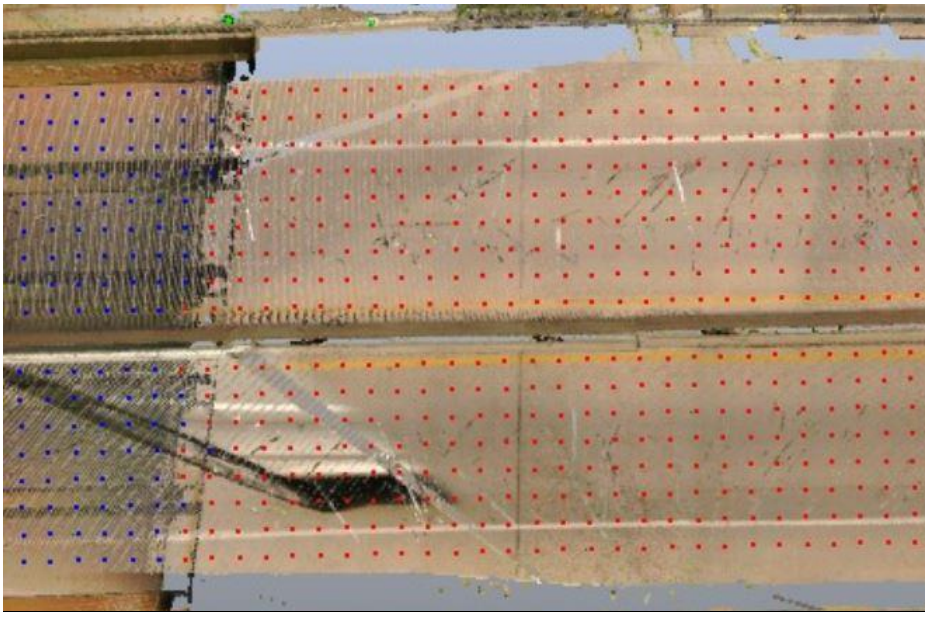

(a)

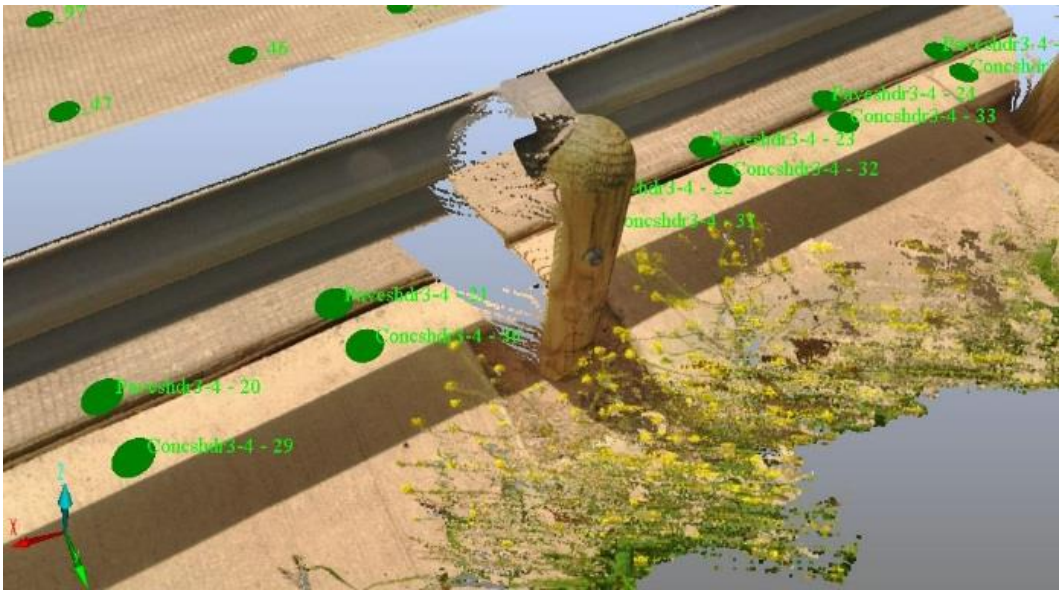

(b)

Figure 4.16 (a) Monitoring points at the top of the pavement surface and (b) concrete shoulders

Preliminary analysis depicted different elevations at the top of the pavement, bridge deck, and the approach slab monitoring zones. Graphical representation of the processed scans (known as heatmap) of the approach embankment and the bridge structure is presented in Figure 4.17.

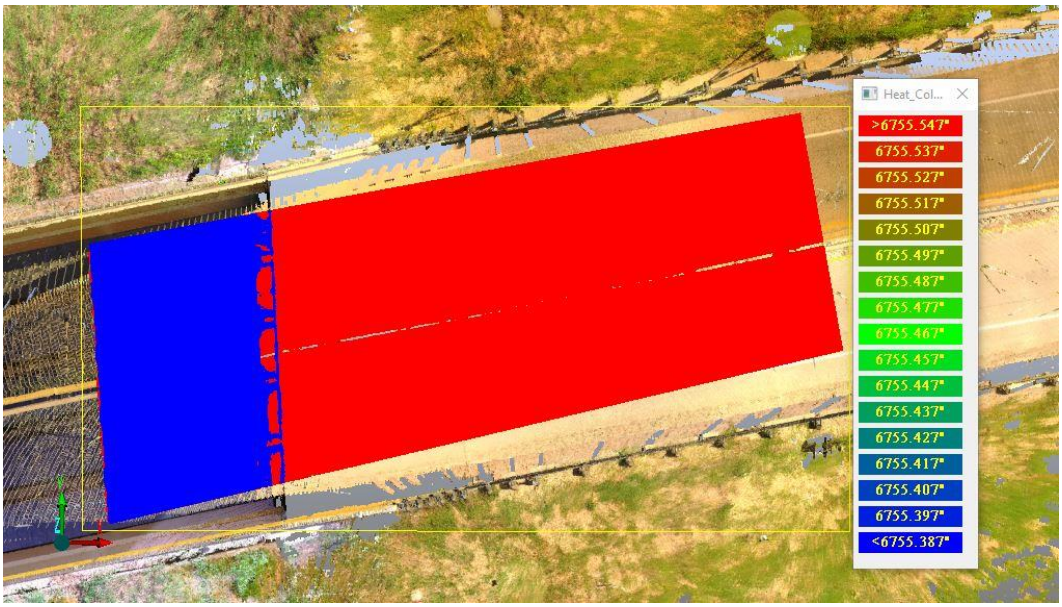

Figure 4.17 Heat color map of the total elevations (in.)

The red zone in Figure 4.17 represents the monitoring area at the top of the approach embankment, and the blue zone demonstrates the monitoring area at the top of the bridge deck. Based on the evaluated total elevations, it is evident that the bridge deck pavement surface has lower elevations than the approach slab pavement surface.

4.11 Evaluate Ground Movements for Periodic Surveying Intervals

Periodic vertical ground movement evaluation was performed at the top of the pavement surface. Approximately 100 ft. of pavement over the bridge deck and the bridge approach embankment was surveyed for vertical deformations. In Figure 4.18, sections A-A and B-B demonstrate a graphical visualization of the longitudinal monitoring sections.

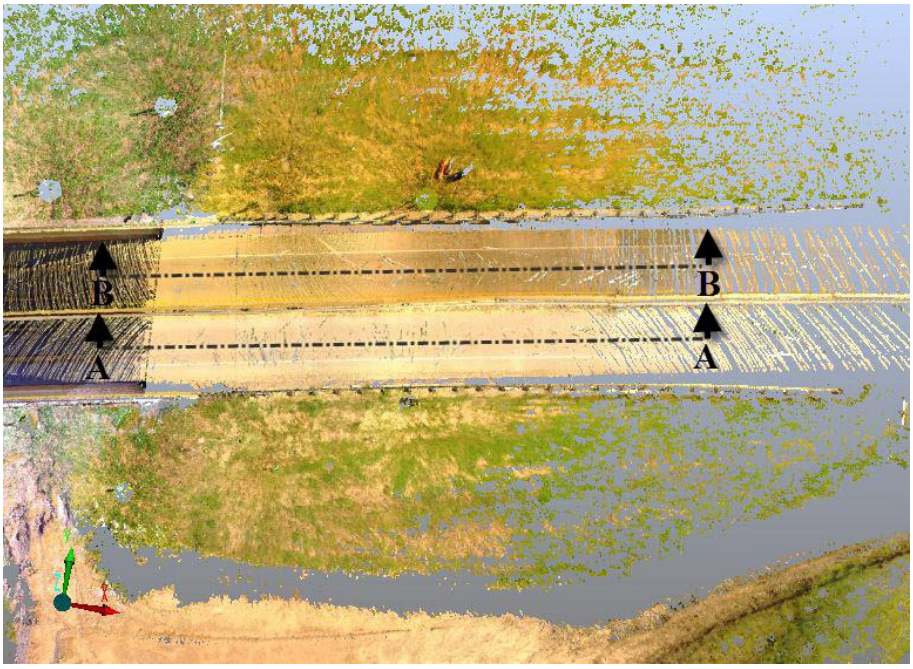

Figure 4.18 Longitudinal monitoring sections

A graphical representation of the measured ground vertical movements over the pavement surface from April to July 2016 is shown in Figure 4.19 ((a) & (b)). Ground movement analysis on the bridge approach embankment from April to May 2016 revealed that heaving had occurred at the bridge approach embankment (Figure 4.19 (a)). However, cumulative total vertical movements at the top of the pavement from April to July 2016 showed that one lane had undergone heaving and the other lane had experienced settlement.

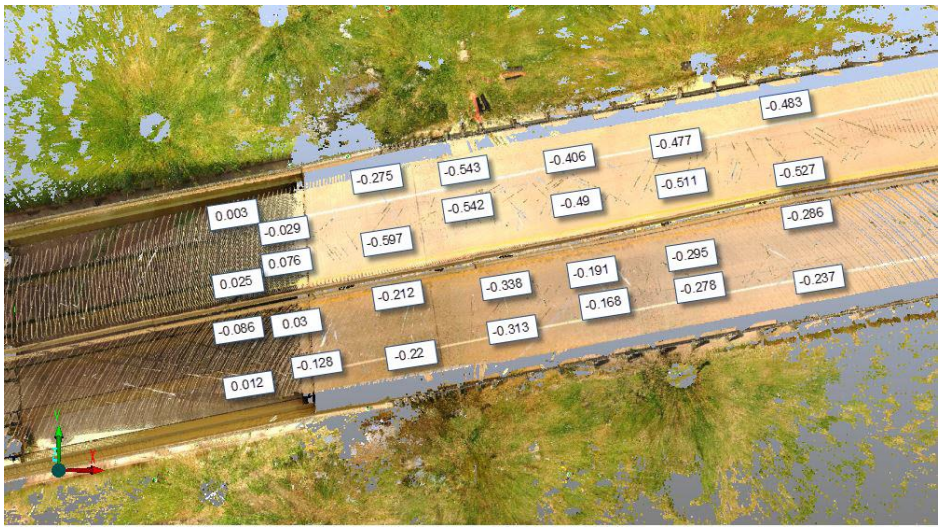

(a)

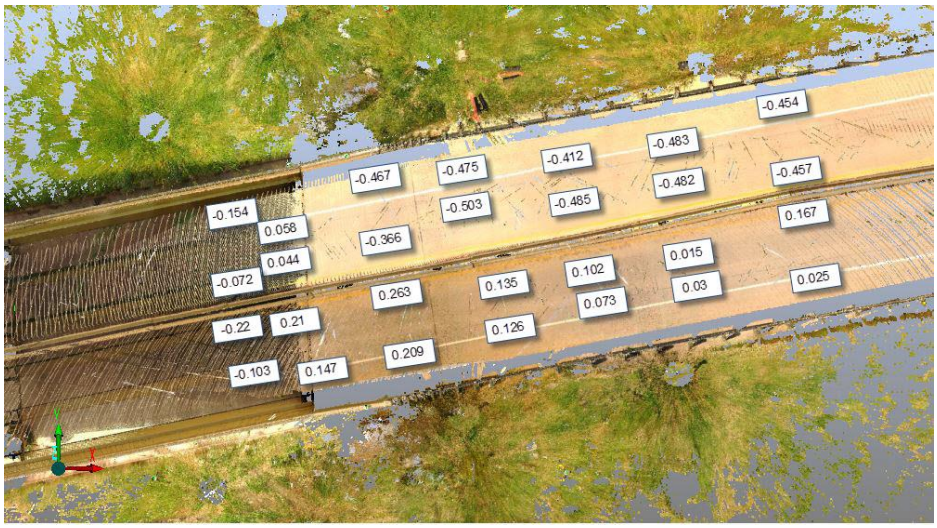

(b)

Figure 4.19 Vertical deformations (in.) (a) April - May 2016 and (b) April - July 2016

It should be noted that the negative values in Figure 4.19 represent heaving and positive values indicate settlement. Measured ground vertical movements in Figure 4.19 are presented in inches. Figures 4.20 (a) and (b) represent a comparative analysis on

vertical movements along sections A-A and B-B for the center line of both US 67-N and US 67-S lanes during the four months from April to July 2016.

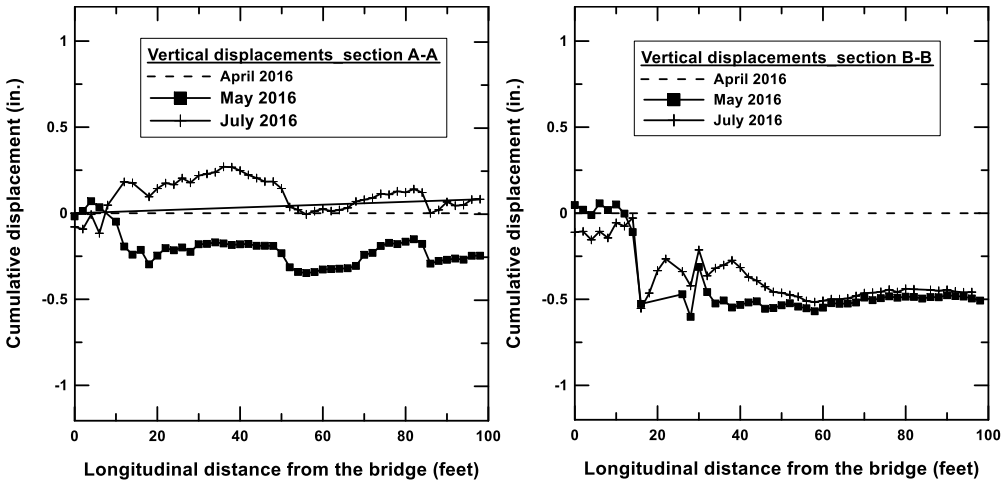

(a) (b)

Figure 4.20 (a) Vertical displacements at section A-A, (b) Vertical displacements at section B-B from the processed scans

In Figure 4.20, the horizontal axis represents the distance from the bridge in inches, and the vertical axis presents cumulative vertical movements in millimeters. Y=0, in both Figures 4.20 (b) and (b), represents the reference date, April 2016, when the first set of scans was performed. The first four meters represent the vertical movements at the top of the bridge deck pavement surface. An abrupt change in the vertical movements from X = 4.3m is observed from the analysis. This section represents the bridge approach embankment (expansion joint). The vertical movements on the bridge structure were smaller than those of the approach slab. This is because the bridge deck is supported on drilled shafts, where the environmental effects are minimal compared to those of the approach slabs, which are underlain by embankment and foundation soils. The swell-shrink

behavior of a moderately plastic clay embankment is more evident from the deformation analysis at the top of the approach embankment pavement surface.

4.12 Validation of LiDAR Data

The reliability of the processed scans was assessed by comparing their magnitudes with the observed vertical movements depicted by the horizontal inclinometer surveys. It should be noted that the horizontal inclinometer data was collected simultaneously with the scanning surveys. Studies on the inclinometer probes show a system accuracy of 0.1 to 0.25in. per 100ft of casing (Machan and Bennett 2008). However, both sets of scans were registered and processed with errors less than $\pm$ 0.078 in.. Figures 4.21 (a) to (d) display vertical movements from both the inclinometer data set and processed scans from April to May 2016.

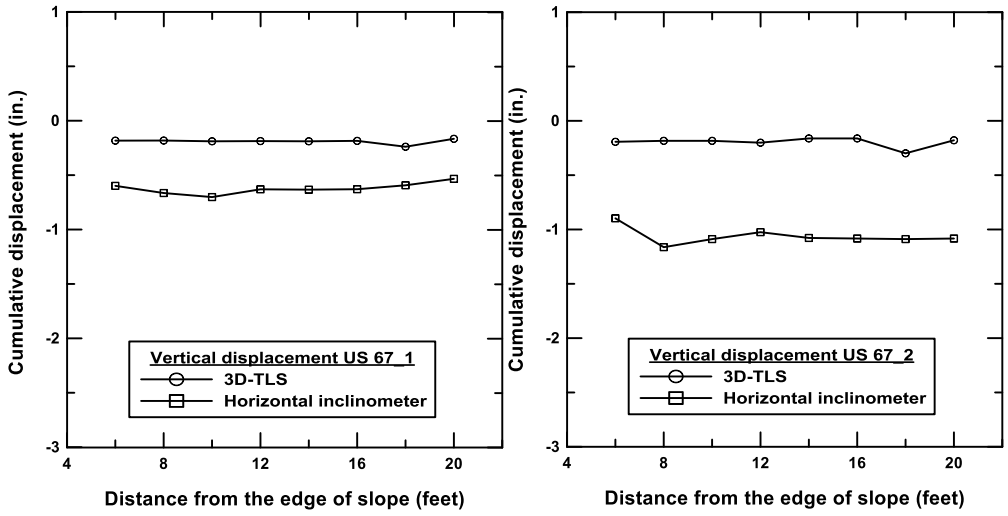

(a) (b)

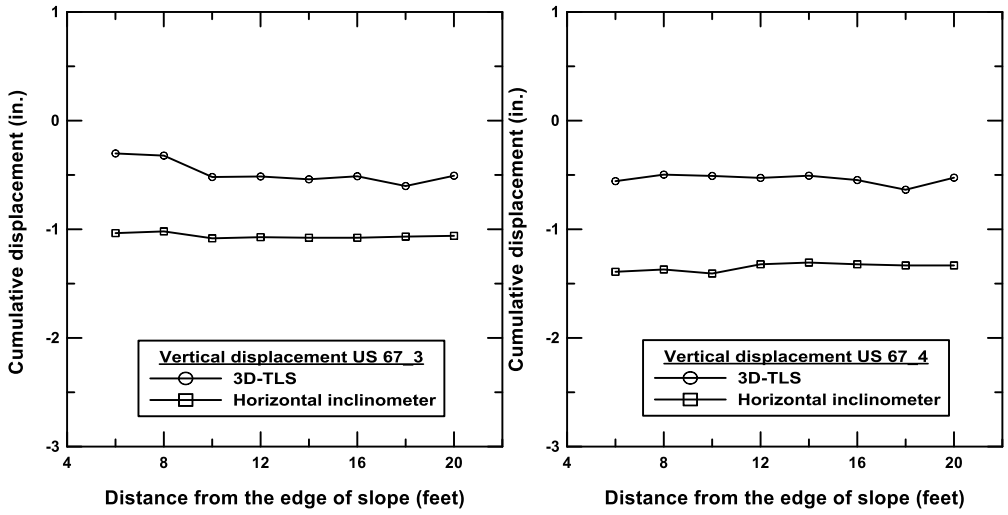

(c) (d)

Figure 4.21 Vertical movements from April 2016 to May 2016: (a) US 67-1, (b) US 67-2, (c) US 67-3, and (d) US 67-4

Inclinometer data depicted vertical movements at the bottom of the pavement, whereas the processed scans from LiDAR showed vertical movements of the four stations at the top of the pavement. It shall be noted that the comparison studies for the movements from horizontal inclinometer and LiDAR studies limits to only trend in the data rather than magnitudes. This is because the magnitude of the movement at the bottom of the pavement may not be completely reflected on the top of the pavement.

It is apparent from Figure 4.21 that both the horizontal inclinometer and LiDAR data sets exhibited swelling from April to May 2016. The average swell displacement obtained by the horizontal inclinometer at the top of the geofoam blocks was 0.97 in.; whereas, the processed scans showed less than 0.4 in. average swell at the top of the pavement. Figures 4.22 (a) to (d) present data from the inclinometer and LiDAR surveys from May to July 2016.

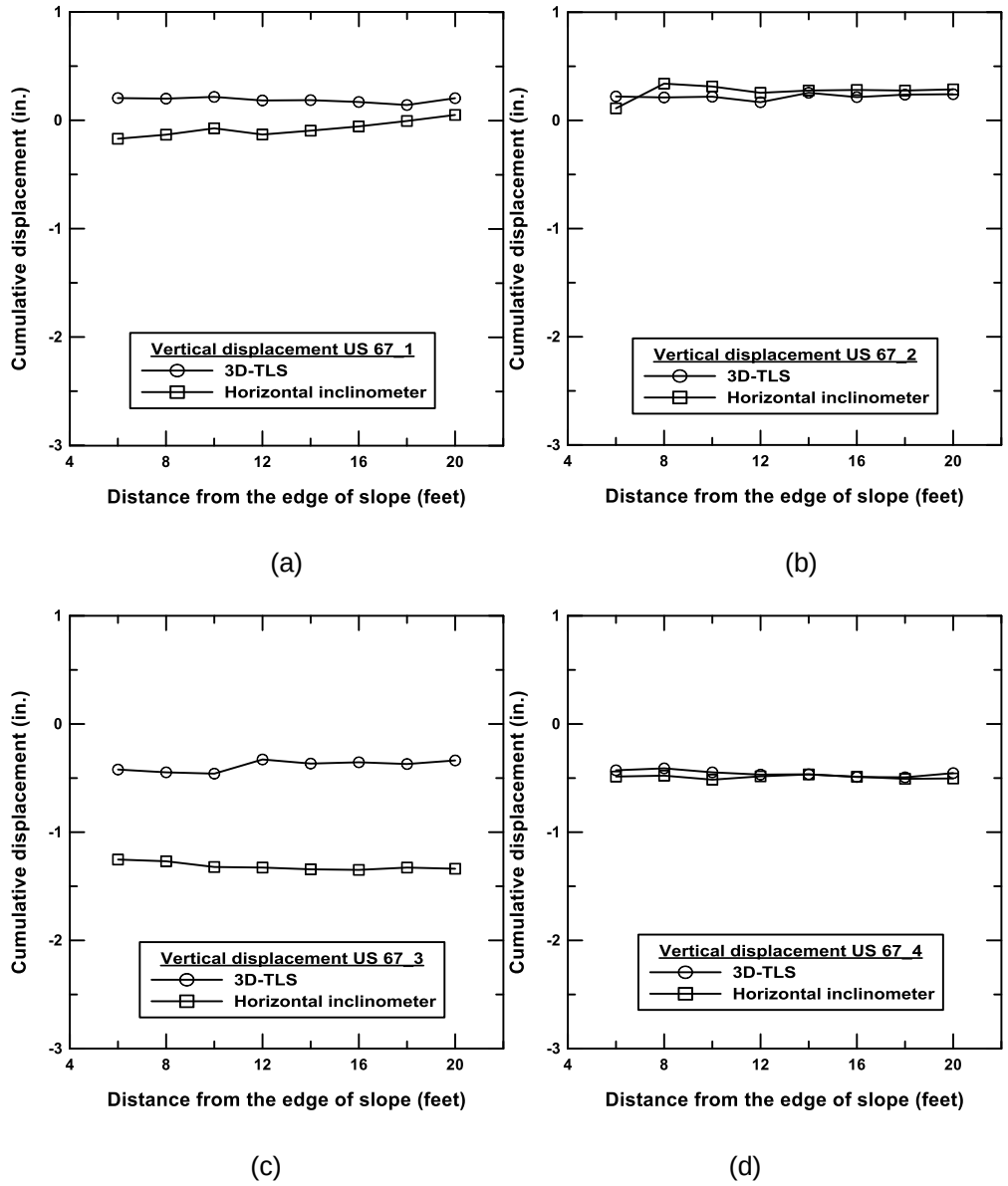

Figure 4.22 Vertical movements from April 2016 to July 2016: (a) US 67-1, (b) US 67-2, (c) US 67-3, and (d) US 67-4

Compared with Figures 4.21 (a) and (c), it is evident that Figures 4.22 (b) and (d) show closer magnitudes for the measured vertical displacements from the LiDAR surveys

and horizontal inclinometer casings. However, all the plots consistently present similar types of vertical displacement (swelling or settlement) captured from the applied methods.

The variations between the magnitudes of measured displacements can be attributed to the different stress-strain behaviors of the rigid pavement and underlying geofoam material (Puppala et al. 2017b, 2018). The data from the horizontal inclinometer showed that more than 1.2 in. of heave was observed during one month at US 67-3 and US 67-4. The deformation tolerance must have been visually evident at the top of the pavement; however, no vertical displacements were observed over the pavement surface during the visual inspection. Hence, it can be concluded that vertical deformations at the top of geofoam blocks cannot represent the deformations at the top of the pavement surface.

Both lanes (US 67 N and US 67 S) experienced heaving from April to May 2016. From May to July 2016, US 67 S experienced negligible vertical movements, but US 67 N underwent noticeable settlements. A comparison between the results from both 3D-TLS and horizontal inclinometer techniques (Figures 4.21 and 4.22) revealed that 3D-TLS technology is a reliable technique for use in evaluating vertical movements at the top of the pavement surface.

4.13 Summary

The reliability of the 3D terrestrial LiDAR technology was evaluated for monitoring of small ground surface vertical movements. The application of the framework was demonstrated by performing the field surveys and analysis on a bridge infrastructure located in North Texas.

Approximately, 26,640 ft^2 of the bridge infrastructure was covered by performing 3D-TLS surveys. Optimization studies revealed that by using artificial targets, the number of scans can be significantly decreased. In the performed analysis of a bridge

infrastructure, the number of scans were significantly decreased from ten to five using artificial targets. This reduction in number of scans still yielded the desired quality for evaluating vertical movement and increased efficiency of field surveys.

More than 800 test points from the processed scans were analyzed over the pavement surface of approach slab and bridge deck without any interruption to traffic. The analysis performed depicted both heave and shrink phenomenon corresponding to different seasonal changes (Shafikhani et al. 2017, 2018b). The trend in the vertical movements determined from 3D-TLS technology were compared and validated with the movements determined from the horizontal inclinometers. Both depicted heave-shrink phenomenon, whereas the 3D-TLS technology provides the data over a wider area, rendering a more reliable assessment of the condition of the bridge infrastructure.

The next chapter provides model identification process of vertical movements at the top of the bridge approach embankment and a mathematical prediction model for ground vertical movements is suggested for potential future concerns.

Chapter 5: Development of Ground Movement Prediction Model

5.1 Introduction

This chapter presents the implementation of the developed framework for predicting ground vertical movements at the top of a rehabilitated bridge approach embankment located at US 67 highway over SH 174, in Cleburne, Texas. The illustration of the developed framework for prediction of ground movements is comprised of three main steps including data acquisition, developing a ground vertical movement prediction model, and validation of the developed model. The database employed to develop and validate the ground movement prediction model is presented in the acquisition step. A detailed illustration of the model identification approach is presented in the autoregressive analysis section. Validation studies is performed by comparing the ground movements from the developed models to actual measurements and predictions from established models in the literature. Detailed information about the data acquisition using different monitoring techniques is presented in the next section.

5.2 Data Acquisition

This section presents the database compiled and utilized for the development of a ground movement prediction model of a slightly over consolidated embankment (OCR=3) soil at US 67 test site. The time-series database at this site consists of measurements of horizontal inclinometer movements, pressure cell readings, temperature and precipitation data from nearby local weather station, and vertical ground movements obtained from LiDAR. Ground vertical movements were monitored monthly from the installed horizontal inclinometer casings below the pavement system. It should be noted that an inclinometer survey consists of collected ground vertical movements from two passes of the inclinometer probe through the installed casings (Figure 5.1).

Figure 5.1 Horizontal inclinometer survey

Figure 5.2 to 5.6 depicts the cumulative ground vertical movements from the horizontal inclinometer casings measured from January 2012 to December 2016.

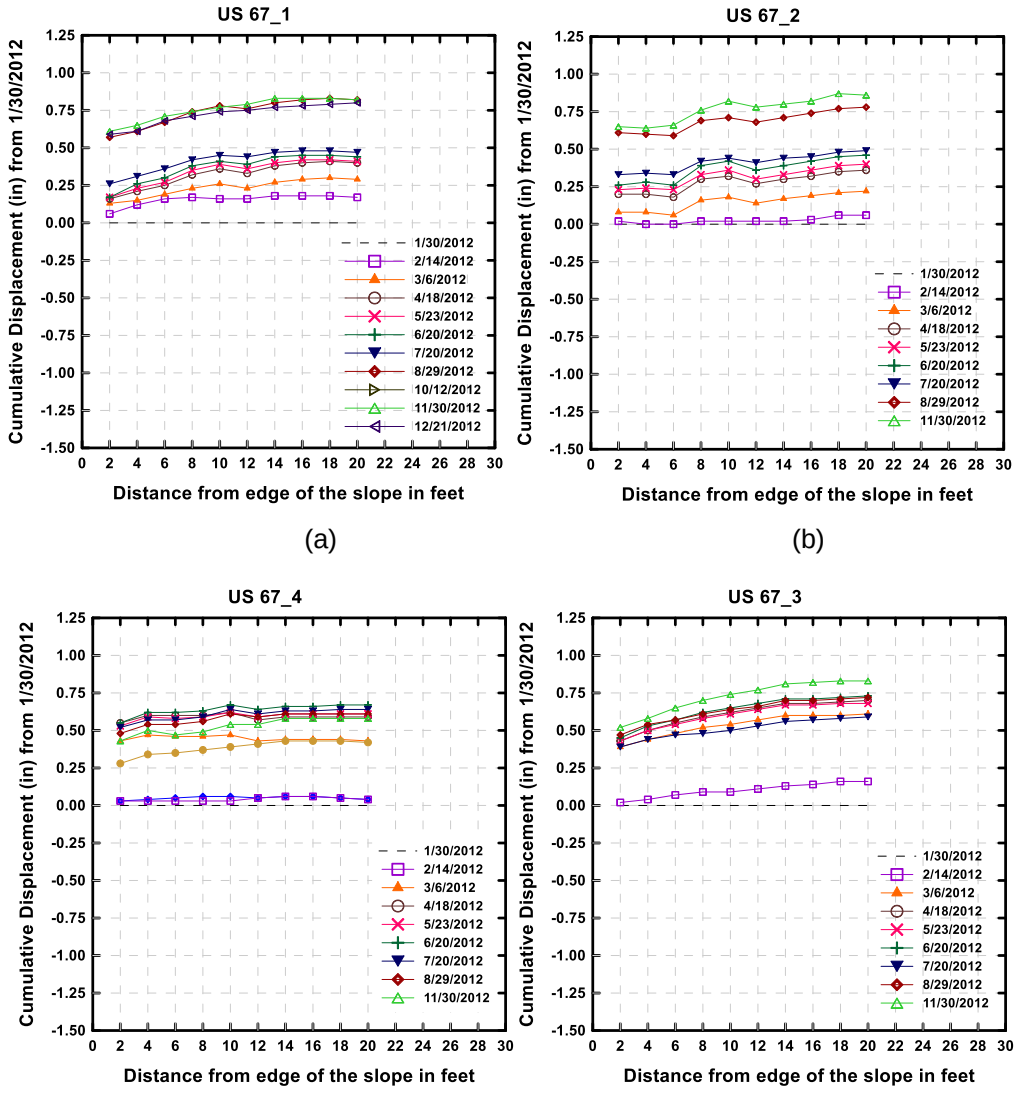

Figure 5.2 Year 2012 measured cumulative ground vertical movements (a) US67-1, (b) US67-2, (c) US67-3, and (d) US67-4

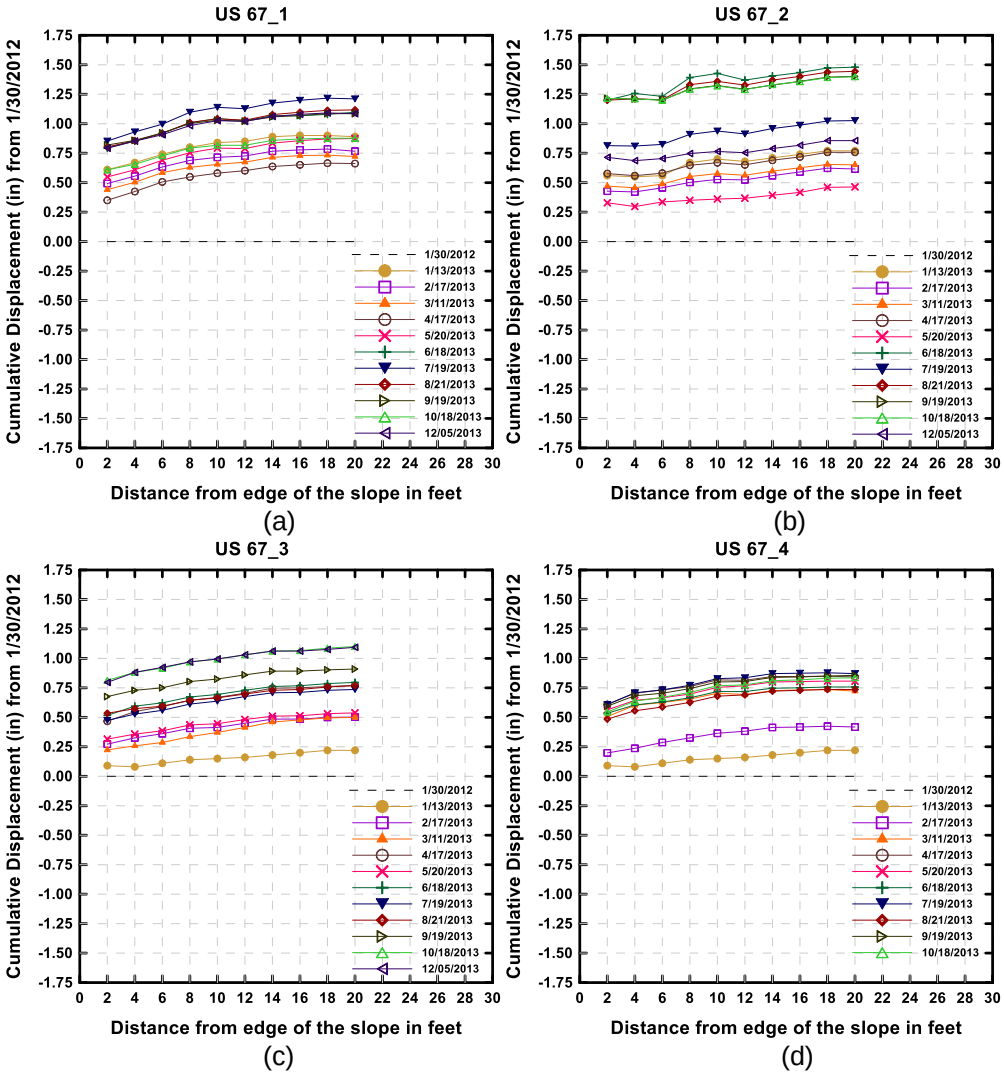

Figure 5.3 Year 2013 cumulative measured ground vertical movements (a) US67-1, (b) US67-2, (c) US67-3, and (d) US67-4

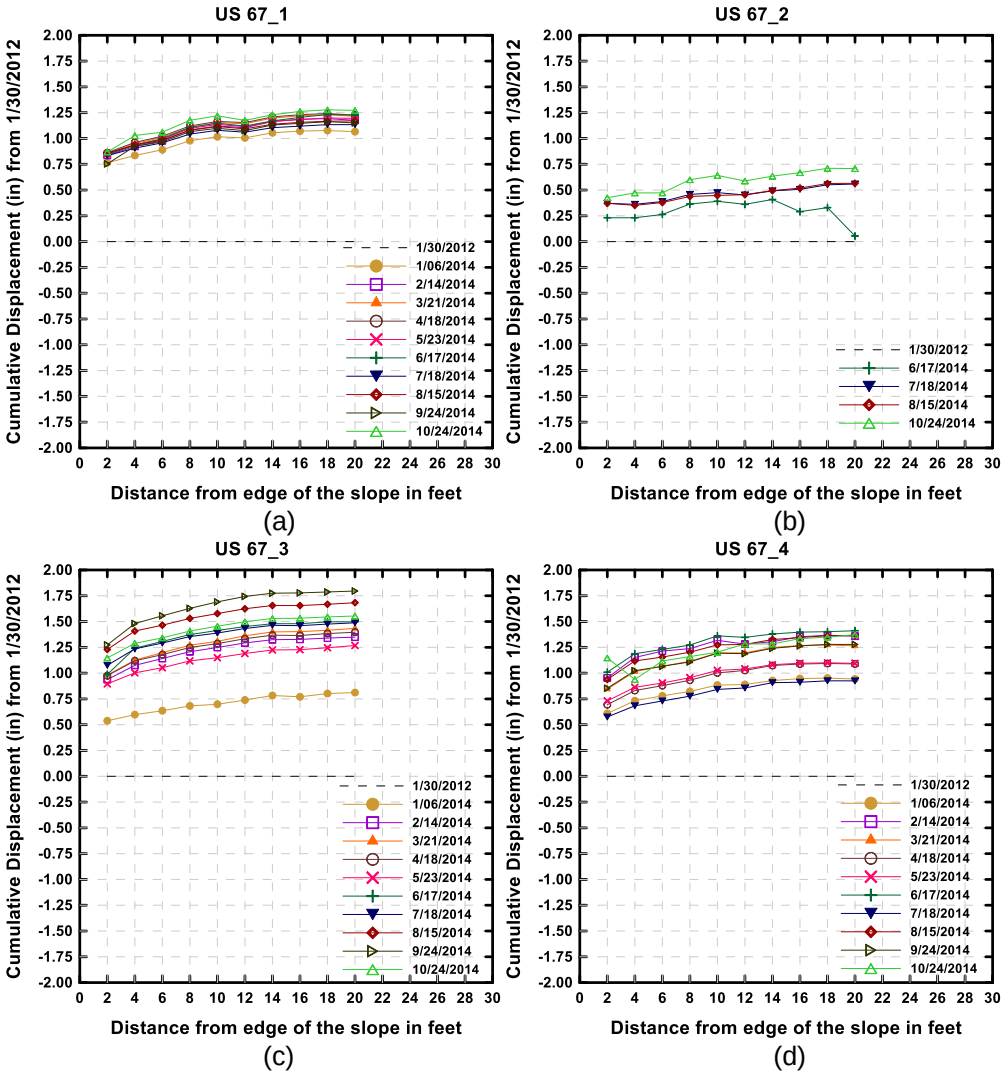

Figure 5.4 Year 2014 cumulative measured ground vertical movements (a) US67-1, (b) US67-2, (c) US67-3, and (d) US67-4

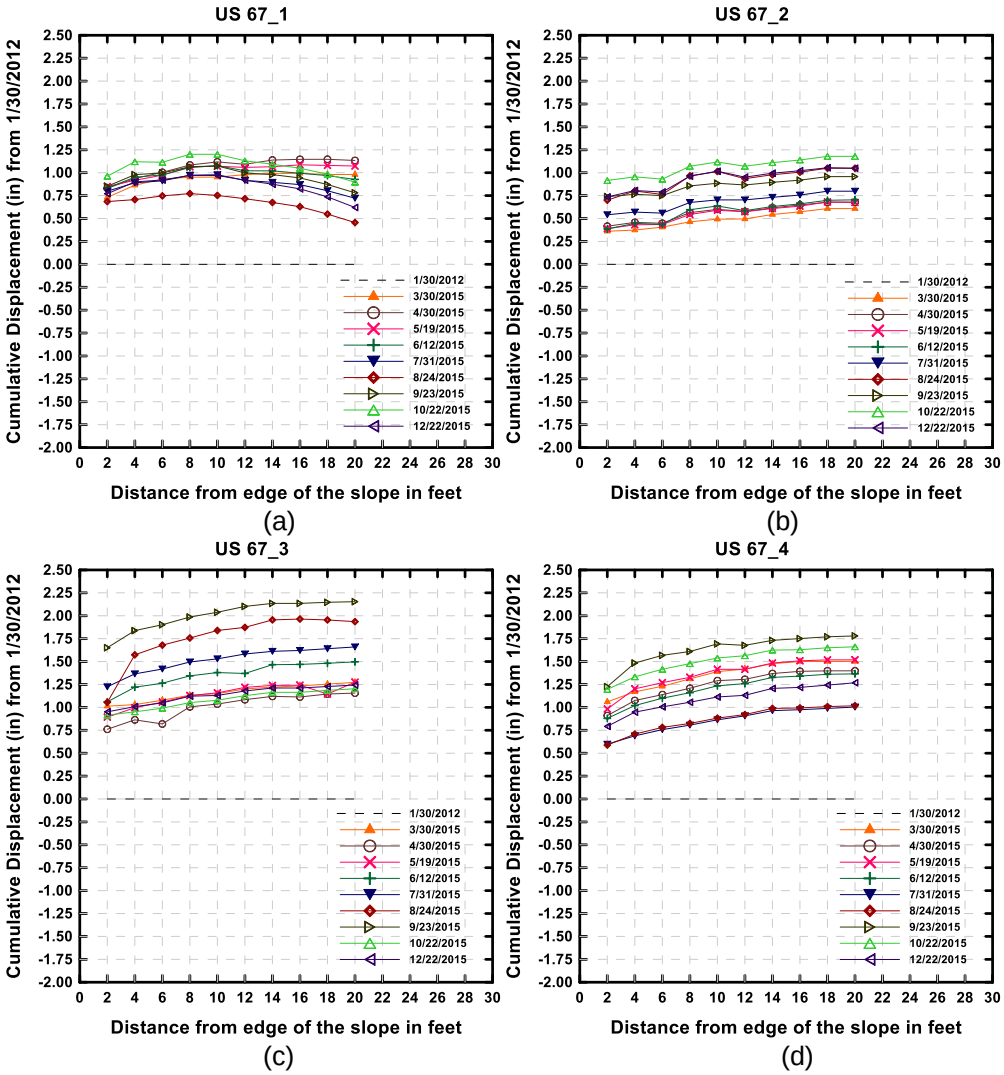

Figure 5.5 Year 2015 cumulative measured ground vertical movements (a) US67-1, (b) US67-2, (c) US67-3, and (d) US67-4

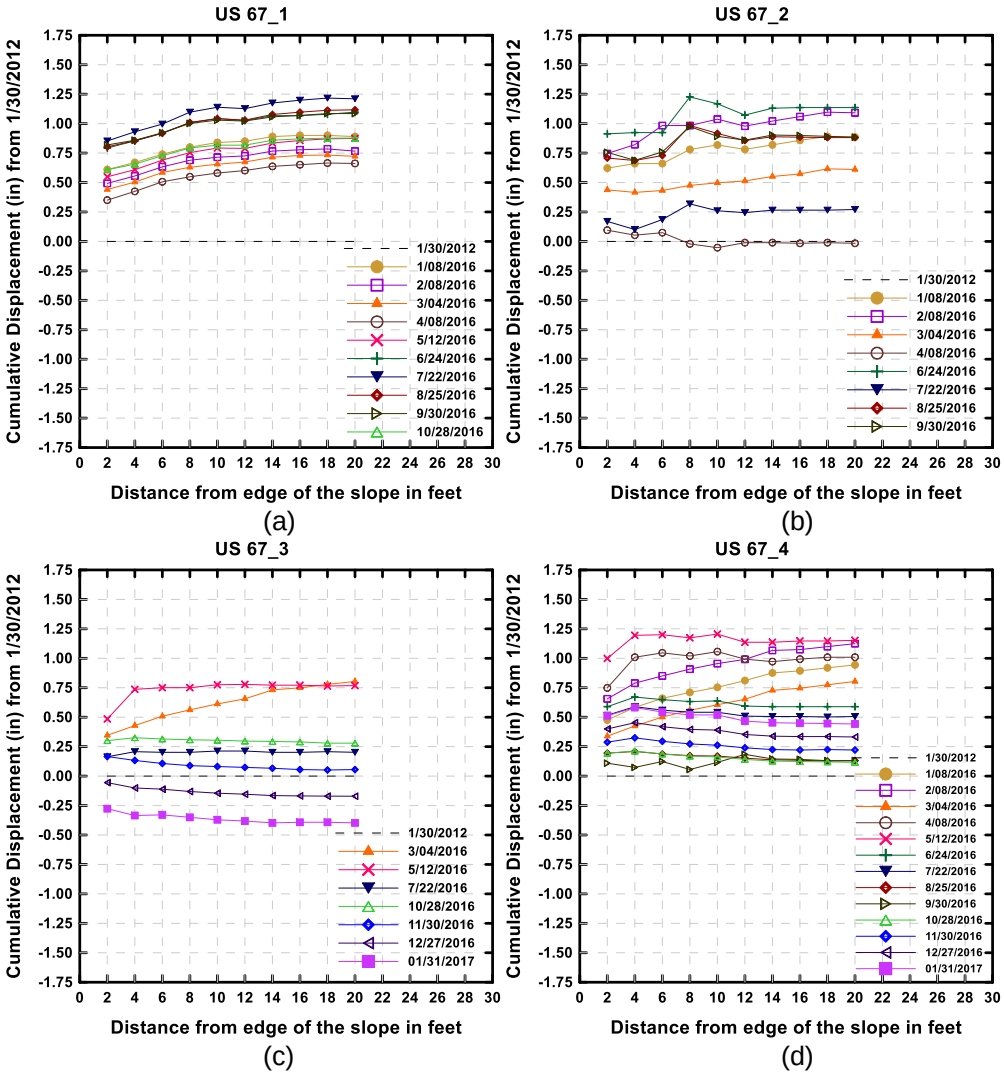

Figure 5.6 Year 2016 cumulative measured ground vertical movements (a) US67-1, (b) US67-2, (c) US67-3, and (d) US67-4

In the Figures 5.2 to 5.6, the X-axis represents the distance from the edge of the approach embankment and the Y-axis demonstrates cumulative ground vertical movements in inches. Vertical pressures from the traffic load and pavement system were also recorded by using the installed pressure cells at the bottom of the pavement system and geofoam layer. Figure 5.7 ((a) to (e)) demonstrates the collected vertical pressures from January 2012 to December 2016.

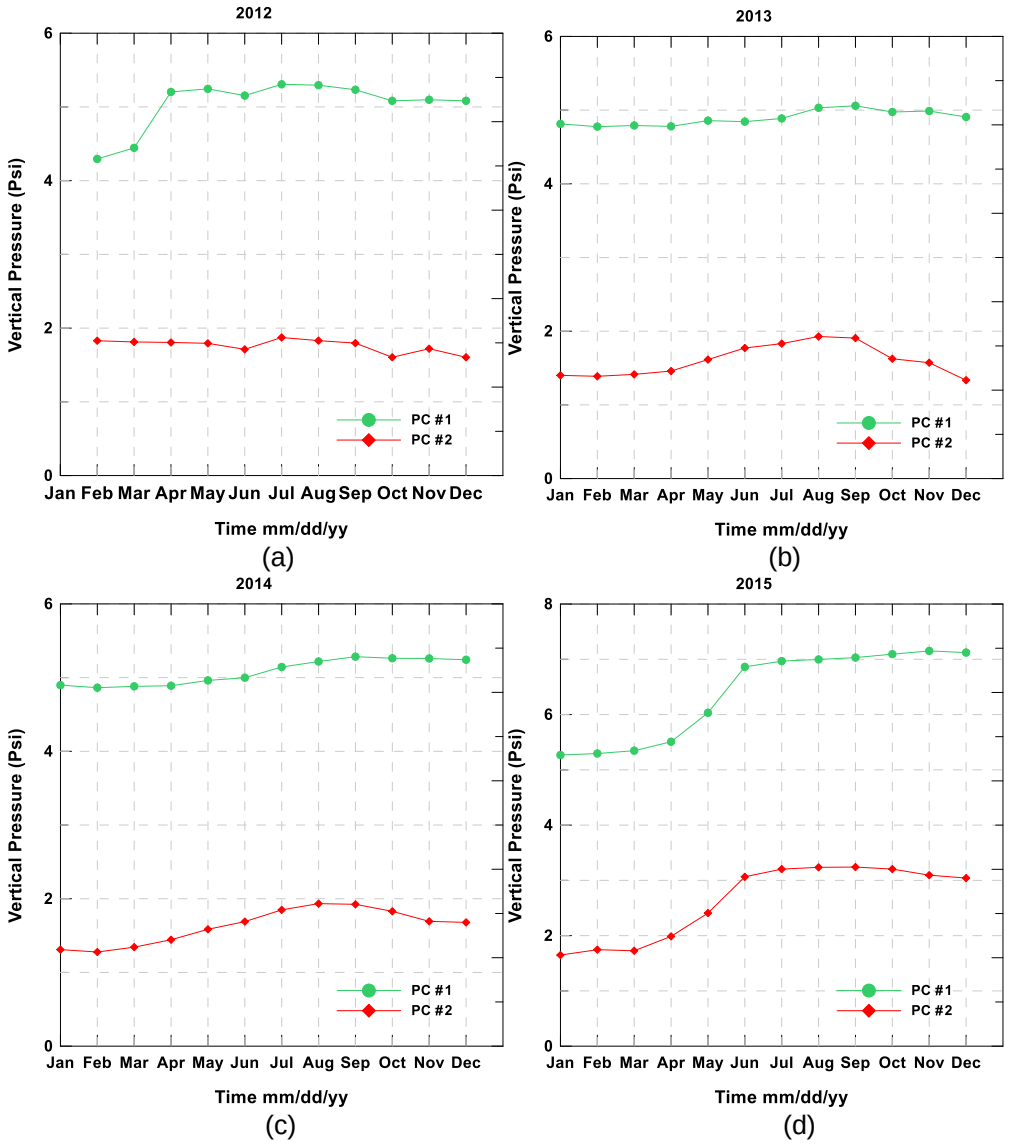
2012
Vertical Pressure (Psi)
Jan Feb Mar Apr May Jun Jul Aug Sep Oct Nov Dec
Time mm/dd/yy
PC #1
PC #2
(a)
2013
Vertical Pressure (Psi)
Jan Feb Mar Apr May Jun Jul Aug Sep Oct Nov Dec
Time mm/dd/yy
PC #1
PC #2
(b)
2014
Vertical Pressure (Psi)
Jan Feb Mar Apr May Jun Jul Aug Sep Oct Nov Dec
Time mm/dd/yy
PC #1
PC #2
(c)
2015
Vertical Pressure (Psi)
Jan Feb Mar Apr May Jun Jul Aug Sep Oct Nov Dec
Time mm/dd/yy
PC #1
PC #2
(d)

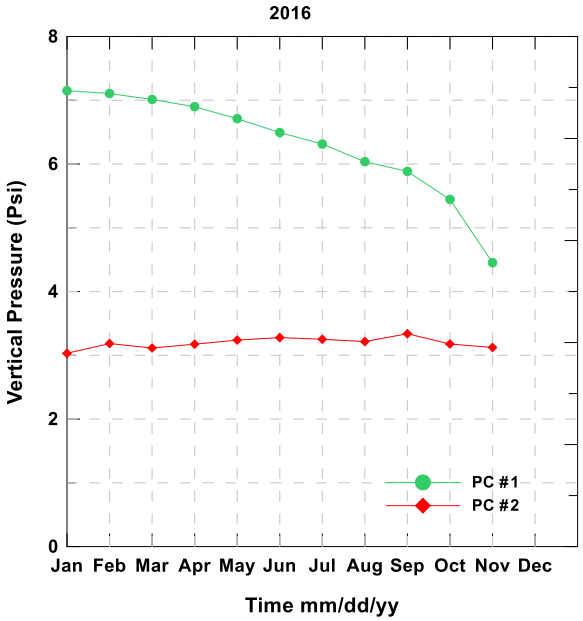

(e)

Figure 5.7 Vertical pressure at the top and bottom of the geofoam layer, (a) 2012, (b) 2013, (c) 2014, (d) 2015, and (e) 2016

In Figure 5.7, pressure cell number 1 (PC #1) depicts vertical pressures below the pavement system. Whereas, pressure cell number 2 (PC #2) illustrates vertical pressures at the bottom of the geofoam layer. The database from the test site was divided into two subset datasets referred to as calibration and validation datasets where the former is used for the purpose of constructing the model (calibration data), while the latter is for subsequent validation of the model (validation data).

In order to have the best prediction model development, the selection of the calibration dataset from the entire database plays a crucial role. The dataset that consists of maximum fluctuations should be considered as the calibration dataset so that the disturbance effects were considered during the model identification process because it can cause extensive shifts in the prediction model. Comparing all the working data combinations for the US 67 site, dominant disturbances were observed during the data

collected over the years 2014 and 2015. Hence, two years of time series data (2014-2015) were analyzed to derive the best prediction model to reflect the disturbance effects in the system.

The model calibration dataset consists of recorded vertical displacements (Y_{1t}) as function of traffic pressures (U_{1t}), temperature data (U_{2t}) and precipitation data (U_{3t}) as effective factors (calibration data). The temperature and precipitation data were collected from the US climate database (U.S. Climate Data 2017). Whereas, the recorded vertical displacements (Y_{1t}) are from horizontal inclinometer casings (output data). Figure 5.8 displays the US 67 site calibration databases.

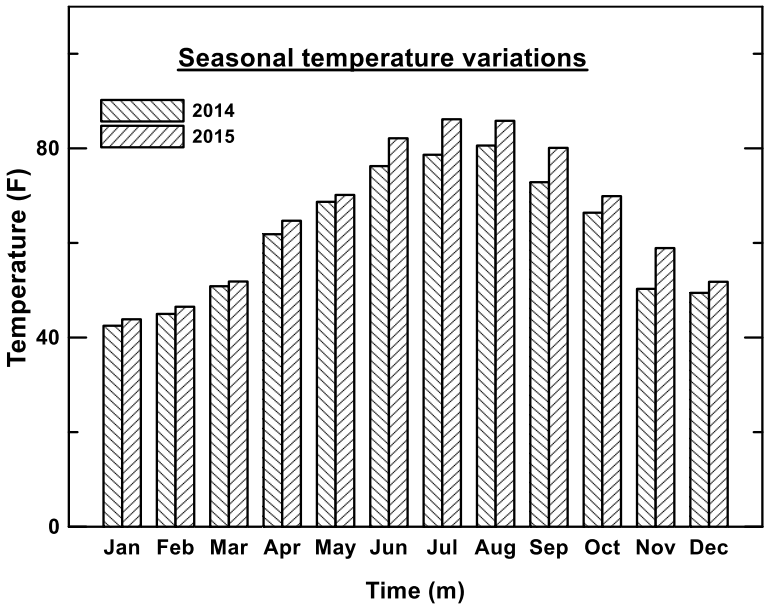

(a)

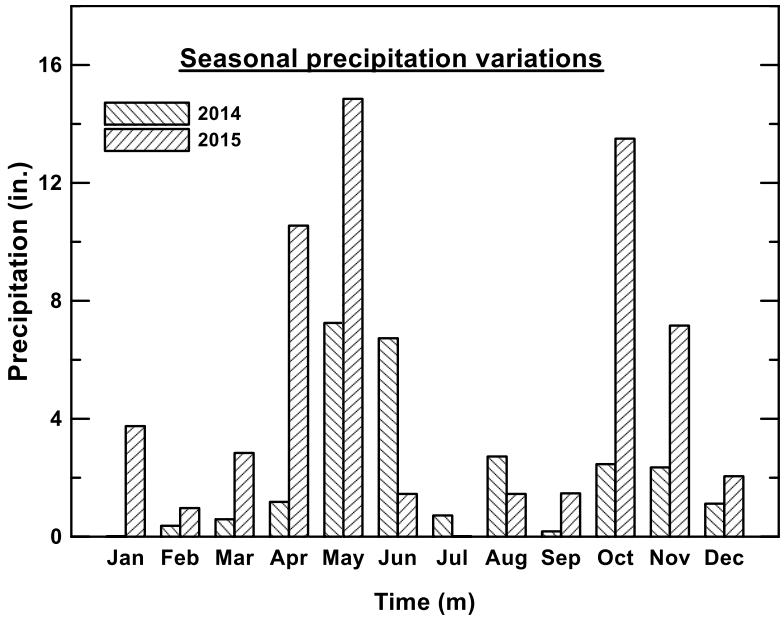
Seasonal precipitation variations
2014
2015
Precipitation (in.)
0
4
8
12
16
Jan
Feb
Mar
Apr
May
Jun
Jul
Aug
Sep
Oct
Nov
Dec
Time (m)

(b)

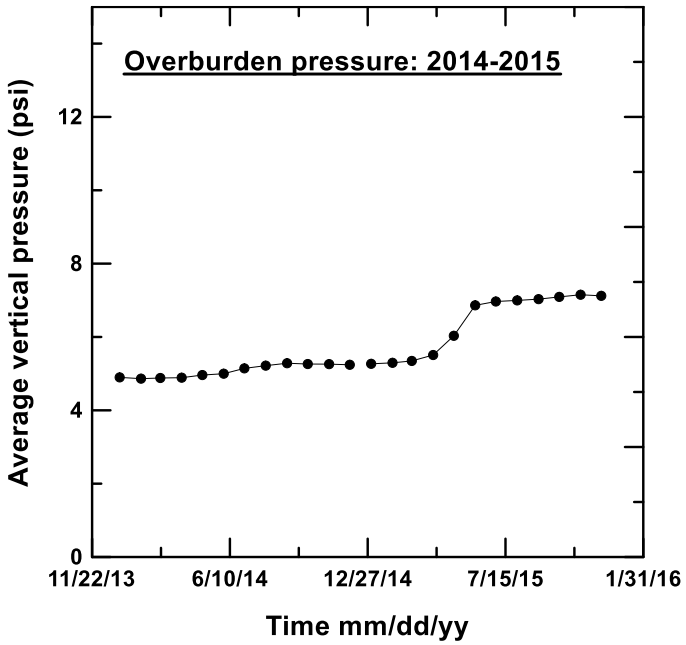
Overburden pressure: 2014-2015
Average vertical pressure (psi)
0
4
8
12
11/22/13
6/10/14
12/27/14
7/15/15
1/31/16
Time mm/dd/yy

(c)

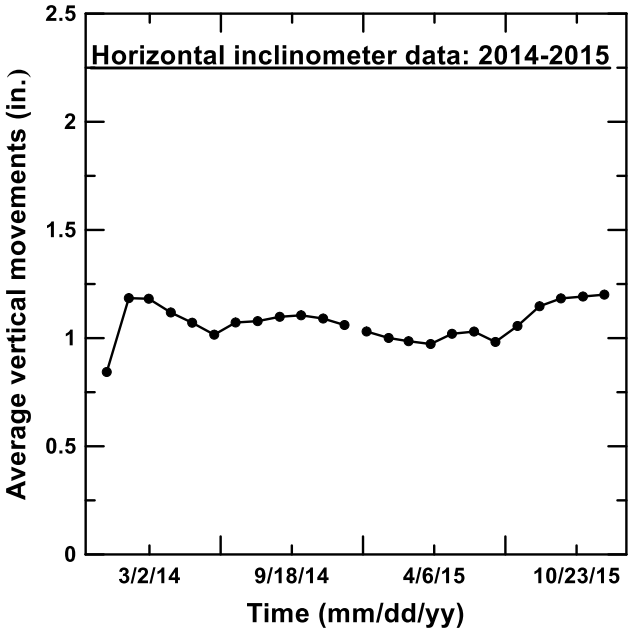

(d)

Figure 5.8 US 67 test site calibration database (2014-2015)

The data collected over years 2012, 2013 and 2016 datasets were used to validate the developed prediction model. Figures 5.9 to Figure 5.11 represent validation datasets for the US 67 site.

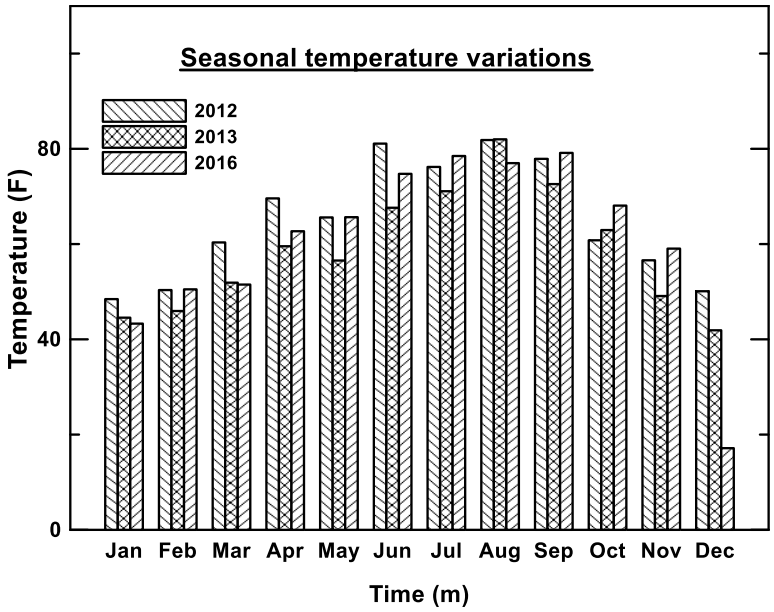

(a)

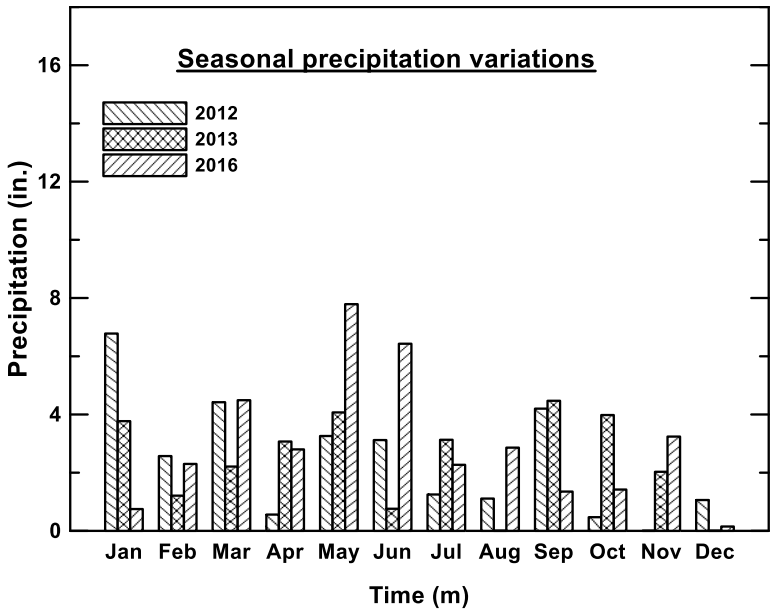

(b)

Figure 5.9 Validation datasets (a) seasonal temperature and (b) precipitation variations (2012, 2013, 2016)

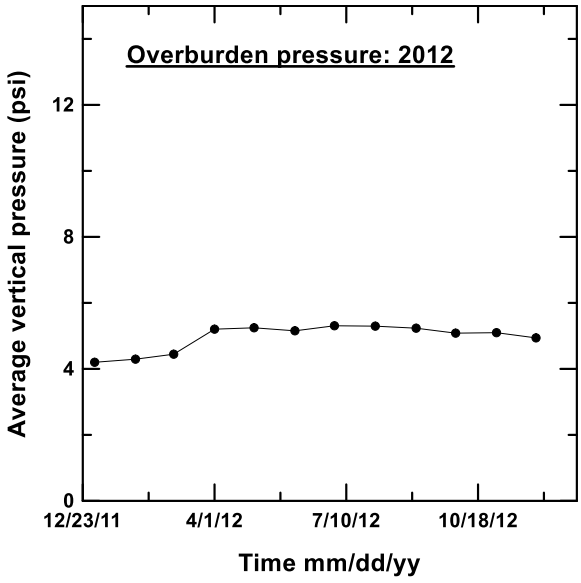
Overburden pressure: 2012
Average vertical pressure (psi)
0
4
8
12
12/23/11
4/1/12
7/10/12
10/18/12
Time mm/dd/yy

(a)

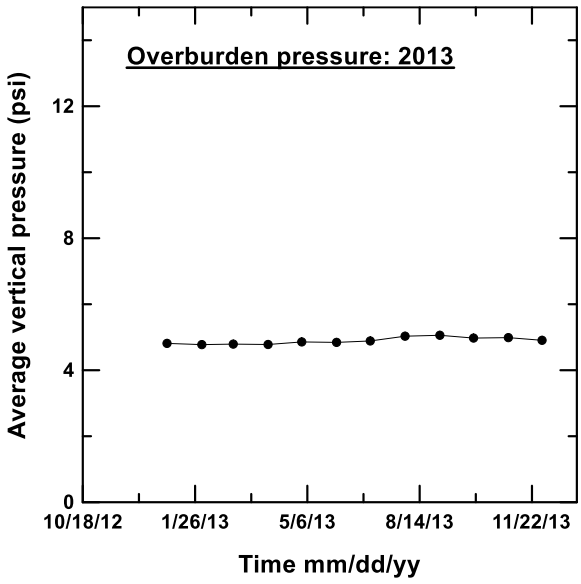
Overburden pressure: 2013
Average vertical pressure (psi)
0
4
8
12
10/18/12
1/26/13
5/6/13
8/14/13
11/22/13
Time mm/dd/yy

(b)

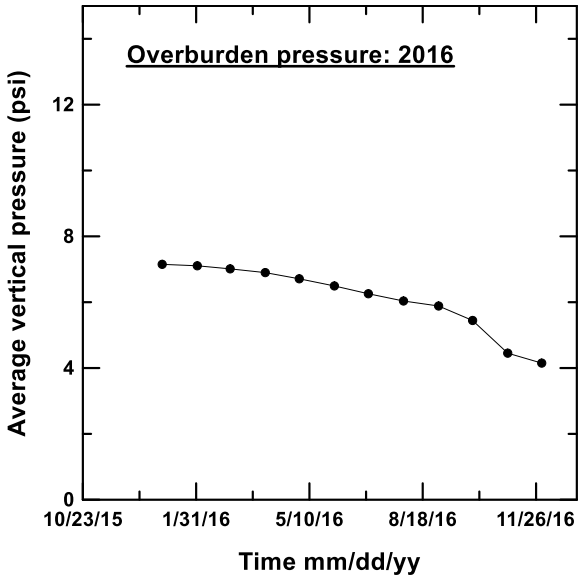

(c)

Figure 5.10 Overburden pressure (validation database 2012, 2013, 2016)

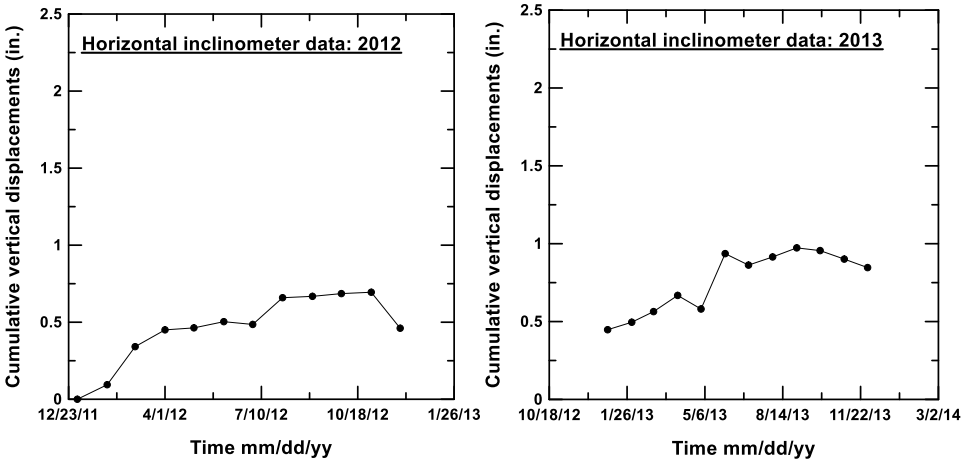

(a) (b)

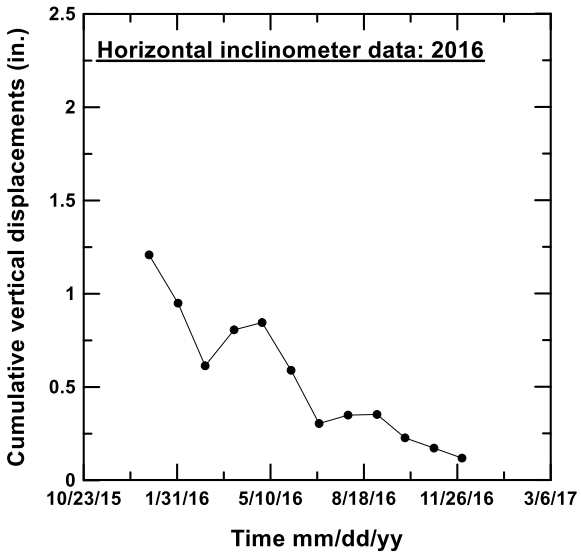

(c)

Figure 5.11 Vertical movements (validation database 2012, 2013, 2016)

In the above figures, Figure 5.9 (a & b) displays the seasonal temperature and precipitation variations for the years 2012, 2013, and 2016. Figure 5.10 (a to c) presents overburden pressure from traffic load and pavement system, and Figure 5.11 (a to c) demonstrates the measured vertical movements form horizontal inclinometer casings. The following section presents the model development using the calibration database.

5.1. Development of Prediction Models for Ground Vertical Movements

This section presents the development of vertical ground movement prediction model using the calibration data at the US 67 test site. The performance monitoring data, including temperature, precipitation, traffic pressures, and vertical movements from years 2014 and 2015 was used to calibrate the model. The precipitation and temperature changes were considered as the climatic excitation factors for triggering the vertical movements at the top of the embankment. The traffic and pavement overburden pressures were contemplated as the major excitation factors for the vertical movements. However, the effect of precipitation and temperature variations were considered as disturbance in

the system. The interdependence of the model parameters including temperature, precipitation, overburden pressure, and vertical movements were evaluated using the Pearson product-moment correlation. The Pearson product-moment correlation coefficient evaluates the strength of the linear correlation between the two variables. The Pearson product-moment correlation for the present data was calculated using the equation (5.1) below:

$$\delta_{ij} = \frac{n(\sum X_i X_j) - (\sum X_i)(\sum X_j)}{\sqrt{\left[n\sum X_i^2 - (\sum X_i)^2\right]\left[n\sum X_j^2 - (\sum X_j)^2\right]}} \qquad 5.1$$

Where, δ_{ij} is the Pearson correlation coefficient between $X_i$and X_j, which are the random variables considered; n is the total number of observations. A δ-value of positive 1 indicates a perfect positive correlation between the two variables, whereas a δ-value of 0 indicates no correlation and a negative 1 indicates a perfect negative correlation between the random variables. It was observed that the vertical ground movements (X_1) have a stronger correlation with precipitation (X_2) and a weaker correlation with overburden pressure (X_4). Similarly, the correlation coefficient between any two parameters can be deduced from the above correlation model. Also, the autocorrelation between the data was determined to evaluate the stationarity, which represents constant mean and variance.

The four linear auto-regressive models with multi-input single-output provided in Table 3.1 were used to identify the best model that translates the interdependence of the considered input variables on output variable. The multi-input variables consist of precipitation, temperature, and vertical pressures, and the output is ground movements observed. Figure 5.12 shows the monitored versus estimated settlements and their confidence levels. ARX, ARMAX, OE, and BJ model.

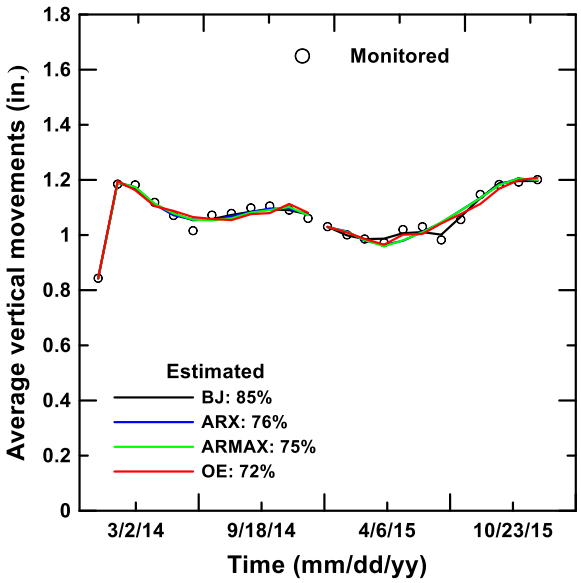

Figure 5.12 Selected calibration models

From Figure 5.12, it can be inferred that the Box Jenkins model structure provided the best estimates of the vertical ground movements with 85% confidence. Whereas, the other models including Auto-Regressive Exogenous (ARX), Auto-Regressive Moving Average Exogenous (ARMAX), and Output Error (OE) provided reasonable estimates of vertical ground movements with confidence values ranging from 72% to 76%. The best performance of the Box-Jenkins model can be attributed to its inherent structure, where the model is less sensitive to the data fluctuations and forecast better with the stationarity in the data. From the earlier autocorrelation plots and product-moment correlation tests, it was identified that the data is stationary. In order to check the reliability of the selected models, validation analysis was performed using the validation data base and the literature review equations as provided in the following sections.

5.3 Model Validation

This section presents the validation analysis of the developed models using the system identification approach. Figure 5.14 depicted that all the models including ARX,

ARMAX, BJ, and OE models performed reasonably well. In order to check the reliability of the selected models, validation analysis of the models was performed using the unused monitoring data from Year 2012, 2013, and 2016. Also, the efficiency of the developed model was determined by comparing the predictions from the developed model with the existing equations provided in the literature. Figure 5.13 ((a) to (c)) represents the performance of the correlated ARX, ARMAX, OE, and BJ models to forecast the monitored settlements during 2012, 2013, and 2016.

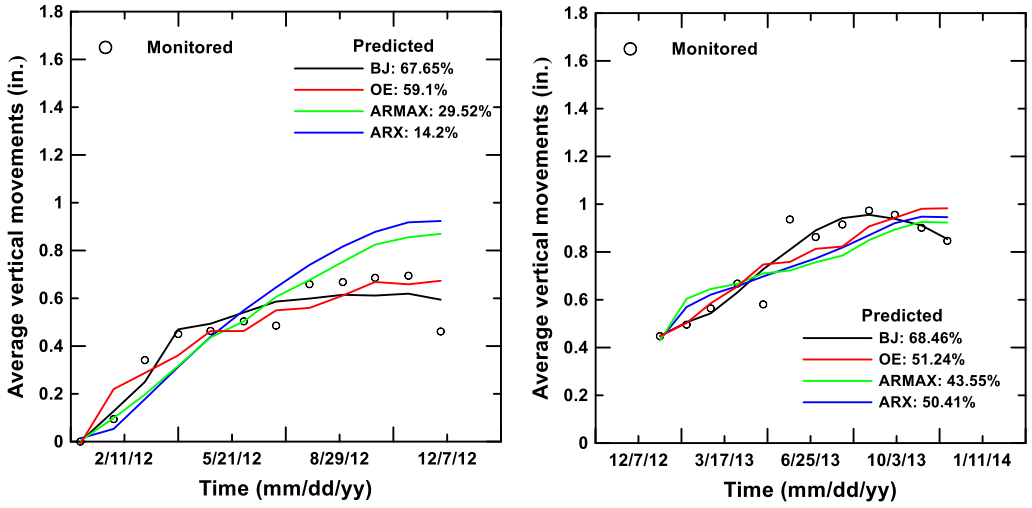

(a) (b)

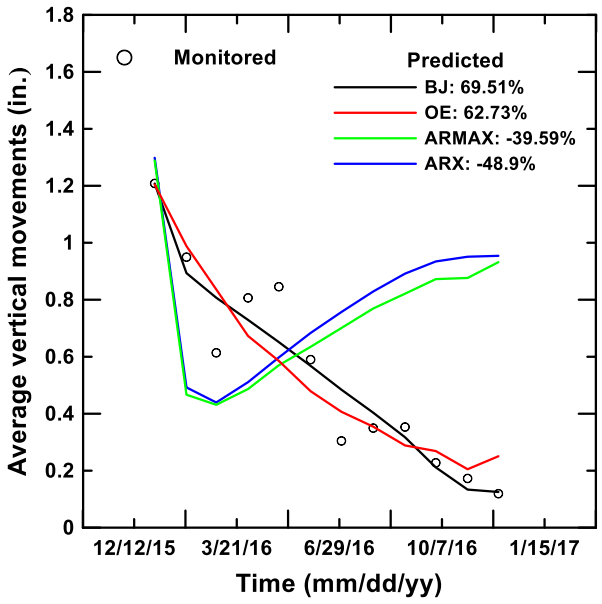

(c)

Figure 5.13 Validation of the selected prediction models: (a) 2012, (b) 2013, and (c) 2016

From the figures, it can be inferred that the ARX and ARMAX models failed to forecast the monitored settlements in 2016. However, they have captured decent trends for the settlements during 2012 and 2013. Evaluation of the estimated results from the OE and BJ models revealed that both models have provided estimates of monitored settlements with more than 50% confidence. It is evident that the best results were achieved from the BJ model during all the calibration and validation periods. It is demonstrated in Figure 3 that the prediction confidence level for the BJ model remains within the same range. However, the accuracy level for other models was changed significantly during the validation period.

Based upon the understanding of the dynamics of a load-settlement system, disturbance from climatic changes might have independently affected the corresponding settlements. Also, the observations exhibited that the influences of the disturbance factors (precipitation and temperature changes) emerged with a delay from the main motive of the

system (load). Hence, BJ can be considered as the best choice of model structure to reflect most characteristics of the studied system, primarily due to the capability of the model structure to provide entirely independent parametrization for the dynamics and the disturbance (climate change) using polynomial functions (Table 3.1).

A Box-Jenkins model structure has been employed to develop a settlement prediction model at the top of the test embankment. Two years of traffic loads, precipitation changes, and temperature variations datasets ($n_u = 3$; Table 3.1) were considered during the model correlation process. Finally, a simple second-degree BJ model (BJ21111) was designed to forecast the ground vertical movements with the minimized average Final Prediction Error (FPE) of 0.001771. Table 5.1 represents the transformation functions (B_i,F_i), the input delay magnitudes (nk_i), function orders, and parameters for the input (u_t) part of the equation (Table 3.1).

Table 5.1 Model parameter magnitudes

i	B_i	Order (B_i)	F_i	Order (F_i)	Delay Factor (n_k)	Input parameter (u_t)
1	-0.15 z^-1 + 0.08 z^-2	2	1 - 0.98 z^-1	1	1	Traffic load
2	-0.002 z^-1	1	1 - 0.76 z^-1	1	1	Precipitation
3	0.0006	1	1 - 0.92 z^-1	1	0	Temperature

The noise transformation functions (C and D) were calculated as the Equations 3.1 and 3.2 for the current case:

$$C(z) = 1 + 0.02z^{-1} \quad (3.1)$$

$$D(z) = 1 - 0.45z^{-1} \quad (3.2)$$

The z description in the presented equations is completely equivalent to the q-transform parameter explained in the Table 3.1.

5.4 Comparison of Box-Jenkins Model with the Hyperbolic Model

This section presents the efficiency of the developed the Box-Jenkins model with a hyperbolic model that is a commonly used for prediction of long-term settlements. In the hyperbolic prediction model, the rate of settlements is assumed to decrease hyperbolically with time (Ruttanaporamakul 2015; TAN 1995). A comparison between the correlated BJ model with the hyperbolic settlement prediction model revealed the robustness of the system identification method to capture the dynamics of the system by considering different settlement motivation factors. Figure 5.14 demonstrates both prediction models over the period of 5 years from January 2012 to December 2015.

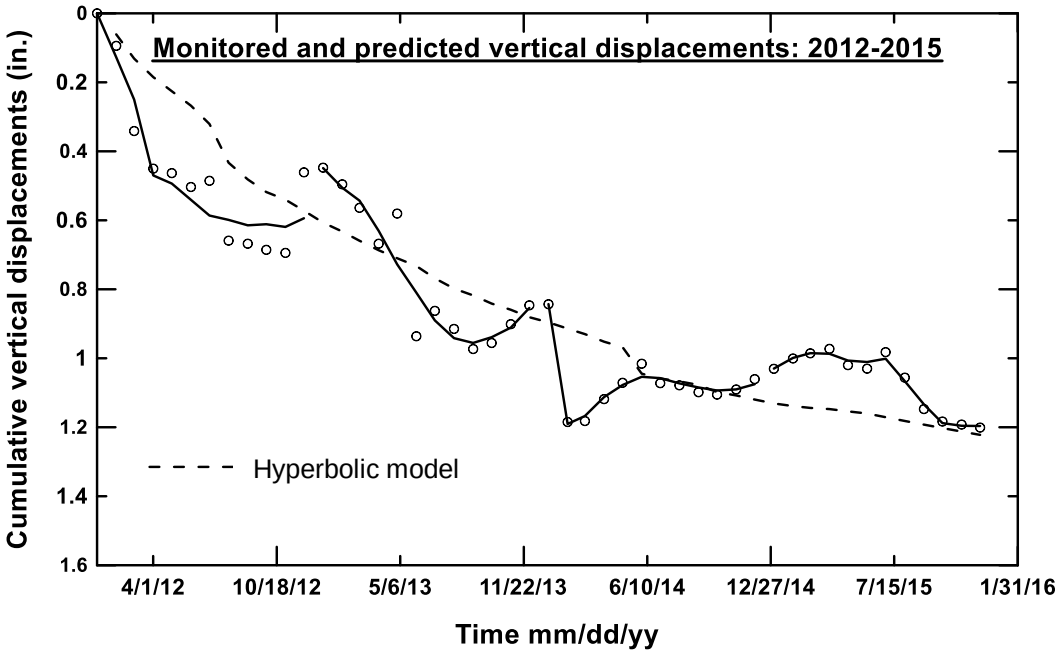

Figure 5.14 Comparison of the developed prediction model with the hyperbolic model

Estimated values from the hyperbolic model reveals a plausible prediction for the overall trend of ground displacements over time. However, the ground movements due to swell-shrink behavior of foundation soil was not captured in the model. Normally, swelling-shrinkage induced ground displacements take place due to a change in moisture condition

of top expansive soil layers, which significantly depends on ambient conditions. Hence, the uncertainty of the hyperbolic model to predict ground displacements due to swell-shrink behavior can be mainly interpreted as the limitation of the model to consider effective factors such as temperature and precipitation variations.

5.5 Summary

Illustration of the developed framework for prediction of ground vertical movements was attempted on a rehabilitated soil-geofoam bridge approach embankment. The system identification approach was implemented to capture the dynamic effects of seasonal ambient conditions on ground vertical movements. Five years of collected time-series data from the site instrumentation and the U.S. climate database, including measured vertical movements, traffic and pavement overburden pressures, temperature and precipitation variations were divided into two categories of calibration and validation datasets to develop and validate the developed models.

Different autoregressive linear model structures, including ARX, ARMAX, OE, and BJ were attempted to develop the most accurate prediction model for ground vertical movements. Model validation studies demonstrated that the developed model from the Box Jenkins (BJ) model structure captured the shrink-swell behavior of the US 67 bridge approach embankment with a maximum confidence level. A comparison between the developed model and the commonly used hyperbolic settlement prediction model disclosed the limitations of the hyperbolic model to contemplate the effectiveness of ambient conditions on cyclic shrink-swell movements of expansive deposits.

The next chapter presents a simple cost benefit analysis on the used ground movement monitoring techniques including horizontal inclinometer casing, LiDAR, and total station surveying techniques.

Chapter 6: Cost Benefit Analysis of Surveying Techniques for Measuring Ground Vertical Movements

6.1 Introduction

In this research study, several instrumentation and surveying techniques were employed at US67 test site to develop visualization models for infrastructure health monitoring and to evaluate the performance of the bridge approach slab infrastructure. The main intent of this chapter is to perform a cost-benefit analysis between three ground movement monitoring techniques including inclinometer instrumentation, total station, and 3D-Terrestrial Laser Scanning (3D-TLS) technology (Figure 6.1). A comparison to each method including equipment operations, data acquisition and analysis, and measurement accuracy are presented. Both cost benefit evaluation and related expenditure analyses are performed based upon the application of each technique to evaluate ground vertical movements at the end of a bridge approach slab for bump phenomenon. Factors such as measurement accuracy and costs are considered in the cost-benefit analysis. Following section presents an overview of the inclinometer instrumentation technique.

(a) (b) (c)

Figure 6.1 (a) Inclinometer (b) total station, and (c) 3D-TLS technology

6.2 Comparison of Inclinometer, Total Station, and 3D-TLS

A thorough introduction to the 3D-TLS technology including history, applications, step by step data acquisition and processing, and measurement accuracy and errors was presented in the earlier chapters. A comparison summary of the three monitoring techniques for determining ground movements is presented in the Table 6.1.

Table 6.1 Comparison of inclinometer, total station, and 3D-TLS monitoring techniques

Parameter	Inclinometer	Total Station	3D-TLS
Accuracy	Maximum accuracy of 0.3 inches can be achieved. The accuracy depends on operator, data acquisition process, casing installation, and length of the casing	Maximum accuracy of less than 0.08 inches can be achieved. The accuracy is significantly depended on the operator, ambient condition, prism type, and distance	Maximum accuracy of less than 0.08 inches can be achieved. The accuracy depends on the angle and distance from the façade
Mobility of System	Construction and maintenance of installed casings are required	Portable system	Portable system
Data points Acquisition	Single point measurement limited to the installed casing section	Single point measurement	Unlimited point measurements by producing dense point cloud
Surficial/Subsurface Technique	Subsurface monitoring technique	Surface monitoring technique	Surface monitoring technique
Practical limitation	Data point movements affect adjacent point movements due to the solid nature of inclinometer casings	Independent point measurements	Independent point measurements

Data Acquisition time	Day or night time data collection	Day time data collection	Day or night time data collection
Data Acquisition process	Direct data acquisition	Indirect data acquisition	Direct data acquisition
Surveying time	Time consuming and labor intensive without traffic disruption	Time consuming surveying process for taking many individual shots with traffic disruption	Quick surveying process without traffic disruption

According to the Table 2.1 and technical capabilities of each technique, maximum accuracy for monitoring of ground vertical movements with minimum chance of random error can be provided by using the 3D-TLS technology. Technical capabilities of each monitoring technique make important contributions to health monitoring and performance evaluation of a bridge infrastructure. However, cost expenditure on each method should be evaluated since the most efficient monitoring approach is the one which can provide accurate information with reasonable costs. Next section provides a Cost-Benefit Analysis (CBA) on the considered monitoring techniques.

6.3 Cost-Benefit Analysis

A cost-benefit analysis is performed by assessing the required costs for the collection and evaluation of each data point for ground vertical movement. All the monitoring techniques are evaluated for surveying of 410 data points over the pavement surface of 100 ft. length and 44 ft. width (two-lane highway). The 410 monitoring points are considered over an area of 4,400 ft^2 based on the bump problem which is a local phenomenon. Approximately one data point is considered per square meter area of the pavement surface to be assessed for ground vertical movements. Several factors including required number of skilled and unskilled operators, time expenditure for surveying and

analysis of each data point, required hardware and software facilities, and time user and environmental costs for traffic congestion are considered during the analysis.

Table 6.2 demonstrates minimum required number of operators and respective costs for performing each monitoring technique.

Table 6.2 Minimum required number of operators and costs

Monitoring Techniques	Required Number of Operators		Cost in $/Hour	
	Skilled	Unskilled	Skilled	Unskilled
Total Station Survey	1	1	14.7	12
Inclinometer	1	2	14.48	12
LiDAR Survey	1	0	20	-

According to the Table 6.2, a total station survey requires at least one skilled operator to design surveying plan, perform readings and calculate ground vertical movements and one unskilled employee to hold the prism pole. In order to carry out the inclinometer readings for measuring ground vertical movements, a crew of one skilled operator and three additional unskilled employees are required to take the readings and to hold the cable casing horizontally while the inclinometer probe is passing through the installed casings respectively (Figure 6.4).

On the other hand, the 3D-TLS surveys can be handled by one skilled operator to collect scans, register them to a single point cloud and perform ground vertical movement analysis. In this study, to conduct each monitoring technique, dry rental cost of each instrumentation and surveying system is considered. A summary of average dry rental costs for each monitoring technique is presented in Table 6.3. It should be noted that dry rent is defined as hiring an equipment or a venue without any accompanying operators or staff.

Table 6.3 Average dry rental costs of considered monitoring techniques

Monitoring techniques	Dry rental cost (US Dollars)		
	Daily	Weekly	Monthly
Total Station Survey	$150	$420	$1,200
Inclinometer	$200	$550	$2,000
LiDAR Survey	$550	$2,000	$5,000

Another considered factor to perform CBA is the time expenditure and costs associated with monitoring surveys and corresponding ground movement analysis (Table 6.4).

Table 6.4 Required time for surveying and analysis of 410 datapoints

Monitoring techniques	Required time for surveying and analysis of 410 datapoints					
	Set-up time/min	Required numbers of setup	Individual survey time (min)	Number of surveying points	Data analysis (hrs.)	Total required time (hrs.)
Total Station Survey	9	1	0.5	410	1	5
Inclinometer	10	20	0.3	410	2	8
LiDAR Survey	5	4	5	_	1	2

Measuring ground vertical movements over the pavement surface using inclinometer instrumentation requires at least 20 casings to be installed below the pavement system in which, initial construction and respective maintenances are inevitable. A total of 8 hours including 6 hours for monitoring and 2 hours for assessing the collected data is estimated for each inclinometer survey (Table 6.4). Using the 3D-TLS monitoring technique, the entire monitoring area can be surveyed and processed for ground vertical movements in less than two hours. However, advanced computational tools and skills are required to perform the analysis. These costs are included in the in Table 2.3.

According to the Table 6.4, the total station can capture all data points in one set-up operation. Total station set-up includes equipment and tripod installation, leveling, and capturing a reference point coordinate system. A total of 410 data points' coordinates should be collected continuously which take at least 4 hours to complete the entire survey. It should be noted that all the monitoring points should be marked during the monitoring period. Considering 1 hour for ground vertical movement analysis, 5 hours is required for completing each survey and respective analysis using total station surveying technique without considering any break time for operators. Another cost factor that should be considered in the total station surveys is the work zone user and environmental costs associated with 4 hours of traffic disruption during each survey.

On-site monitoring activities can result in significant adverse mobility and safety impacts to road users. Also, traffic disruption due to the presence of work zone can result in noise and negative environmental impacts (Daniels et al. 1999; Mallela and Sadasivam 2011; New Jersey Dept. of Transportation (NJDOT) 1999; Rezaeifar et al. 2017). According to the U.S. Federal Highway Administration (FHWA), work zone user costs is defined as the additional costs borne by motorists and the community as a result of work zone activity (Mallela and Sadasivam 2011). Work zone user costs include travel delay costs, vehicle operating costs, crash costs, emission costs, and impact of nearby projects. According to the NCHRP report 133 and TxDOT construction division report, total estimated values of work zone user and environmental costs for personal and commercial travels is presented in Table 6.5. The total user costs include travel delay, vehicle operating, excess fuel burn, crash, and impact on nearby projects costs. Whereas, environmental costs include noise and air pollution due to excessive emission (Ellis and Ph 2018; Ljung 1999; Rezaeifar 2018; Transportation Research Board 2016).

Table 6.5 User and environmental costs

Vehicle class	Total user cost per vehicle-hour ($)	Environmental cost per vehicle-hour ($)	Average cost value per vehicle-hour ($)
Car	28.69	3	36.48
Truck	36.28	5	

In this study, an average cost value of $36.48 per vehicle-hour is assumed along with minimum 5 minutes delay for each motorist's travel time due to 4 hours of total station survey. Also, ideal capacity of 1400 passenger cars per hour for the US 67 two-lane highway is assumed according to the highway capacity manual (Transportation Research Board 2016). Hence, an average user and environmental cost value of $1702 is estimated for taking 2 minutes of traffic delay during 4 hours of traffic interruption to perform each total station survey.

Total estimated costs per surveyed datapoint corresponding with each monitoring technique are illustrated in the Figure 6.2.

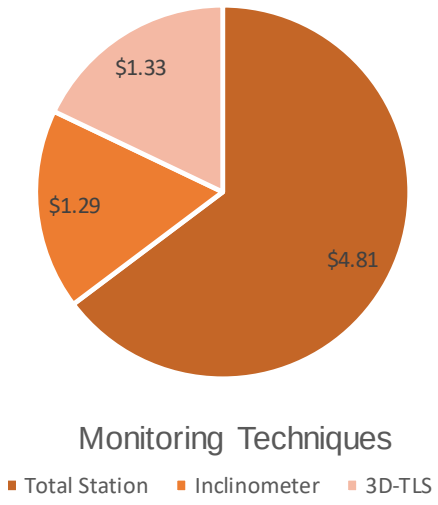

Figure 6.2 Total surveying costs per point

According to the Figure 6.2, total station cannot be considered as a cost-effective technique for monitoring ground vertical movements over the pavement surface. It is mainly because of its traffic interruption and respective environmental negative impacts. However, inclinometer and 3D-TLS techniques both can be considered as cost-effective approaches for monitoring ground vertical movements over the pavement surface. It should be noted that technical assessment of the monitoring techniques revealed that using the inclinometer for monitoring ground vertical movements require initial construction for installing casings and respective maintenance. Also, it should be noted that the casings installed within the infrastructure reduces the structural integrity of different component encompassing the casing. Whereas, 3D-TLS saves more time by providing more accurate results with the least chance of random error. Instead, sophisticated computational hardware and software tools are required for performing ground movement analysis.

6.4 Summary

A Cost-Benefit Analysis (CBA) is performed on three ground movement monitoring techniques including total station, inclinometer, and 3D-Terrestrial Laser Scanning (3D-TLS) techniques. Several factors such as required number of skilled and unskilled workers, time expenditure for surveying and analysis of each data point, required hardware and software facilities, and time user and environmental costs for traffic congestion are considered during the analysis. It was observed that monitoring ground vertical movements using total station and inclinometer are time consuming and labor intensive. From the technical point of view, the 3D-TLS technique provided more accurate results without causing any traffic interruption and negative environmental impacts. Also, the total station and inclinometer can monitor vertical movements along specified points or sections respectively. Based on the monetary assessment of each technique, the total station was found as an unprofitable monitoring approach mainly due to its traffic disruption and

respective environmental costs. Total surveying costs per collected datapoint revealed that both inclinometer and 3D-TLS techniques can be considered as cost-effective monitoring alternatives for the sake of ground vertical movements. However, 3D-TLS monitoring technique does not require any construction or high maintenance costs. Instead, advanced computer hardware and software systems are required to process and analyze the collected scans from the 3D-TLS technique.

Next chapter presents a summary, conclusions, and recommendations for future research of the performed study on the performance evaluation of bridge infrastructure using terrestrial LiDAR and system identification approach.

Chapter 7: Summary, Conclusions and Recommendations

7.1 Summary and Conclusions

This dissertation focusses on the performance evaluation of bridge infrastructure using terrestrial LiDAR and system identification approaches. A framework is developed for health monitoring and performance assessment of bridge approach slab infrastructure by focusing on evaluating vertical ground movements of bridge embankment induced settlements. The developed framework mainly consists of four major steps including project requirements, developing a monitoring approach using 3D-TLS LiDAR technology, studying and assessing long-term ground movement prediction models using system identification approach, and performing validation studies for determining the accuracy of the developed models. A Cost-Benefit Analysis (CBA) is performed on three ground movement monitoring approaches including the total station, inclinometer, and terrestrial LiDAR techniques. The illustration of the developed framework is performed on a rehabilitated soil-geofoam bridge approach embankment located in Cleburne, Texas. Based on the performed studies, the following conclusions are deduced:

1. A framework is developed to assess the reliability of the 3D-TLS technology to monitor vertical movements over the pavement surface of a bridge approach embankment. Optimization studies revealed that the number of scans can be significantly decreased. In the performed analysis on a bridge infrastructure, the number of scans were significantly decreased from ten (10) to five (5) by using artificial targets. This reduction in number of scans still yielded desired quality for evaluating vertical movement, and increased efficiency and effective field surveys.
2. Field surveys were performed over a span of 18 months to evaluate the efficiency of 3D-TLS technology to capture the vertical movements corresponding to different seasonal changes. More than 800 test points from the processed scans were

analyzed over the pavement surface of approach slab and bridge deck without any interruption to traffic. The analysis performed depicted both heave and shrink phenomenon corresponding to different seasonal changes.

3. The trend in the vertical movements determined from the 3D-TLS technology were compared and validated with the movements determined from the horizontal inclinometers. Both depicted heave-shrink phenomenon, whereas the 3D-TLS technology provides the data over a wider area, rendering a more reliable assessment of the condition of the bridge infrastructure.
4. Unlike the data collected from the in-situ instrumentation, such as the horizontal inclinometer, processed scans can be used for several other monitoring purposes. Structural element displacements such as bridge deck deflections and foundation movements are prime examples. Scanning surveys can be performed anytime during or after the construction of a test site; however, installing instrumentation such as horizontal casings must be planned during construction works. In contrast, the 3D-TLS is a non-destructive, non-invasive, environmentally friendly, and robust technology that can be used for different geotechnical and geological monitoring purposes, including tracking ground movements efficiently and accurately.
5. System identification approach was applied for a better understanding of the dynamics of a traffic loads-climate changes induced ground movement system and expressing it through a mathematical model structure layout. A specific order of a particular linear polynomial autoregressive model structure (BJ) was shown to be consistent among ARX, ARMAX, and OE model structures to predict the movements at the top of the studied embankment.
6. A long-term settlement prediction model was developed based on the average monthly monitored data for 5 years. Not only the precipitation and temperature

changes effects were considered, the model can also capture any delay or disturbance (climate changes) and noise (from installed instrumentation) induced independent effects in a system. The presented model can be updated simply by operating the common computational tools such as the MATLAB system identification toolbox for the similar situations.

7. A comparison between the developed model and the commonly used hyperbolic settlement prediction model disclosed the limitations of the hyperbolic model to account for the ambient conditions on cyclic shrink-swell movements of expansive deposits. On the other hand, the developed BJ model was able to forecast long-term ground vertical movements by considering the aforementioned effects with a reasonable confidence level.
8. Cost-Benefit Analysis (CBA) of all three monitoring methods including total station, horizontal inclinometer, and 3D-TLS technique demonstrated that monitoring ground vertical movements using total station and inclinometer tools are time and labor intensive. From the technical point of view, it was revealed that the 3D-TLS technique can provide more accurate results without causing any traffic interruption and negative environmental impacts. However, the total station and inclinometer can monitor vertical movements along specified points or sections respectively.
9. Based on the monetary assessment of each technique, the total station was found as a non-profitable monitoring approach mainly due to its traffic disruption and respective environmental costs. Total surveying costs per collected data point revealed that both inclinometer and 3D-TLS techniques can be considered as more cost-effective monitoring alternatives for ground vertical movements. Among these two, the 3D-TLS monitoring technique does not require any construction or

maintenance costs which are needed for installation of inclinometer casings. Instead, advanced 3D terrestrial scanners are costly to purchase, and sophisticated computer hardware and software systems are required to process and analyze the collected scans from the 3D-TLS technique.

7.2 Limitation of the Developed Framework

The developed framework using the 3D-TLS LiDAR technology for monitoring of bridge infrastructure have some limitations due to LiDAR and system identification restrictions. The developed framework cannot be implemented on the vegetated embankment slopes. It is not feasible to perform terrestrial LiDAR surveys in hard to access areas and projects such as in highly elevated steep natural slopes and huge infrastructure projects mainly due to the portability limitations of the terrestrial LiDAR. However, the application of LiDAR technology has been adapted for different types of surveying areas by using the developed aquatic and UAV LiDAR systems. Performing LiDAR surveys for long distances will become labor intensive and not feasible due to the energy source limitations (battery). Performing LiDAR surveys in very low temperatures (below 14°F) can cause technical problems since at this temperature, ice crystals are started to form in the atmosphere and LiDAR may capture these crystal points as data points. 3D-TLS systems cannot be operated in snow or rainy weather conditions. Developing analytical models are very expensive in both time and data. In this dissertation, it was attempted to develop a linear simple model to capture the dynamic trend of ground movements. However, in some cases, it is not always feasible to identify a linear simple model structure to capture the dynamic behavior of a system and developed complex high degree model structures will not be user friendly to implement in practice.

7.3 Recommendations for Future Research

Several recommendations can be made based on the developed framework including:

1. Illustration of the developed framework is performed on a rehabilitated soil-geofoam bridge approach embankment. However, the application of the developed framework can be extended to other civil infrastructure projects such as buildings, dams, tunnels, and slopes.
2. Automatic data logger systems can be used along with the developed ground movement prediction model identification algorithms in the site instrumentations such as settlement cells, magnet extensometers, and Shape Array Accelerometer MEMS (SAA MEMS) to establish automatic monitoring systems in which, unique ground movement prediction models can be developed and updated automatically.
3. Different types of soils represent diverse behavior under loading and seasonal ambient conditions. Advanced machine learning and artificial neural network approaches are highly recommended to be employed to develop more accurate ground movement prediction models with the least data acquisition costs.

References

Aarts, R. (2012). “System identification and parameter estimation.” *Lecture Notes (University of Twente, 2012). https://www. utwente. nl/ctw/wa/web_dev/old/lectures/113170/notes/notes. pdf*.

Acharya, R., Bheemasetti, T. V., Ruttanaporamakul, P., Chittoori, B., and Puppala, A. J. (2014). “Numerical modeling of a highway embankment using geofoam material as partial fill replacement.” *Geo-Congress 2014 Technical Papers: Geo-characterization and Modeling for Sustainability*, ASCE, 2986–2995.

Adeli, H., and Hung, S.-L. (1994). *Machine learning: neural networks, genetic algorithms, and fuzzy systems*. John Wiley & Sons, Inc.

Adem, H. H., and Vanapalli, S. K. (2013). “Constitutive modeling approach for estimating 1-D heave with respect to time for expansive soils.” *International Journal of Geotechnical Engineering*, Taylor & Francis, 7(2), 199–204.

Aggarwal, S. (2004). “Principles of remote sensing.” *Satellite remote sensing and GIS applications in agricultural meteorology*, 23.

Akaike, H. (1974). “A new look at the statistical model identification.” *IEEE transactions on automatic control*, Ieee, 19(6), 716–723.

Akshaykumar, N., and Subbulekshmi, D. (2016). “Process identification with autoregressive linear regression method using experimental data: Review.” *Indian Journal of Science and Technology*, 9(39), 1–7.

Al-Rawabdeh, A., He, F., Moussa, A., El-Sheimy, N., and Habib, A. (2016). “Using an unmanned aerial vehicle-based digital imaging system to derive a 3D point cloud for landslide scarp recognition.” *Remote sensing*, Multidisciplinary Digital Publishing Institute, 8(2), 95.

Alonso, E. E., Vaunat, J., and Gens, A. (1999). “Modelling the mechanical behaviour of

expansive clays.” *Engineering geology*, Elsevier, 54(1), 173–183.

Anderson, N. L., Torgashov, E. V, and Rogers, J. D. (2016). “Imaging Reinforced Concrete: A comparative Study of Ground Penetration Radar and Rebarscope.”

Andersson, L., Jönsson, U., Johansson, K. H., and Bengtsson, J. (1998). “A manual for system identification.” *Laboratory Exercises in System Identification. KF Sigma i Lund AB. Department of Automatic Control, Lund Institute of Technology, Box*, 118.

Antova, G. (2007). “3D LASER SCANNING FOR DAM DEFORMATION MONITORING.” *7th International Scientific Conference-SGEM2007*, SGEM Scientific GeoConference.

ASCE. (2017). “Infrastructure report card.” *ASCE News*, 53(September 2017), 1–36.

Åström, K. J., and Eykhoff, P. (1971). “System identification—a survey.” *Automatica*, Elsevier, 7(2), 123–162.

Authority, E. R. (2002). “Bridge Design Manual.” *Addis Ababa: ERA*.

Baecher, G. B., and Christian, J. T. (2005). *Reliability and statistics in geotechnical engineering*. John Wiley & Sons.

Baker, M. R., Crain, K., and Nazarian, S. (1995). *Determination of pavement thickness with a new ultrasonic device.*

Banerjee, A. (2017). “Response of Unsaturated Soils under Monotonic and Dynamic Loading over moderate Suction States.” Doctoral Dissertation, University of Texas at Arlington, Arlington, Texas.

Banerjee, A., Patil, U. D., Puppala, A. J., and Hoyos, L. R. (2018a). “Suction-controlled Repeated Load Triaxial Test of Subgrade Soil at High Suction States.” *Proc: 7th International Conference on Unsaturated Soils*, Hong Kong.

Banerjee, A., Patil, U. D., Puppala, A. J., and Hoyos, L. R. (2018b). “Evaluation of Liquefaction Resistance in Silty Sand via Suction Controlled Cyclic Triaxial Tests.”

PanAm Unsaturated Soils 2017, GSP 301, Dallas, Texas, 543–552.

Banerjee, A., and Viladkar, M. N. (2015). “Ground Subsidence due to Construction of Shallow twin Tunnels near Adjacent Structures.” *Proc: 50th Indian Geotechnical Conference*, Pune, India.

Bartlett, S. F., and Youd, T. L. (1995). “Empirical prediction of liquefaction-induced lateral spread.” *Journal of Geotechnical Engineering*, American Society of Civil Engineers, 121(4), 316–329.

Bender, E. A. (2012). *An introduction to mathematical modeling*. Courier Corporation.

Berns, M., Bigelow, J., Phares, B. M., White, D. J., and Zhang, J. (2011). “Identification and Evaluation of Pavement-Bridge Interface Ride Quality Improvement and Corrective Strategies.” (134375), 264.

Biggs, A. J. W., and Mahony, K. M. (2004). “Is soil science relevant to road infrastructure?” *ISCO 2004-13th International Soil Conservation Organisation Conference*.

Bouali, E. H., Oommen, T., Vitton, S., Escobar-Wolf, R., and Brooks, C. (2017). “Rockfall Hazard Rating System: Benefits of Utilizing Remote Sensing.” *Environmental & Engineering Geoscience*, Assoc Eng Geologists, 23(3), 165–177.

Bovenga, F., Wasowski, J., Nitti, D. O., Nutricato, R., and Chiaradia, M. T. (2012). “Using COSMO/SkyMed X-band and ENVISAT C-band SAR interferometry for landslides analysis.” *Remote Sensing of Environment*, Elsevier, 119, 272–285.

Brenan, K. E., Campbell, S. L., and Petzold, L. R. (1996). *Numerical solution of initial-value problems in differential-algebraic equations*. Siam.

Briaud, J.-L., Maher, S. F., and James, R. W. (1997). “Bump at the End of the Bridge.” *Civil Engineering*, American Society of Civil Engineers, 67(5), 68.

Briaud, J.-L., Zhang, X., and Moon, S. (2003). “Shrink test–water content method for

shrink and swell predictions." *Journal of geotechnical and geoenvironmental engineering*, American Society of Civil Engineers, 129(7), 590–600.

Brinkgreve, R. B. J. (2013). *Validating numerical modelling in geotechnical engineering*. NAFEMS.

Brownjohn, J. M. W. (2007). "Structural health monitoring of civil infrastructure." *Philosophical Transactions of the Royal Society of London A: Mathematical, Physical and Engineering Sciences*, The Royal Society, 365(1851), 589–622.

Brylawski, E., and Asce, M. (2007). "Embankment Dam with an Upstream Concrete Slab and Cutoff Wall." (Fmgm), 1–14.

Caltrans. (2011). "Terrestrial Laser Scanning Specifications." *Surveys Manual*, (January), 32.

Campbell, J. B., and Wynne, R. H. (2011). *Introduction to remote sensing*. Guilford Press.

Carter, J. P. (2001). "Solving boundary value problems in geotechnical engineering." *Proc. 2nd International Symposium on Pre-Failure Deformation Characteristics of Geomaterials*, 1113–1141.

Carter, J., Schmid, K., Waters, K., Betzhold, L., Hadley, B., Mataosky, R., and Halleran, J. (2012). "Lidar 101: An introduction to lidar technology, data, and applications." *National Oceanic and Atmospheric Administration (NOAA) Coastal Services Center*, 7–11.

Catbas, F. N., Susoy, M., and Frangopol, D. M. (2008). "Structural health monitoring and reliability estimation: Long span truss bridge application with environmental monitoring data." *Engineering Structures*, Elsevier, 30(9), 2347–2359.

Chakraborty, S., Banerjee, A., Das, J. T., Mosadegh, L., and Puppala, A. J. (2018). "Impact of Variation of Small Strain Shear Modulus on Seismic Slope Stability Analysis of a Levee: A Sensitivity Analysis." *IFCEE 2018*, American Society of Civil

Engineers, Reston, VA, 302–313.

Chakraborty, S., Bheemasetti, T. V, Puppala, A. J., and Nazarian, S. (2017). “A rational approach to select the number of field tests required to determine subgrade properties.” *International Journal of Pavement Engineering*, Taylor & Francis, 1–9.

Chakraborty, S., and Nair, S. (2018). “Impact of different hydrated cementitious phases on moisture-induced damage in lime-stabilised subgrade soils.” *Road Materials and Pavement Design*, Taylor & Francis, 19(6), 1389–1405.

Chang, P. C., Flatau, A., and Liu, S. C. (2003). “Health monitoring of civil infrastructure.” *Structural health monitoring*, Sage Publications, 2(3), 257–267.

Chen, E. W., Duan, L., and Wang, L. (2000). “Wang, L., Gong, C. ‘Abutments and Retaining Structures.’”

Chen, F. H. (2012). *Foundations on expansive soils*. Elsevier.

Chen, H.-F. (2009). “Recursive system identification.” *Acta Mathematica Scientia*, Elsevier, 29(3), 650–672.

Chen, S., Billings, S. A., and Grant, P. M. (1990). “Non-linear system identification using neural networks.” *International journal of control*, Taylor & Francis, 51(6), 1191–1214.

Chen, Y.-T., and Chai, Y. H. (2010). “Experimental study on the performance of approach slabs under deteriorating soil washout conditions.” *Journal of Bridge Engineering*, American Society of Civil Engineers, 16(5), 624–632.

Childs, D. (1998). “Bridge Design and Assessment.”

Chinarro, D. (2014). *System Engineering Applied to Fuenmayor Karst Aquifer (San Julián de Banzo, Huesca) and Collins Glacier (King George Island, Antarctica)*.

Choudhury, S. (2008). *An Introduction to geographic information technology*. IK International Pvt Ltd.

Clouston, P., Bathon, L. A., and Schreyer, A. (2005). “Shear and bending performance of a novel wood–concrete composite system.” *Journal of Structural Engineering*, American Society of Civil Engineers, 131(9), 1404–1412.

Combs, J. H., and Kemeny, J. (2011). “DOT study of LIDAR geotechnical applications in eight states.” *45th US Rock Mechanics/Geomechanics Symposium*, American Rock Mechanics Association.

Covello, F., Battazza, F., Coletta, A., Lopinto, E., Fiorentino, C., Pietranera, L., Valentini, G., and Zoffoli, S. (2010). “COSMO-SkyMed an existing opportunity for observing the Earth.” *Journal of Geodynamics*, Elsevier, 49(3–4), 171–180.

Covello, F., Battazza, F., Coletta, A., Manoni, G., and Valentini, G. (2009). “COSMO-SkyMed mission status: Three out of four satellites in orbit.” *Geoscience and Remote Sensing Symposium, 2009 IEEE International, IGARSS 2009*, IEEE, II-773.

Croarkin, C., Tobias, P., and Zey, C. (2002). *Engineering statistics handbook*. NIST iTL.

Curran, P. J. (1985). *Principles of remote sensing.* Longman Inc.

Cuypers, W., Van Gestel, N., Voet, A., Kruth, J.-P., Mingneau, J., and Bleys, P. (2009). “Optical measurement techniques for mobile and large-scale dimensional metrology.” *Optics and Lasers in Engineering*, Elsevier, 47(3–4), 292–300.

Daniels, G., Ellis, D. R., and Stockton, W. R. (1999). “Techniques for Manually Estimating Road User Costs Associated with Construction Projects.” *LCS-u*, (December), 111p.

Das, J. T., Samuel, R. A., George, A. M., Chakraborty, S., Bheemasetti, T. V, and Puppala, A. J. (2018). “Establishing a Threshold Sustainability Index for a Geotechnical Construction.” *IFCEE 2018*, 222–232.

Davenport, G. C. (2001). “Remote sensing applications in forensic investigations.” *Historical Archaeology*, Springer, 35(1), 87–100.

Dewitte, O., Jasselette, J.-C., Cornet, Y., Van Den Eeckhaut, M., Collignon, A., Poesen, J., and Demoulin, A. (2008). “Tracking landslide displacements by multi-temporal DTMs: a combined aerial stereophotogrammetric and LIDAR approach in western Belgium.” *Engineering Geology*, Elsevier, 99(1–2), 11–22.

Dong, W. (2017). *On the role of constitutive behaviour in the response of squeezing ground to tunnelling*. vdf Hochschulverlag AG.

Drains, D., Minimum, D., and Thickness, D. (2011). “Concrete Decks.”

Duan, L., and Chen, W.-F. (1999). *Bridge engineering handbook*. CRC press.

Dunnicliff, J. (1993). *Geotechnical instrumentation for monitoring field performance*. John Wiley & Sons.

Eberhardt, E. (2003). “Rock slope stability analysis–utilization of advanced numerical techniques.” *Earth and Ocean sciences at UBC*.

Eberhardt, E., and Stead, D. (2011). “Geotechnical instrumentation.” *SME mining engineering handbook*, 1(8.5), 551–572.

Eggert, H., and Kauschke, W. (2002). *Structural bearings*. John Wiley & Sons.

Ehlers, M., Gähler, M., and Janowsky, R. (2003). “Automated analysis of ultra high resolution remote sensing data for biotope type mapping: new possibilities and challenges.” *ISPRS Journal of Photogrammetry and Remote Sensing*, Elsevier, 57(5–6), 315–326.

Ellis, D. R., and Ph, D. (2018). “Updated Estimate of Roadway User Cost for Personal Vehicles and Commercial Trucks.” 1–15.

Ettouney, M. M., and Alampalli, S. (2011). *Infrastructure health in civil engineering: Applications and management*. CRC press.

FARO Technologies. (2011). “FARO SCENE User Manual.” 2011.

FARO Technologies. (2016). “FARO ® Laser Scanner Focus 3D X 330 HDR The

Imaging Laser Scanner for extended ranges.” 3–4.

Farrar, C. R., and Worden, K. (2007). “An introduction to structural health monitoring.” *Philosophical Transactions of the Royal Society of London A: Mathematical, Physical and Engineering Sciences*, The Royal Society, 365(1851), 303–315.

Fassois, S. D., and Rivera, D. E. (2007a). “Applications of system identification.” *IEEE Control Systems*, IEEE, 27(5), 24–26.

Fassois, S. D., and Rivera, D. E. (2007b). “INTRODUCTION TO THE SPECIAL SECTION.” *IEEE Control Systems Magazine*, 1066(033X/07).

Fekete, S., Diederichs, M., and Lato, M. (2009). “Geotechnical applications of Lidar scanning in tunnelling.” *RockEng. Diederichs and Grasselli, Toronto*, 1–12.

Fenton, G. A., and Griffiths, D. V. (2008). *Risk assessment in geotechnical engineering*. Wiley Online Library.

Forssell, U., and Lindskog, P. (1996). *Combining semi-physical and neural network modeling: an example of its usefulness*. Linköping University Electronic Press.

Frangopol, D. M., and Liu, M. (2007). “Maintenance and management of civil infrastructure based on condition, safety, optimization, and life-cycle cost∗.” *Structure and infrastructure engineering*, Taylor & Francis, 3(1), 29–41.

Fröhlich, C., and Mettenleiter, M. (2004). “Terrestrial laser scanning—new perspectives in 3D surveying.” *International archives of photogrammetry, remote sensing and spatial information sciences*, 36(Part 8), W2.

Fu, L., and Li, P. (2013). “The research survey of system identification method.” *Intelligent Human-Machine Systems and Cybernetics (IHMSC), 2013 5th International Conference on*, IEEE, 397–401.

Gahalaut, V. K. (2011). “M 6.9 September 18, 2011 Sikkim earthquake.” *Geomatics, Natural Hazards and Risk*, Taylor & Francis, 2(4), 325–328.

Galetzka, J., Melgar, D., Genrich, J. F., Geng, J., Owen, S., Lindsey, E. O., Xu, X., Bock, Y., Avouac, J.-P., and Adhikari, L. B. (2015). “Slip pulse and resonance of the Kathmandu basin during the 2015 Gorkha earthquake, Nepal.” *Science*, American Association for the Advancement of Science, 349(6252), 1091–1095.

Gao, J. (2008). *Digital analysis of remotely sensed imagery*. McGraw-Hill Professional.

Gawthrop, P. J., Jezek, J., Jones, R. W., and Sroka, I. (1993). “Gray-Box Model Identification.” *Control-Theory and Advanced Technology*, MITA Press Ochanomizu Center BLDG 2-12 Hongo-3 Bunkyo-KU, Tokyo, 113, Japan, 9(1), 139–157.

Geo-Enterprises, D. (2006). “Digitilt Inclinometer Probe.” *Mukilteo, WA: Durham Geo Slope Indicator*.

George, A. M., Chakraborty, S., Das, J. T., Pedarla, A., and Puppala, A. J. (n.d.). “Understanding Shallow Slope Failures on Expansive Soil Embankments in North Texas Using Unsaturated Soil Property Framework.” *PanAm Unsaturated Soils 2017*, 206–216.

Ghanem, R., and Shinozuka, M. (1995). “Structural-system identification. I: Theory.” *Journal of Engineering Mechanics*, American Society of Civil Engineers, 121(2), 255–264.

Goldberg, D. E., and Holland, J. H. (1988). “Genetic algorithms and machine learning.” *Machine learning*, Springer, 3(2), 95–99.

Grejner-Brzezinska, D. A., Toth, C., Wu, T. H., and Shakoor, A. (2015). *Probabilistic Use of LiDAR Data to Detect and Characterize Landslides*.

Grosse, C. U., Beutel, R., Reinhard, H. W., and Kruger, M. (2005). “Impact-echo techniques for non-destructive inspection of concrete structures.” *Concrete Repair, Rehabilitation and Retrofitting*, Taylor & Francis London.

Gupta, R. P. (2017). *Remote sensing geology*. Springer.

Habib, M. (2016). *Empirical Modeling and Its Applications*. InTech.

Hanna, T. H. (1985). “Field instrumentation in geotechnical engineering.” Trans Tech Pub., Rockport, MA.

Hashash, Y. M. A., and Whittle, A. J. (1996). “Ground movement prediction for deep excavations in soft clay.” *Journal of geotechnical engineering*, American Society of Civil Engineers, 122(6), 474–486.

Hassona, F., Hashem, M. D., Abdelmalak, R. I., and Hakeem, B. M. (2017). “Bumps at Bridge Approaches: Two Case Studies for Bridges at El-Minia Governorate, Egypt.” *International Congress and Exhibition" Sustainable Civil Infrastructures: Innovative Infrastructure Geotechnology"*, Springer, 265–280.

Hausamann, D., Zirnig, W., Schreier, G., and Strobl, P. (2005). “Monitoring of gas pipelines–a civil UAV application.” *Aircraft Engineering and Aerospace Technology*, Emerald Group Publishing Limited, 77(5), 352–360.

Hicher, P.-Y., and Shao, J.-F. (2013). *Constitutive modeling of soils and rocks*. John Wiley & Sons.

Hicks, M. A., Brinkgreve, R. B. J., and Rohe, A. (2014). *Numerical Methods in Geotechnical Engineering*. CRC Press.

Hoensheid, R. C., Dean, D. B., Brooks, C., Ahlborn, T. M., Harris, D. K., and Dobson, R. J. (2012). *An Evaluation of Surface Defect Detection in Reinforced Concrete Bridge Decks Using Terrestrial LiDAR*.

Hoła, J., and Schabowicz, K. (2010). “State-of-the-art non-destructive methods for diagnostic testing of building structures–anticipated development trends.” *Archives of civil and mechanical engineering*, Elsevier, 10(3), 5–18.

Hooks, J. M., and Frangopol, D. M. (2013). *LTBP bridge performance primer.* United States. Federal Highway Administration. Office of Infrastructure Research and

Development.

Hoppe, E. J. (1999). “Guidelines for the use, design, and construction of bridge approach slabs.” Virginia. Dept. of Transportation.

Horvath, A., and Hendrickson, C. (1998). “Steel versus steel-reinforced concrete bridges: Environmental assessment.” *Journal of Infrastructure Systems*, American Society of Civil Engineers, 4(3), 111–117.

Hu, H., Fernandez-Steeger, T. M., Dong, M., Nguyen, H. T., and Azzam, R. (2010). “3D modeling using LiDAR data and its geological and geotechnical applications.” *2010 18th International Conference on Geoinformatics*, IEEE, 1–6.

Huston, D. (2010). *Structural sensing, health monitoring, and performance evaluation*. CRC Press.

Hvorslev, M. J. (1976). *The Changeable Interaction betweeen Soils and Pressure Cells; Tests and Reviews at the Waterways Experiment Station*. Army Engineer Waterways Experiment Station Vicksburg MS.

Indicator, S. (2004). “Guide to geotechnical instrumentation.” *Washington, USA*.

Isermann, R. (1981). “Practical aspects of process identification.” *System Identification*, Elsevier, 575–587.

Islam, A. K. M. (2010). “On reducing bumps at pavement-bridge interface.”

Jaboyedoff, M., Oppikofer, T., Abellán, A., Derron, M.-H., Loye, A., Metzger, R., and Pedrazzini, A. (2012). “Use of LIDAR in landslide investigations: a review.” *Natural hazards*, Springer, 61(1), 5–28.

Jackson, T. J. (1993). “III. Measuring surface soil moisture using passive microwave remote sensing.” *Hydrological processes*, Wiley Online Library, 7(2), 139–152.

Jensen, J. R. (2005). “Introductory digital image processing 3rd edition.” *Upper saddle river: Prentice hall*.

Johansen, T. A., and Foss, B. (1993). “Constructing NARMAX models using ARMAX models.” *International Journal of Control*, Taylor & Francis, 58(5), 1125–1153.

Johnson, A. I. (1988). *Geotechnical Applications of Remote Sensing and Remote Data Transmission: A Symposium*. ASTM International.

Jones, L. D. (2006). “Monitoring landslides in hazardous terrain using terrestrial LiDAR: an example from Montserrat.” *Quarterly journal of engineering geology and hydrogeology*, GeoScienceWorld, 39(4), 371–373.

Jooste, M. A., and Cawood, F. T. (2006). “Survey slope stability monitoring: Lessons from Venetia diamond mine.” *International Symposium on Stability of Rock Slopes in Open Pit Mining and Civil Engineering*, 3–6.

Kailath, T. (1980). *Linear systems*. Prentice-Hall Englewood Cliffs, NJ.

Karbhari, V. M. (2009). *Design principles for civil structures*. Wiley Online Library.

Karbhari, V. M., and Ansari, F. (2009). *Structural health monitoring of civil infrastructure systems*. Elsevier.

Kayen, R., Pack, R. T., Bay, J., Sugimoto, S., and Tanaka, H. (2006). “Terrestrial-LIDAR visualization of surface and structural deformations of the 2004 Niigata Ken Chuetsu, Japan, earthquake.” *Earthquake Spectra*, 22(S1), 147–162.

Keesman, K. J. (2011). *System identification: an introduction*. Springer Science & Business Media.

Keller, H. B. (1992). *Numerical methods for two-point boundary-value problems*. Dover Pubns.

Kellndorfer, J. M., Dobson, M. C., and Ulaby, F. T. (1996). “Geocoding for classification of ERS/JERS-1 SAR composites.” *Geoscience and Remote Sensing Symposium, 1996. IGARSS’96.’Remote Sensing for a Sustainable Future.’, International*, IEEE, 2335–2337.

Kerr, J. T., and Ostrovsky, M. (2003). “From space to species: ecological applications for remote sensing.” *Trends in ecology & evolution*, Elsevier, 18(6), 299–305.

Kirkham, R. J., Alisa, M., Pimenta da Silva, A., Grindley, T., and Brondsted, J. (2004). “EUROLIFEFORM: An integrated probabilistic whole life cycle cost and performance model for buildings and civil infrastructure.” *Proceedings of International Construction Research Conference of the Royal Institution of Chartered Surveyors (COBRA 2004)*.

Klaiber, F. W., White, D. J., Wipf, T. J., Phares, B. M., Robbins, V. W., Division, H., and Highway, I. (2004). “Development of Abutment Design Standards for Local Bridge Designs Volume 1 of 3 Final Department of Civil and Construction Engineering.” *Design*, 1.

Kogias, G. (2007). “Ultrasonic Testing.” *High frequency ultrasonic testing*, 4544, 1–36.

Kolay, P. K., Rosmina, A. B., and Ling, N. W. (2008). “Settlement prediction of tropical soft soil by artificial neural network (ANN).” *The 12th international conference of international association for computer methods and advances in geomechanics (IACMAG), Goa, India*, 1843–1849.

Koliji, A. (2013). “Guide to numerical modeling in geomechanics.” *Geotechdata.info*.

Kramer, S. L., and Sajer, P. (1991). *Bridge Approach Slab Effectiveness. Final Report*.

Kramer, S. L., and Wang, C.-H. (2015). “Empirical model for estimation of the residual strength of liquefied soil.” *Journal of Geotechnical and Geoenvironmental Engineering*, American Society of Civil Engineers, 141(9), 4015038.

Kromel, E., and Maher, K. (2010). *Second Generation Precast Deck Panel (Nudeck) System*.

La, H. M., Gucunski, N., Kee, S.-H., and Van Nguyen, L. (2015). “Data analysis and visualization for the bridge deck inspection and evaluation robotic system.”

Visualization in Engineering, Nature Publishing Group, 3(1), 6.

Lato, M. (2010). “Geotechnical applications of LiDAR pertaining to geomechanical evaluation and hazard identification.” Canadian theses.

Lazecky, M., Perissin, D., Bakon, M., de Sousa, J. M., Hlavacova, I., and Real, N. (2015). “Potential of satellite InSAR techniques for monitoring of bridge deformations.” *Urban Remote Sensing Event (JURSE), 2015 Joint*, IEEE, 1–4.

Lefsky, M. A., Cohen, W. B., Acker, S. A., Parker, G. G., Spies, T. A., and Harding, D. (1999). “Lidar remote sensing of the canopy structure and biophysical properties of Douglas-fir western hemlock forests.” *Remote sensing of environment*, Elsevier, 70(3), 339–361.

Leontaritis, I. J., and Billings, S. A. (1985). “Input-output parametric models for non-linear systems part I: deterministic non-linear systems.” *International journal of control*, Taylor & Francis, 41(2), 303–328.

Lim, K., Treitz, P., Wulder, M., St-Onge, B., and Flood, M. (2003). “LiDAR remote sensing of forest structure.” *Progress in physical geography*, Sage Publications Sage CA: Thousand Oaks, CA, 27(1), 88–106.

Lin, W., and Yoda, T. (2017). *Bridge Engineering: Classifications, Design Loading, and Analysis Methods*. Butterworth-Heinemann.

Lipiński, M., and Wdowska, M. (2011). “A stress history and strain dependent stiffness of overconsolidated cohesive soil.” *Annals of Warsaw University of Life Sciences-SGGW. Land Reclamation*, Versita, 43(2), 207–216.

LIU, J., LUAN, M., and WANG, J. (2007). “Analysis on Limitation of Inclinometer in Measuring Lateral Displacement of Soft Soil Foundation Under Embankment [J].” *Journal of Yangtze River Scientific Research Institute*, 5, 18.

Ljung, L. (1992). *System identification toolbox*. Math Works.

Ljung, L. (1998). “System identification.” *Signal analysis and prediction*, Springer, 163–173.

Ljung, L. (1999). “System identification: Theory for the user, ptr prentice hall information and system sciences series.” *ed: Prentice Hall, New Jersey*.

Ljung, L., and Söderström, T. (1983). *Theory and practice of recursive identification*. MIT press.

Lorito, F. (1998). “Identification of a grey-box model of nonlinear current transformers for simulation purposes.” *Control Engineering Practice*, Elsevier, 6(11), 1331–1339.

Lowe, S. R., Improvement, H., Project, W., and Eir, D. (2006). “Santa Rosa Lowe’s Home Improvement Warehouse Project Draft EIR Geology, Soils, and Seismicity 4.5 -.” 1–14.

Lyzenga, D. R. (1978). “Passive remote sensing techniques for mapping water depth and bottom features.” *Applied optics*, Optical Society of America, 17(3), 379–383.

Machan, G., and Bennett, V. G. (2008). “Use of inclinometers for geotechnical instrumentation on transportation projects: State of the practice.” *Transportation Research E-Circular*, (E-C129).

Malheiro, R. L. M. C., Camões, A., and Meira, G. (2018). “Behaviour of concrete under severe environment: effect of carbonation on the chloride diffusion coefficient from non-steady-state migration test.” *Romanian Journal of Materials*, Foundation for Materials Science and Engineering “serban Solacolu,” 48(1), 64–69.

Mallela, J., and Sadasivam, S. (2011). “Work Zone Road User Costs – Concepts and Applications.” (December).

Manconi, A., Casu, F., Ardizzone, F., Bonano, M., Cardinali, M., De Luca, C., Gueguen, E., Marchesini, I., Parise, M., and Vennari, C. (2014). “Brief Communication: Rapid mapping of landslide events: the 3 December 2013 Montescaglioso landslide, Italy.”

Natural Hazards and Earth System Sciences, Copernicus GmbH, 14(7), 1835–1841.

Manos, G. C., Kourtides, V., and Sextos, A. (2008). “Model bridge pier-foundation-soil interaction implementing in-situ/shear stack testing and numerical simulation.” *14th World conference on earthquake engineering, Beijing*.

Marano, S. A. (1994). “Boundary Value Problem.” *Journal of Mathematical Analysis and Applications*, 183, 518–522.

Mark, C. (2016). “Science of empirical design in mining ground control.” *International Journal of Mining Science and Technology*, Elsevier, 26(3), 461–470.

Matthews, J. (2017). “Laboratory Testing of Transverse Joints in Precast-Panel Bridge-Deck Replacement Systems.”

Mazroi, A., Wang, L. L., and Murray, T. M. (1983). “Effective coefficient of friction of steel bridge bearings.” *Transportation Research Record*, 903, 79–86.

Mikkelsen, P. E., and Wilson, S. D. (1983). “Field instrumentation: accuracy performance, automation and procurement.” *International Symposium on Field Measurements in Geomechanics. Zürich*, 251–272.

Morgan, D., and Falkner, E. (2001). *Aerial mapping: methods and applications*. CRC Press.

Mukoyama, S. (2011). “Estimation of ground deformation caused by the earthquake (M7. 2) in Japan, 2008, from the geomorphic image analysis of high resolution LiDAR DEMs.” *Journal of Mountain Science*, Springer, 8(2), 239–245.

Murray, C. J. L., Lopez, A. D., and Wibulpolprasert, S. (2004). “Monitoring global health: time for new solutions.” *BMJ: British Medical Journal*, BMJ Publishing Group, 329(7474), 1096.

Nageh, W., and Saturday, M. A. (2014). “The Usage And Applications of Remote Sensing

Science & Satellite Image Processing in Engineering Geology And Geotechnical Engineering."

Nakase, A., Kamei, T., and Kusakabe, O. (1988). "Constitutive parameters estimated by plasticity index." *Journal of Geotechnical Engineering*, American Society of Civil Engineers, 114(7), 844–858.

Narayanan, S. (2017). "Accelerated Bridge Construction With Folded steel Plate Girders." *Journal of the Indian National Group of The International Association for Bridge & Structural Engineering*, 47(March).

Natke, H. G. (2014). *Application of system identification in engineering*. Springer.

Nazarian, S., Baker, M., and Crain, K. (1997). "Assessing quality of concrete with wave propagation techniques." *Materials Journal*, 94(4), 296–305.

Nelson, J. D., Chao, K.-C., and Overton, D. D. (2007). "Definition of Expansion Potential for Expansive Soils." *Proceedings of the Third Asian Conference on Unsaturated Soils*, Citeseer.

Nelson, J., and Miller, D. J. (1997). *Expansive soils: problems and practice in foundation and pavement engineering*. John Wiley & Sons.

New Jersey Dept. of Transportation (NJDOT). (1999). "Road user cost manual, Trenton, N.J." *Scientific American*, 284(6), 5–6.

Nguyen, V. V. (2018). "Damage identification of a bridge component using model updating and artificial neural network techniques based on frequency response functions."

Nicks, J. E. (2009). "The bump at the end of the railway bridge." Texas A&M University.

Njoku, E. G., and Entekhabi, D. (1996). "Passive microwave remote sensing of soil moisture." *Journal of hydrology*, Elsevier, 184(1–2), 101–129.

O'reilly, M. P., and New, B. M. (1982). *Settlements above tunnels in the United Kingdom-*

their magnitude and prediction.

O'rourke, T. D. (1993). "Base stability and ground movement prediction for excavations in soft clay." *Retaining Structures. Proceedings of the Conference Organized by the Institution of Civil Engineers and Held on 20-23 JULY, 1992 at Robinson College, Cambridge*.

Oh, W. T., Vanapalli, S. K., and Puppala, A. J. (2009). "Semi-empirical model for the prediction of modulus of elasticity for unsaturated soils." *Canadian Geotechnical Journal*, NRC Research Press, 46(8), 903–914.

Onoufriou, T., and Casciati, F. (2015). "Condition assessment of civil infrastructure." Taylor & Francis.

Oskay, C., and Zeghal, M. (2011). "A survey of geotechnical system identification techniques." *Soil Dynamics and Earthquake Engineering*, Elsevier, 31(4), 568–582.

Overton, D. D., Chao, K.-C., and Nelson, J. D. (2006). "Time rate of heave prediction for expansive soils." *GeoCongress 2006: Geotechnical Engineering in the Information Technology Age*, 1–6.

Päivinen, R., and Anttila, P. (2000). "How Reliable Is a Satellite Forest Inventory?" *Silva Fennica*, 35(1), 125–127.

Panigrahi, B., and Goyal, M. R. (2016). *Modeling Methods and Practices in Soil and Water Engineering*. Apple Academic Press.

Papadimitriou, C. H. (2003). *Computational complexity*. John Wiley and Sons Ltd.

Papadopoulos, E., Cortes, D. D., and Carlos Santamarina, J. (2016). "In-situ assessment of the stress-dependent stiffness of unbound aggregate bases: application in inverted base pavements." *International Journal of Pavement Engineering*, Taylor & Francis, 17(10), 870–877.

Paraschos, A., Amde, A. M., and Moumena, L. (2016). "Bridge Approach Slabs."

4(November), 71–82.

Park, G., Cudney, H. H., and Inman, D. J. (2000). “Impedance-based health monitoring of civil structural components.” *Journal of infrastructure systems*, American Society of Civil Engineers, 6(4), 153–160.

Pedarla, A., Puppala, A. J., Hoyos, L. R., and Chittoori, B. (2015). “Evaluation of swell behavior of expansive clays from internal specific surface and pore size distribution.” *Journal of Geotechnical and Geoenvironmental Engineering*, American Society of Civil Engineers, 142(2), 4015080.

Pelckmans, K. (2015). “Recursive identification.” *Lecture Notes for a Course on System Identification*, 119–128.

Petite, T. D., and Huff, R. M. (2002). “System and method for monitoring and controlling remote devices.” Google Patents.

Phanikumar, B. R., and Singla, R. (2016). “Swell-consolidation characteristics of fibre-reinforced expansive soils.” *Soils and Foundations*, Elsevier, 56(1), 138–143.

Pulvirenti, L., Chini, M., Pierdicca, N., Guerriero, L., and Ferrazzoli, P. (2011). “Flood monitoring using multi-temporal COSMO-SkyMed data: Image segmentation and signature interpretation.” *Remote Sensing of Environment*, Elsevier, 115(4), 990–1002.

Punthutaecha, K., Puppala, A. J., Vanapalli, S. K., and Inyang, H. (2006). “Volume change behaviors of expansive soils stabilized with recycled ashes and fibers.” *Journal of materials in Civil Engineering*, American Society of Civil Engineers, 18(2), 295–306.

Puppala, A. J., Bheemasetti, T. V., and Shafikhani, A. (2017a). *Pilot Implementation Using Geofoam for Repair of Bridge Approach Slabs and Adjoining Roadway*. Arlington.

Puppala, A. J., Bheemasetti, T. V., and Shafikhani, A. (2017b). *Investigations of Geofoam as an Embankment Fill Material for Bridge at Eden Road – US 287 in Arlington , Texas*. Arlington.

Puppala, A. J., Manosuthikij, T., and Chittoori, B. C. S. (2014). “Swell and shrinkage strain prediction models for expansive clays.” *Engineering Geology*, Elsevier, 168, 1–8.

Puppala, A. J., Pedarla, A., Hoyos, L. R., Zapata, C., and Bheemasetti, T. V. (2016). “A semi-empirical swell prediction model formulated from ‘clay mineralogy and unsaturated soil’properties.” *Engineering Geology*, Elsevier, 200, 114–121.

Puppala, A. J., Punthutaecha, K., and Vanapalli, S. K. (2006). “Soil-water characteristic curves of stabilized expansive soils.” *Journal of Geotechnical and Geoenvironmental Engineering*, American Society of Civil Engineers, 132(6), 736–751.

Puppala, A. J., Ruttanaporamakul, P., Bheemasetti, T. V., and Shafikhani, A. (2018). “Laboratory and Field Investigations on Geofoam - A Light Weight Fill Material.” *ASCE Journal of Pipeline Systems Engineering and Practice*, In Press.

Rabbani, M. J., Hussain, K., and Ali, A. (2013). “Model identification and validation for a heating system using Matlab system identification toolbox.” *IOP Conference Series: Materials Science and Engineering*, IOP Publishing, 12022.

Rachad, S., Nsiri, B., and Bensassi, B. (2015). “System Identification of Inventory System Using ARX and ARMAX Models.” *International Journal of Control and Automation*, 8(12), 283–294.

Rai, D. C., Singhal, V., Mondal, G., Parool, N., Pradhan, T., and Mitra, K. (2012). “The M 6.9 Sikkim (India–Nepal Border) earthquake of 18 September 2011.” *Current Science*, JSTOR, 1437–1446.

Rana, S. (2017). *Risk-Targeted Ground Motion for Performance-Based Bridge Design*. Southern Illinois University at Carbondale.

Rashidi, M., Gibson, P., and Ho, T. K. (2013). “A new approach to bridge infrastructure management.”

Reilly, D. P. (1980). “Experiences with an Automatic Box-Jenkins Modeling Algorithm.” *Time Series Analysis, ed. OD*.

Rezaeifar, F. (2013). “The Role of Social Security Spaces of Traditional Iranian Cities in Urban Crimes Reduction: With Emphasis on CPTED* Approach.” *The International Journal of Humanities*, Tarbiat Modarres University, 19(1), 51–68.

Rezaeifar, F. (2018). “Developing a Framework to Optimize the Operations of an Intermodal Underground Freight Transportation Terminal Using Simulation.” University of Texas at Arlington.

Rezaeifar, F., Najafi, M., Ardekani, S. A., and Shahooei, S. (2017). “Optimized Terminal Design for UFT Systems in Integrated Subterranean Pipeline Infrastructure.” *Pipelines*, 528–539.

Ruttanaporamakul, P. (2015). “Evaluation Of Lightweight Geofoam For Mitigating Bridge Approach Slab Settlements.” Civil & Environmental Engineering.

Ruttanaporamakul, P., Puppala, A. J., Pedarla, A., Bheemasetti, T. V., and Williammee, R. S. (2016). “Settlement Mitigation of a Distressed Embankment in Texas by Utilization of Lightweight EPS Geofoam Material.” *Transportation Research Board 95th Annual Meeting*.

Ryan, T. W., EricMann, J., Chill, Z. M., and Ott, B. T. (2012). “Bridge Inspector’s Reference Manual.” *Fhwa*, BIRM 1, 1020.

Sabins, F. F. (2007). *Remote sensing: principles and applications*. Waveland Press.

Samanta, B., Al-Balushi, K. R., and Al-Araimi, S. A. (2003). “Artificial neural networks and

support vector machines with genetic algorithm for bearing fault detection." *Engineering applications of artificial intelligence*, Elsevier, 16(7–8), 657–665.

Sanchez, J., Denis, F., Checchin, P., Dupont, F., and Trassoudaine, L. (2017). "Global Registration of 3D LiDAR Point Clouds Based on Scene Features: Application to Structured Environments." *Remote Sensing*, Multidisciplinary Digital Publishing Institute, 9(10), 1014.

Sanford, K. L., Loehr, J. E., and Huaco, D. (2003). "Asset management framework for geotechnical infrastructure." *Journal of infrastructure systems*, American Society of Civil Engineers, 9(3), 107–116.

Saygili, G., and Rathje, E. M. (2008). "Empirical predictive models for earthquake-induced sliding displacements of slopes." *Journal of Geotechnical and Geoenvironmental Engineering*, American Society of Civil Engineers, 134(6), 790–803.

Scaioni, M., Longoni, L., Melillo, V., and Papini, M. (2014). "Remote sensing for landslide investigations: An overview of recent achievements and perspectives." *Remote Sensing*, Multidisciplinary Digital Publishing Institute, 6(10), 9600–9652.

Schofield, A., and Wroth, P. (1968). *Critical state soil mechanics*. McGraw-Hill London.

Scott, M., Rezaizadeh, A., Delahaza, A., Santos, C. G., Moore, M., Graybeal, B., and Washer, G. (2003). "A comparison of nondestructive evaluation methods for bridge deck assessment." *NDT & E International*, Elsevier, 36(4), 245–255.

Selig, E. T. (1980). "Soil stress gage calibration." *Geotechnical Testing Journal*, ASTM International, 3(4), 153–158.

Seo, J. B. (2005). "The bump at the end of the bridge: an investigation." Texas A&M University.

Shafikhani, A., Bheemasetti, T. V., and Puppala, A. J. (2018a). "Performance Evaluation

of a Bridge Superstructure Using Terrestrial Laser Scanning Technology." *Geotechnical testing journal*, In Press.

Shafikhani, A., Bheemasetti, T. V, and Puppala, A. J. (2017). "Effect of Seasonal Changes on a Hybrid Soil–Geofoam Embankment System." *International Journal of Geosynthetics and Ground Engineering*, Springer, 3(4), 39.

Shafikhani, A., Bheemasetti, T. V, Puppala, A. J., and Banerjee, A. (2018b). "Analysis and Interpretation of Inclinometer and Pressure Cell Data on a Soil-Geofoam Embankment." *GeoShanghai International Conference*, Springer, 410–418.

Shahin, M. A., Jaksa, M. B., and Maier, H. R. (2001). "Artificial neural network applications in geotechnical engineering." *Australian geomechanics*, Citeseer, 36(1), 49–62.

Shinners, S. M. (1998). *Modern control system theory and design*. John Wiley & Sons.

Siegal, B. S., and Gillespie, A. R. (1980). *Remote sensing in geology*. Wiley New York.

Silvestrin, P., Berger, M., Kerr, Y., and Font, J. (2001). "ESA's second earth explorer opportunity mission: The soil moisture and ocean salinity mission-SMOS." *IEEE Geoscience and Remote Sensing Newsletter*, 118, 11–14.

Simard, M., Grandi, G. De, Saatchi, S., and Mayaux, P. (2002). "Mapping tropical coastal vegetation using JERS-1 and ERS-1 radar data with a decision tree classifier." *International Journal of Remote Sensing*, Taylor & Francis, 23(7), 1461–1474.

Sjöberg, J., and De Raedt, P. (1997). "Nonlinear system identification: a software concept and examples." *IFAC Proceedings Volumes*, Elsevier, 30(11), 657–662.

Söderström, T., and Stoica, P. (1989). "System identification." Prentice-Hall.

Spathonis, J. (2011). *Queensland roads*. Queensland Government.

Stewart, J. P., Hu, J., Kayen, R. E., Lembo Jr, A. J., Collins, B. D., Davis, C. A., and O'Rourke, T. D. (2009). "Use of airborne and terrestrial lidar to detect ground

displacement hazards to water systems." *Journal of Surveying Engineering*, American Society of Civil Engineers, 135(3), 113–124.

Su, Y. Y., Hashash, Y. M. A., and Liu, L. Y. (2006). "Integration of construction as-built data via laser scanning with geotechnical monitoring of urban excavation." *Journal of construction engineering and management*, American Society of Civil Engineers, 132(12), 1234–1241.

Talesnick, M. (2013). "Measuring soil pressure within a soil mass." *Canadian Geotechnical Journal*, NRC Research Press, 50(7), 716–722.

Tan, K. C., and Li, Y. (2002). "Grey-box model identification via evolutionary computing." *Control Engineering Practice*, Elsevier, 10(7), 673–684.

TAN, S. (1995). "Validation of hyperbolic method for settlement in clays with vertical drains." *Soils and Foundations*, The Japanese Geotechnical Society, 35(1), 101–113.

Theroux, B., Labuz, J. F., and Drescher, A. (2000). "Calibration of an earth pressure cell."

Thyagarajan, K. N., and Minden, G. (2002). "Earth Observation System Satellite Communication Characteristics." 1–227.

Ti, K. S., Huat, B. B. K., Noorzaei, J., Jaafar, M. S., and Sew, G. S. (2009a). "A review of basic soil constitutive models for geotechnical application." *Electronic Journal of Geotechnical Engineering*, 14, 1–18.

Ti, K. S., Huat, B. B. K., Noorzaei, J., Jafar, M. S., and Sew, G. S. (2009b). "A Review of Basic Soil Constitutive Models for Geotechnical Application." *Electronic Journal of Geotechnical Engineering*, 14, 18.

TN, D., and SM, D. (n.d.). "A Review on Pressure Measurement using Earth Pressure Cell." Citeseer.

Transportation Research Board. (2016). *Highway Capacity Manual*. *National Research*

Council, Washington, DC.

Troyano, L. F. (2003). *Bridge engineering: a global perspective*. Thomas Telford.

Tsang, L., Kong, J. A., and Shin, R. T. (1985). "Theory of microwave remote sensing."

U.S. Climate Data. (2017). "U.S. Climate Data."

Ulaby, F. T., Moore, R. K., and Fung, A. K. (1986). *Microwave Remote Sensing, Active and Passive, Volume I, Microwave Remote Sensing Fundamentals and Radiometry*. Reading, MA: Addison-Wesley.

Vanapalli, S., and Lu, L. (2012). "A state-of-the art review of 1-D heave prediction methods for expansive soils." *International Journal of Geotechnical Engineering*, Taylor & Francis, 6(1), 15–41.

Vu, H. Q., and Fredlund, D. G. (2004). "The prediction of one-, two-, and three-dimensional heave in expansive soils." *Canadian Geotechnical Journal*, NRC Research Press, 41(4), 713–737.

Wachman, G. S., and Labuz, J. F. (2011). "Soil-structure interaction of an earth pressure cell." *Journal of Geotechnical and Geoenvironmental Engineering*, American Society of Civil Engineers, 137(9), 843–845.

Wang, D. (2017). "Application and evaluation of non-destructive testing methods for buried pipes." Queen's University (Canada).

Wanyan, Y., Abdallah, I., Nazarian, S., and Puppala, A. J. (2014). "Moisture content-based longitudinal cracking prediction and evaluation model for low-volume roads over expansive soils." *Journal of Materials in Civil Engineering*, American Society of Civil Engineers, 27(10), 4014263.

Weibelzahl, S., and Weber, G. (2002). "Advantages, opportunities and limits of empirical evaluations: Evaluating adaptive systems." *KI*, 16(3), 17–20.

Weiler, W. A., and Kulhawy, F. H. (1982). "Factors affecting stress cell measurements in

soil.” *Journal of the Geotechnical Engineering Division*, ASCE, 108(12), 1529–1548.

Whitman, R. V. (2000). “Organizing and evaluating uncertainty in geotechnical engineering.” *Journal of Geotechnical and Geoenvironmental Engineering*, American Society of Civil Engineers, 126(7), 583–593.

Woodhouse, I. H. (2017). *Introduction to microwave remote sensing*. CRC press.

Wray, W. K., El-Garhy, B. M., and Youssef, A. A. (2005). “Three-dimensional model for moisture and volume changes prediction in expansive soils.” *Journal of Geotechnical and Geoenvironmental Engineering*, American Society of Civil Engineers, 131(3), 311–324.

writers, C. R. I. (2018). “Rip up roads at the right time only: Your research round-up for Q1 2018.” *Construction Research and Innovation*, Taylor & Francis, 9(1), 26–30.

X-engineer.org. (2018). “Methods of Mathematical Modeling.”

Xiao, M., Qiu, T., Khosrojerdi, M., Basu, P., and Withiam, J. L. (2016). *Synthesis and Evaluation of the Service Limit State of Engineered Fills for Bridge Support*.

Xue, D., and Chen, Y. (2013). *System simulation techniques with MATLAB and Simulink*. John Wiley & Sons.

Yamamuro, J. A., and Kaliakin, V. N. (2005). “Soil constitutive models: evaluation, selection, and calibration: January 24-26, 2005, Austin, Texas.” American Society of Civil Engineers.

Yang, Y., and Yu, X. B. (2016). “Real time measurement of the dynamic displacement field of a large-scale arch-truss bridge by remote sensing technology.” *SENSORS, 2016 IEEE*, IEEE, 1–3.

Yari, N. (2018). “New Model for Bridge Management System (BMS): Bridge Repair Priority Ranking System (BRPRS), Case Based Reasoning for Bridge Deterioration , Cost Optimization , and Preservation Strategy . BY Nasser Yari

Bachelor of Science in Civil Engineering , Univ." (May).

Yehia, S., Abudayyeh, O., Nabulsi, S., and Abdelqader, I. (2007). "Detection of common defects in concrete bridge decks using nondestructive evaluation techniques." *Journal of Bridge Engineering*, American Society of Civil Engineers, 12(2), 215–225.

Yun, H.-B., and Reddi, L. N. (2011). "Nonparametric monitoring for geotechnical structures subject to long-term environmental change." *Advances in Civil Engineering*, Hindawi, 2011.

Zhang, G., Fu, P., and Liang, F. (2013). "Mathematical and numerical modeling in geotechnical engineering." *Journal of Applied Mathematics*, Hindawi, 2013.

Zhang, X. (2005). "Consolidation theories for saturated-unsaturated soils and numerical simulation of residential buildings on expansive soils." Texas A&M University.

Zwissler, B., Oommen, T., Vitton, S., and Seagren, E. A. (2017). "Thermal remote sensing for moisture content monitoring of mine tailings: laboratory study." *Environmental & Engineering Geoscience*, Assoc Eng Geologists, 1078–7275.

Biographical Information

Ali Shafikhani is a geotechnical engineer originally from Shiraz, Iran. He received his bachelor's degree in civil engineering from Yasuj University in 2005. He worked for more than one year in Salman Farsi Concrete Dam project in several fields including concrete geotechnical engineering laboratories and dam bearings water-tight grout curtains in karst zones. He accomplished his master's Degree in Civil Engineering majoring in Geotechnical Engineering from Shiraz University in February 2010. His research was concentrated on effective zone radius of sand compaction piles as a remedial measure against soil liquefaction by implementing cavity expansion theory and numerical modeling using ABAQUS and PLAXIS 2D. He established his own consultant company and worked for more than four years in several tunneling, subway, and building projects.

In August 2015, he possessed the opportunity to pursue his PhD at The University of Texas at Arlington, under the supervision of Dr. Anand J. Puppala. His research was focused on the performance evaluation of a rehabilitated soil-geofoam bridge infrastructure using terrestrial LiDAR and system identification approach. He developed a retaining wall system design guideline applicable for high flood zone areas. He has collaborated actively on writing several high-quality journal and conference papers on his field of research. His main goal is to establish his own interdisciplinary science foundation center to develop new generations of geotechnical engineering health monitoring instrumentation systems based on artificial intelligence and machine learning techniques.